

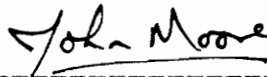
LASER DOPPLER ANEMOMETER MEASUREMENTS OF REYNOLDS
STRESSES IN A FULLY DEVELOPED PIPE FLOW

by

Mark C. Doty

Thesis submitted to the Faculty of the
Virginia Polytechnic Institute and State University
in partial fulfillment of the requirements
for the degree of
MASTER OF SCIENCE
in Mechanical Engineering

APPROVED:



J. Moore, Chairman



C.L. Dancey



F.J. Pierce

December, 1992

Blacksburg, VA

C.2

LD
5655
V855
1992
D689

LASER DOPPLER ANEMOMETER MEASUREMENTS OF REYNOLDS
STRESSES IN A FULLY DEVELOPED PIPE FLOW

by

Mark C. Doty

Committee Chairman: Prof. J. Moore

Mechanical Engineering Department

(ABSTRACT)

A laser Doppler Anemometer (LDA) is used to make Reynolds stress measurements in a fully developed, turbulent pipe flow. Traverses are made to measure shear stress, normal stresses, and the correlation coefficient. To assess the accuracy of this system, these measurements are compared with results from other published investigations. The differences between the published reports are discussed to emphasize how much turbulence measurements can vary, even in a well studied flow. Descriptions are included about LDA theory and turbulence measurement techniques. The techniques discussed include the selection of proper sampling rate, the reduction of statistical bias, the choice of amplification, and optimization practices.

ACKNOWLEDGMENTS

This project would not have been possible without the help of several people. I am indebted to Dr. J. Moore who's thoughtful guidance and encouragement brought me to a successful conclusion of this project. He provided a supportive environment and was always willing to spend time with me. I owe a great deal of thanks to Dr. C. L. Dancey who was an invaluable source of information and guidance throughout the project. He was always willing to discuss LDA concepts and lend me his equipment. I am also grateful to Dr. F. J. Pierce for serving on my committee and lending me the use of the LDA equipment. Finally, I would like to thank my parents for encouraging me throughout my life and for providing the opportunity to get a college education.

TABLE OF CONTENTS

	<u>Page</u>
ABSTRACT	
ACKNOWLEDGMENTS	iii
TABLE OF CONTENTS	iv
LIST OF FIGURES	vii
NOMENCLATURE	x
1. INTRODUCTION	1
2. LITERATURE REVIEW	2
2.1 Turbulence and the Significance of Reynolds Stresses	2
2.2 Flow Description	5
2.3 Comparison of Laufer's and Lawn's Results ...	9
2.4 Review of Turbulence Measurement and Laser Anemometry	17
2.5 Previous Studies by Graduate Students	21
3. BASIC LDA THEORY	23
4. APPARATUS AND METHODS	37
4.1 Pipe Description.....	37
4.2 LDA Equipment Description	39
4.2.1 Laser	39
4.2.2 Optical System	40
4.2.3 Signal Processing	42
4.2.3.1 Frequency Shifter	45
4.2.3.2 Signal Conditioners	45
4.2.3.3 Frequency Counters	46

TABLE OF CONTENTS (continued)

	<u>Page</u>
4.2.3.4 Coincidence Interface	48
4.2.3.5 Computer and Software	49
4.2.4 Seeding System	50
4.2.5 Traverse System and Velocity Sensitivity	53
4.2.5.1 Traverse System and Optical Bench Orientation	53
4.2.5.2 Measurement Plane	55
4.2.5.3 Velocity Sensitivity	58
4.2.5.4 Statistics of Interest and Coordinate Transformation	58
4.2.6 Beam Angle Determination	62
5.0 TURBULENCE MEASUREMENTS WITH AN LDA..	67
5.1 Turbulence Scales and Sampling Rate	67
5.1.1 Statistical Independence	67
5.1.2 Sampling Rate of This System	71
5.2 Statistical Bias	73
5.2.1 Fringe Bias	73
5.2.2 Filter Bias	74
5.2.3 Velocity Bias	76
5.3 Residence Time Weighting and Software Algorithms	77
5.4 Errors Due to Finite Sample Size	78
6.0 OPTIMIZATION OF THIS LDA SYSTEM	80
6.1 Alignment.....	80

TABLE OF CONTENTS (continued)

	<u>Page</u>
6.2 Choice of Amplification	81
6.3 Use of Filters and Flow Rate Selection	82
6.4 Coincidence Window	84
7.0 RESULTS AND DISCUSSION	90
7.1 Mean Velocity Profile	90
7.2 Velocity Fluctuations	93
7.3 Reynolds Shear Stress	98
7.4 Correlation Coefficient	100
8.0 CONCLUSIONS	102
REFERENCES	104
APPENDICES	109
Appendix A. Beam Angle Determination Program ...	109
Appendix B. Experimental Data	110
Appendix C. Probe Volume Dimensions	111
VITA	112

TABLE OF FIGURES

<u>Figure</u>	<u>Page</u>
1. Cylindrical Control Volume	6
2. Shear Stress Across a Channel [8]	8
3. Comparison of Laufer's and Lawn's Results for u'/U_t vs. r'/R [1], [2]	11
4. Comparison of Laufer's and Lawn's Results for v'/U_t vs. r'/R [1], [2]	12
5. Comparison of Laufer's and Lawn's Results for w'/U_t vs. r'/R [1], [2]	13
6. Comparison of Laufer's and Lawn's Results for \overline{uv}/U_t^2 vs. r'/R [1], [2]	15
7. Comparison of Laufer's and Lawn's Results for $\overline{uv}/u'v'$ vs. r'/R [1], [2]	16
8. Beam Intersection and Formation of Probe Volume [31].....	24
9. Velocity Sensitivity of Dual Beam LDA [41]	26
10. Fringe Formation [31]	27
11. Doppler Burst [31]	29
12. Gaussian Distribution Of Intensity Across a Laser Beam [31]	30
13. Doppler Spectrum [31]	31
14. Filtered Doppler Burst [6]	32
15. Polar Intensity Plot of Scattered Light [33] ..	33
16. Forward Scatter And Back Scatter LDA Systems	34
17. Three Beam LDA System and Fringe Formation [31]	36
18. Pipe and Blower [7]	38
19. Transmitting Path of LDA Optics [41]	41

TABLE OF FIGURES (continued)

<u>Figure</u>	<u>Page</u>
20. Recieving Path of LDA Optics [41]	43
21. Signal Path of LDA Signal Processing	44
22. LDA Counter Operation [31]	47
23. Seeding System	52
24. Scanning Electron Microscope View of Seed Particles	54
25. Traverse System and Orientation to Pipe	56
26. Measurement Plane Orientation	57
27. Traverse Direction for U and V Sensitivity	59
28. Traverse Direction for U and W Sensitivity	60
29. Half Angle Determination [37]	64
30. Spatial Correlation of Two Signals [45]	69
31. Sampling Methods	72
32. Dead Zone in Unshifted LDA Measurements [31] ..	75
33. Clipped Doppler Spectrum	83
34. Delay Due to Disparate Signal Strength	85
35. Coincident Data Rate vs Coincidence Window Size	87
36. Measurement Variability vs. Coincidence Window Size	89
37. Comparison of U/U_0 vs. r'/R to Reference Curve [1]	92
38. Comparison of u'/U_t vs. r'/R to Reference Curves [1], [2], [7]	94
39. Comparison of v'/U_t vs. r'/R to Reference Curves [1], [2], [7]	96

TABLE OF FIGURES (continued)

<u>Figure</u>		<u>Page</u>
40.	Comparison of w'/Ut vs. r'/R to Reference Curves [1], [2], [7]	97
41.	Comparison of \overline{uv}/Ut^2 vs. r'/R to Reference Curves [1], [2], [7]	99
42.	Comparison of $\overline{uv}/u'v'$ vs. r'/R to Reference Curves [1], [2], [7]	101

NOMENCLATURE

A	Amplitude
B	Angle defining dead zone in unshifted LDA
c	Distance used for angle measurement
C	Spatial correlation
Cv	Percent error in mean velocity
Cv'	Percent error in standard deviation
d	Distance used for angle measurement
Df	Distance between fringes
fd	Doppler Frequency
FFT	Fast Fourier transform
I	Intensity
I _o	Intensity at center of laser beam
I.D.	Inner diameter
L	Length scale
LDA	Laser Doppler anemometer
N	Number of samples
P	Pressure
P	Average pressure
p	Fluctuation from average pressure
PMT	Photomultiplier tube
r	Radius
R	Pipe radius
ReD	Reynolds number based on diameter
RMS	Root-mean-square

NOMENCLATURE (continued)

SNR	Signal to noise ratio
t	Time
T	Time scale
Tf	Total number of fringes
U, V, W	Total velocity in axial, radial, and tangential directions
U, V, W	Mean velocity
V _m	Measured velocity
V'	True standard deviation
V _p	Particle velocity
u, v, w	Fluctuation from mean velocity
u', v', w'	RMS value of u
u _g , u _b	Velocity measured with green and blue channels
U _t	Friction velocity
Greek Symbols	
θ	Angle
ϕ	Angle of velocity vector
λ	Laser light wavelength
π	3.1415927...
μ	Viscosity of air
ρ	Density
τ_5	Time for 5 fringes
τ_8	Time for 8 fringes
τ	Shear stress
τ_w	Wall shear stress

NOMENCLATURE (continued)

ΔT

Residence time

ΔT_{uv}

Smaller of the residence times
in the two channels

1. INTRODUCTION

The ability to make turbulence measurements is of significant value to fluid dynamicists. Experimental analysis of turbulence not only extends basic knowledge about fluid flow but also serves as a basis for comparison with computational codes. One of the primary means of turbulence measurement is the laser Doppler anemometer (LDA). The LDA is a non-intrusive instrument that measures the velocity of reflective particles in a fluid. The measured velocity of these particles is related to the Doppler shift of reflected laser light as they pass through the laser beam.

A two component, three beam LDA system has been available in this department for approximately ten years but was never used to make Reynolds shear stress measurements. The main concern was whether coincident velocity measurements could be made. To assess the potential of the system, the LDA was refurbished and the radial distributions of Reynolds shear stress and normal stress were measured in a fully developed pipe flow. The results are compared to comprehensive pipe flow studies by Laufer [1] and Lawn [2].

Although measurements with LDA systems have been made since the late sixties, there is still quite a lot of subtle expertise required to make high quality turbulence measurements. Therefore, the following chapters describe

not only the results but the problems and procedures of making turbulence measurements. First, a general overview of turbulence is presented along with a description of the previous work about pipe flows and LDA. Later chapters describe LDA theory, LDA equipment, turbulence measurement difficulties with an LDA, and the optimization of this LDA system.

Beyond the results presented, this investigation is significant since the ability to make turbulent shear stress measurements is demonstrated by careful use of existing departmental equipment. In the future, this system could be utilized to make turbulence measurements in many other flows of research interest.

2. LITERATURE REVIEW

2.1 Turbulence and the Significance of Reynolds Stresses

The investigation of fluid turbulence has been carried out since the pioneering work of O. Reynolds in 1883 [3]. He was the first to show that the transition from laminar to turbulent flow depended on the ratio of inertial to viscous forces, i.e. the Reynolds number, of the flow. With the advent of modern computers, fluid dynamicists began to investigate turbulence through numerical solutions to a modified form of the Navier-Stokes equations:

$$\rho \left(\frac{\partial U_i}{\partial t} + U_j \frac{\partial U_i}{\partial x_j} \right) = -\frac{\partial P}{\partial x_i} + \mu \frac{\partial^2 U_i}{\partial x_j \partial x_j} \quad (1)$$

This form of the Navier-Stokes equations is in Cartesian tensor notation and is for incompressible flow with constant density and viscosity and no body forces. One method of solution is to eliminate time as an independent variable [5,6]. This is done by introducing the definition of $U_i = \bar{U}_i + u_i$ and $P = \bar{P} + p$. In these definitions, \bar{U}_i and \bar{P} are the time averages of U and P respectively while u_i and p are the instantaneous variations from those averages. When these are introduced into Eq. 1 and the equations are time averaged, the following set of equations results:

$$\bar{U}_j \rho \left(\frac{\partial \bar{U}_i}{\partial x_j} \right) = -\frac{\partial \bar{P}}{\partial x_i} + \mu \frac{\partial^2 \bar{U}_i}{\partial x_j \partial x_j} - \frac{\partial}{\partial x_j} (\rho \overline{u_i u_j}) \quad (2)$$

The numerical solutions to these equations are not exact since they rely on turbulence models to provide information about the last term in Eq. 2 and effect closure of the problem. This term is the Reynolds stress tensor which describes the stresses due to turbulent fluid motion. The need for turbulence models is the reason that the experimental investigation of fluid turbulence is still necessary. The information about the Reynolds stress distribution can either furnish constants for turbulence models or serve as a basis for comparison after the simulation is complete. The Reynolds stress distribution in a flow can also identify regions of high turbulence production. In these regions, the turbulent shear stresses tend to decrease the mean kinetic energy of the flow and transform it into turbulence kinetic energy [4].

Physically, the Reynolds stresses arise from the momentum transfer between regions of faster and slower moving fluid. The momentum transfer occurs due to the random fluctuations in the motion of the fluid. This motion may be in any direction including the streamwise direction. The stress is created when slower moving fluid interacts with faster moving layers by tending to slow them down. Recalling the term: $-\frac{\partial}{\partial x_j}(\rho \overline{u_i u_j})$, when i equals j , the stress is normal and when i is not equal to j , the stress is in shear.

2.2 Flow Description

To assess the accuracy of Reynolds stress measurements with the present LDA system, measurements were taken at the end of a pipe with fully developed flow. This flow has been well documented by other experimentalists so it is ideal for comparison.

Fully developed pipe flow ideally has a linear profile of stress across the radius. To prove this, consider Fig. 1, where a cylindrical control volume is shown. We first assume an incompressible flow with constant wall stress and axial pressure gradient. Eq. 3 shows the conservation of momentum equation.

$$P\pi r^2 - (P + \Delta P)\pi r^2 + \tau 2\pi rL = 0 \quad (3)$$

The sum of the forces is equal to zero since there are no inertial forces (on average) in fully developed flow. In other words, the axial velocity profile does not vary with axial position. The shear stress is solved for as:

$$\tau = \frac{r \Delta P}{2L} \quad (4)$$

The stress varies linearly across the pipe and reaches its maximum, τ_w , at the wall where $r = R$. The friction velocity is defined by dividing τ_w by the density, ρ , such

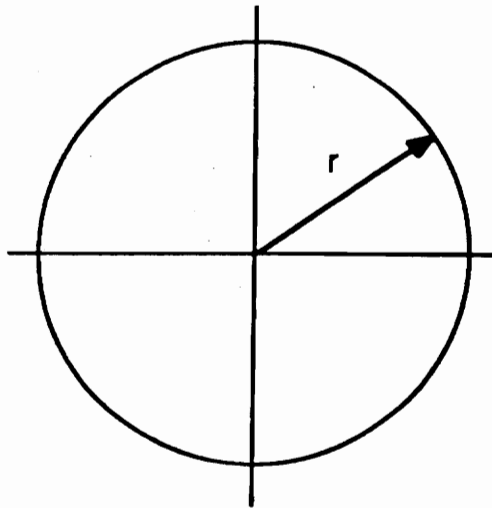
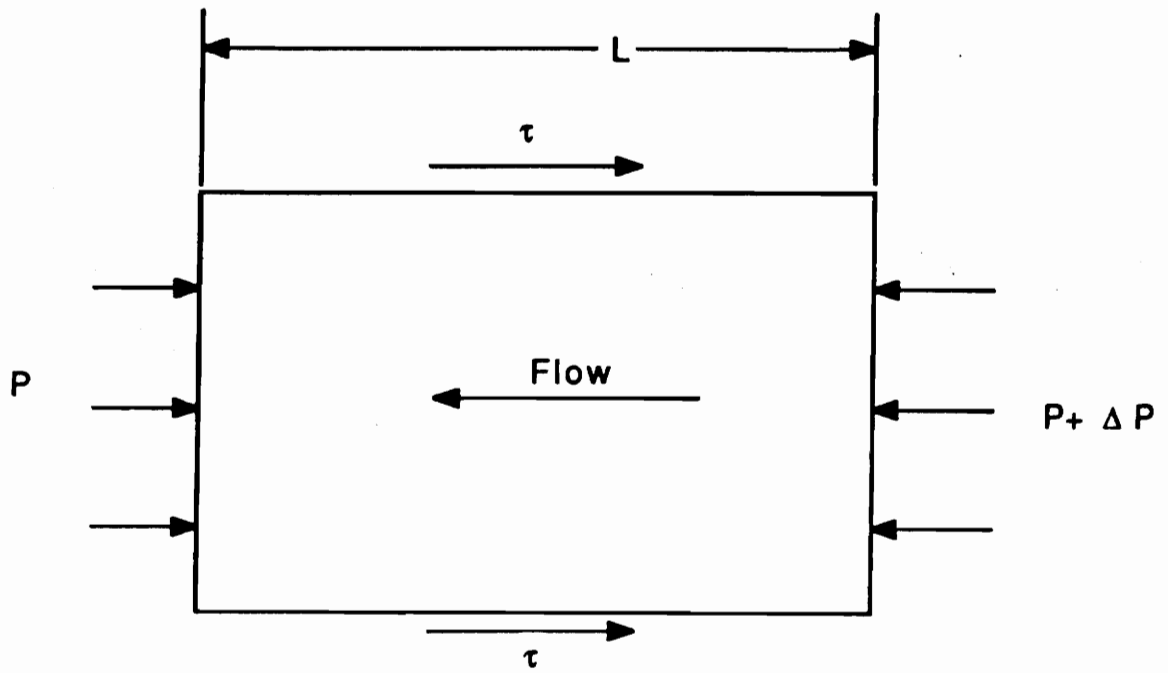


Fig. 1 Cylindrical Control Volume

that:

$$U_\tau = \sqrt{\frac{\tau_w}{\rho}} = \frac{R \Delta P}{2\rho L} \quad (5)$$

The friction velocity is a turbulence scale and is used to nondimensionalize the Reynolds stress for comparison purposes. The shear stress in Eq. 4, is a combination of laminar and turbulent stresses:

$$\tau = \mu \frac{\partial U_x}{\partial r} - \rho \overline{u_r u_x} \quad (6)$$

where u_r and u_x are the fluctuations from the mean in the radial and axial directions [7]. Shown in Fig. 2 is the total shear stress and the turbulent shear stress profile across a channel [8]. In the core of the flow, the turbulent stress is the only contributor to the total shear stress. However, near the wall, viscosity effects dominate and the laminar stress becomes the largest part of the total shear stress.

There are many investigations of pipe flow in the literature. However, none of them uses an LDA to investigate Reynolds stress in the core region of the pipe flow. For example, LDA pipe flow measurements by Berman and Dunning [9] are somewhat related, but they use an FFT analyzer while a more accurate frequency counter was used in

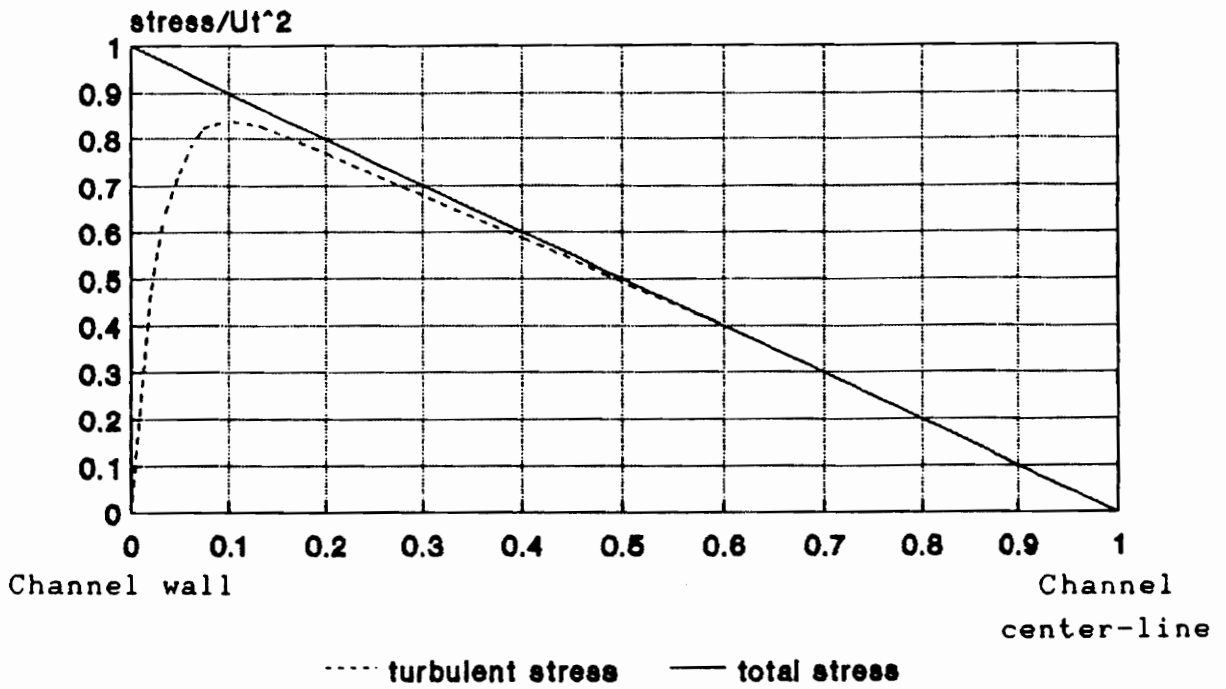


Fig. 2 Shear Stress Across a Channel [8]

this study. In addition, they do not make Reynolds shear stress measurements so a comparison of results is not possible. Kim, Moin and Moser [10] made good quality Reynolds stress measurements in a channel. However, their results are only for the near wall region so they are not candidates for comparison to this data.

The best sources of information for comparison are the investigations by Lawn [2] and Laufer [1]. They used hot-wire anemometers to measure all of the Reynolds stresses of interest here. While these are both excellent references, there are some significant differences between them. The next section will compare and contrast their results.

2.3 Comparison of Laufer's and Lawn's Results

Both Laufer and Lawn collected data using hot-wire anemometers but with somewhat different methods. Laufer used a constant-current system without linearizers while Lawn used a more modern constant-temperature system with linearizers.

Laufer's and Lawn's data are presented in Figs. 3-7. Laufer's curves are for Reynolds numbers based on diameter (ReD) of 50,000 and 500,000. The curve from Lawn's paper is a mean curve that Lawn selected as representative of his data for a range of ReD from 38,000 to 250,000. All of the curves are plotted versus r'/R , where R is the pipe radius,

r is the radial location, and $r' = R-r$. A value of $r'/R = 1$ indicates the pipe center while $r'/R = 0$ is at the wall. Note that the three components of velocity are U , V , and W which are in the axial, radial and tangential directions respectively. u' is defined as the RMS value of u , where $U = \bar{U} + u$, and v' and w' are defined similarly. These RMS values are the square root of the Reynolds normal stresses.

The axial velocity fluctuation, u' , is shown in Fig. 3. It displays the increase in u' from the center line to the vicinity of the wall. These curves are taken from the data outside the "wall" region of the boundary layer in order to coincide with the experimental data from this system. Lawn's data shows a higher turbulence level throughout the core of the flow. In addition, Lawn did not show the same Reynolds number dependence that Laufer did. In fact, Lawn could not separate the effect of Reynolds number from the experimental errors that he experienced.

The radial fluctuations, v' , are shown in Fig. 4. Again, Lawn's curve shows higher turbulent fluctuations except near the center line. Lawn's data also does not show the large drop off near the wall that Laufer shows for $ReD = 50,000$.

The w' distribution from the two authors is shown in Fig. 5. In this case, Lawn's data agrees with Laufer's data through the core of the flow. Near the wall, Lawn's curve

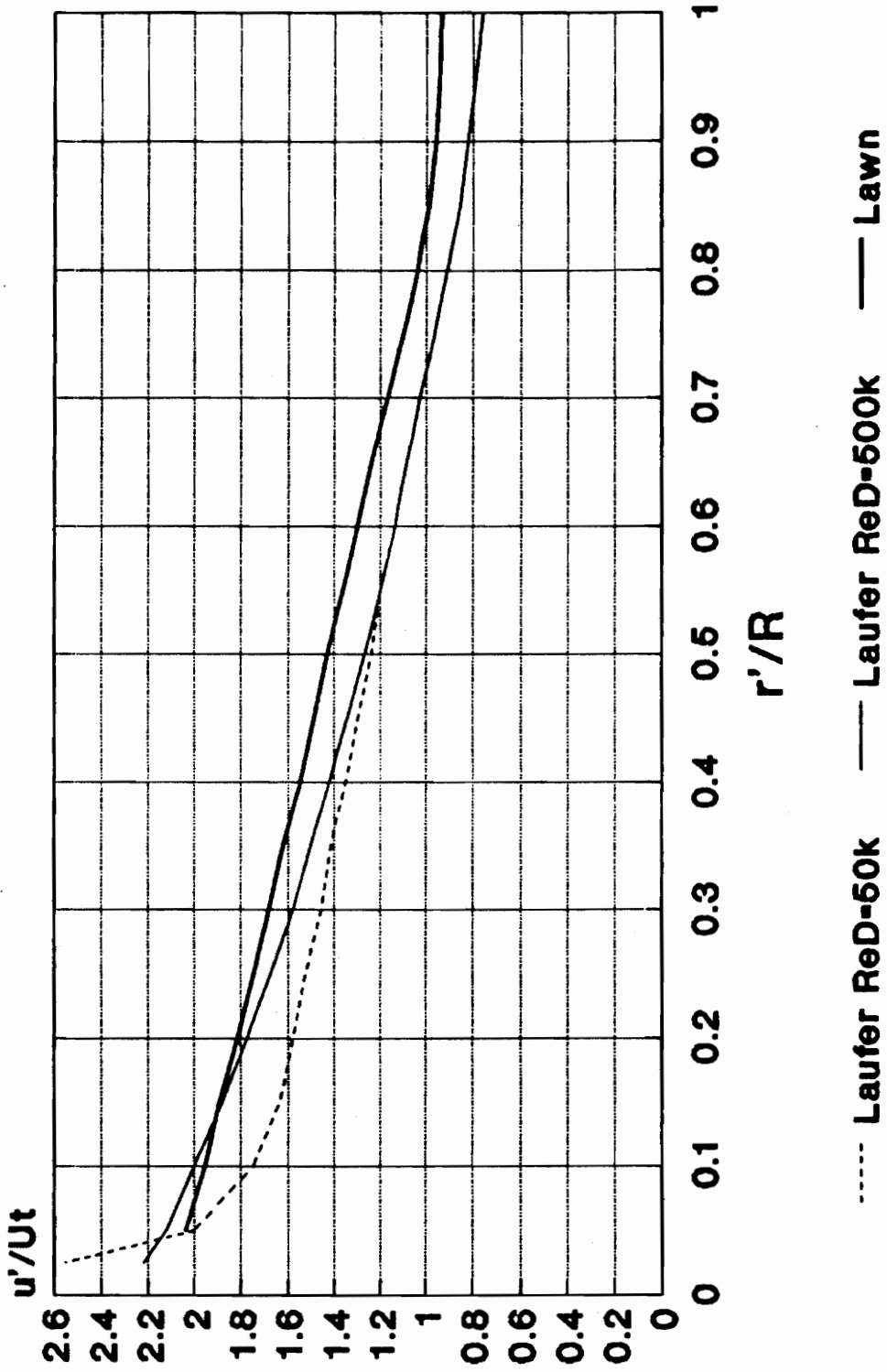


Fig. 3 Comparison of Laufer's and Lawn's Results for u'/Ut vs. r'/R [1], [2]

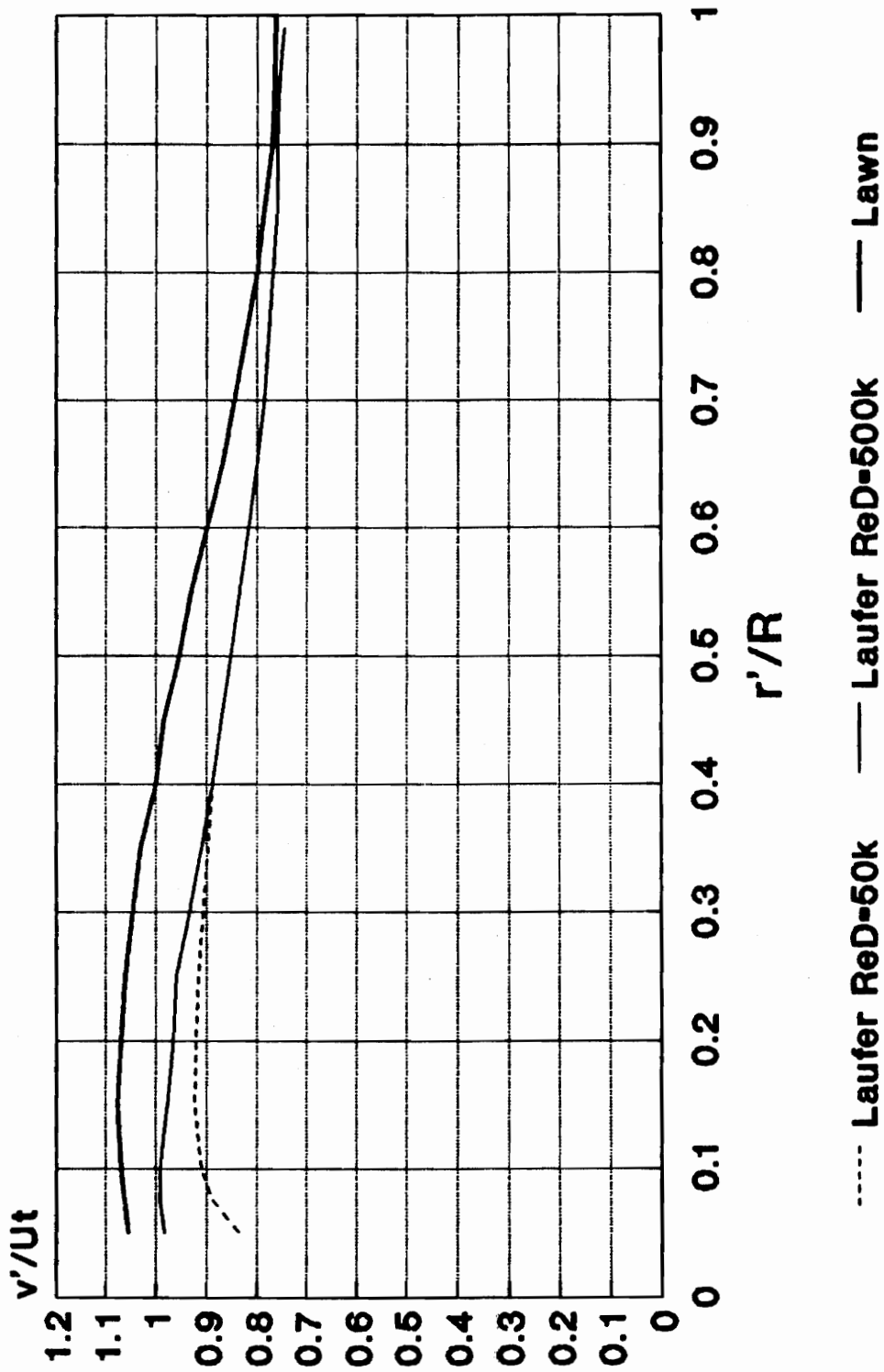


Fig. 4 Comparison of Laufer's and Lawn's Results for v'/Ut vs. r'/R [1], [2]

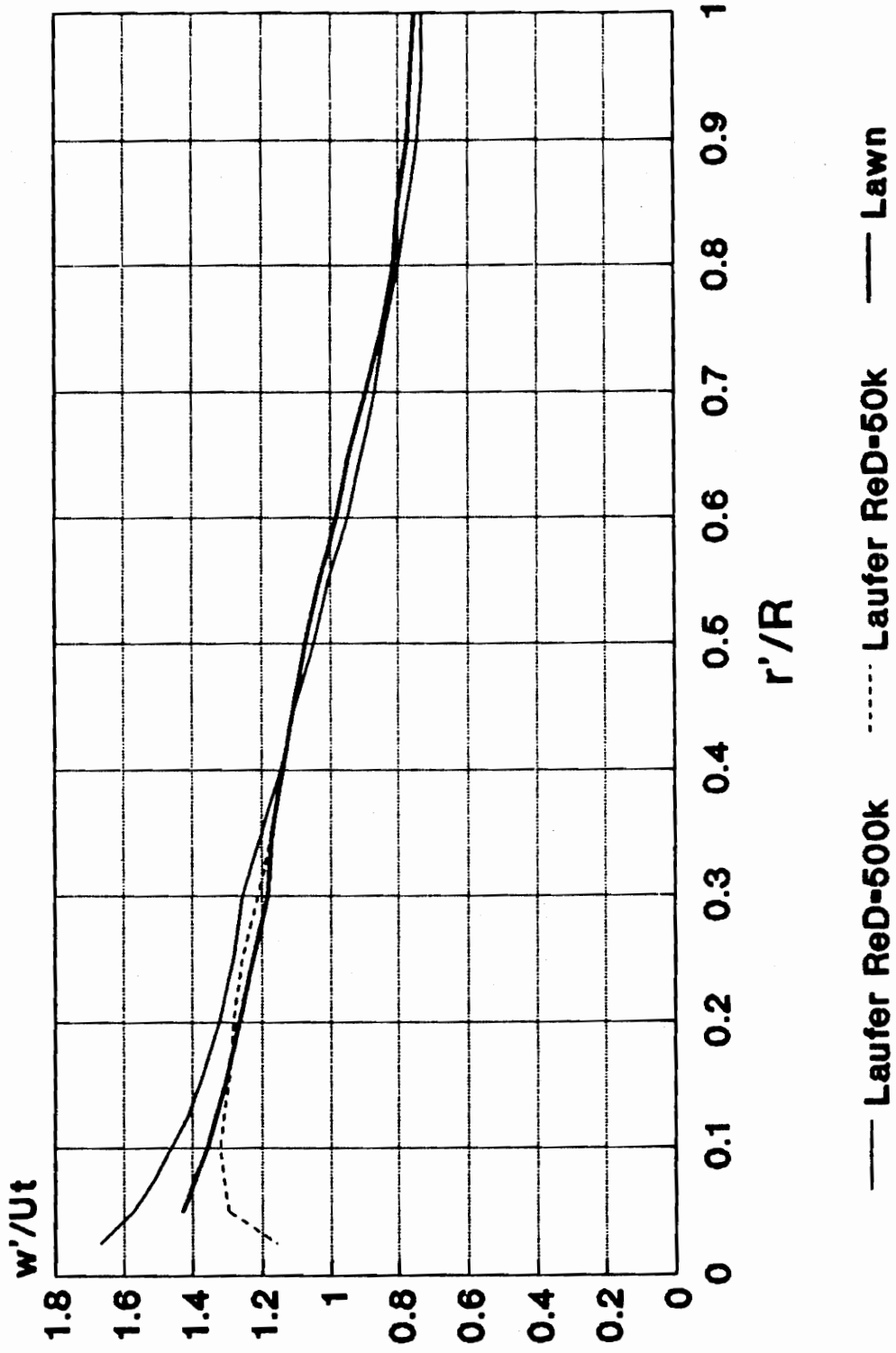


Fig. 5 Comparison of Laufer's and Lawn's Results for w'/Ut vs. r'/R [1], [2]

is in between Laufer's two curves. Lawn only showed the results for one Reynolds number (90,000) so the Reynolds number dependence cannot be compared.

The shear stress in the axial-radial plane is shown in Fig. 6. It is important to note that Laufer's curve was calculated based upon the velocity profile and the friction velocity. All of his experimental points fell in a $\pm 5\%$ band around this theoretical curve. Similar to previous figures, Lawn's curve was the mean curve from his data. All of his data fell in a $\pm 4\%$ band around this curve. Both Laufer's and Lawn's results show the expected linear variation in the core of the flow. However, Lawn's data had an approximately constant offset from the linear distribution of about $.03R$ toward the pipe wall. This made his shear stress negative at the center line affected the correlation coefficient. Lawn indicated that this error was due to asymmetries in his velocity distribution.

The correlation coefficients presented in Fig. 7 show the greatest discrepancy between the two investigations. As shown by Lawn, this quantity should be independent of Reynolds number. However, Laufer showed an upper branch of his curve for $ReD = 50,000$ and attributed it to experimental error. Lawn's data, while correct in shape, was about $.05$ lower in magnitude than Laufer's $ReD = 500,000$ curve since Lawn's Reynolds stresses were offset. However, an

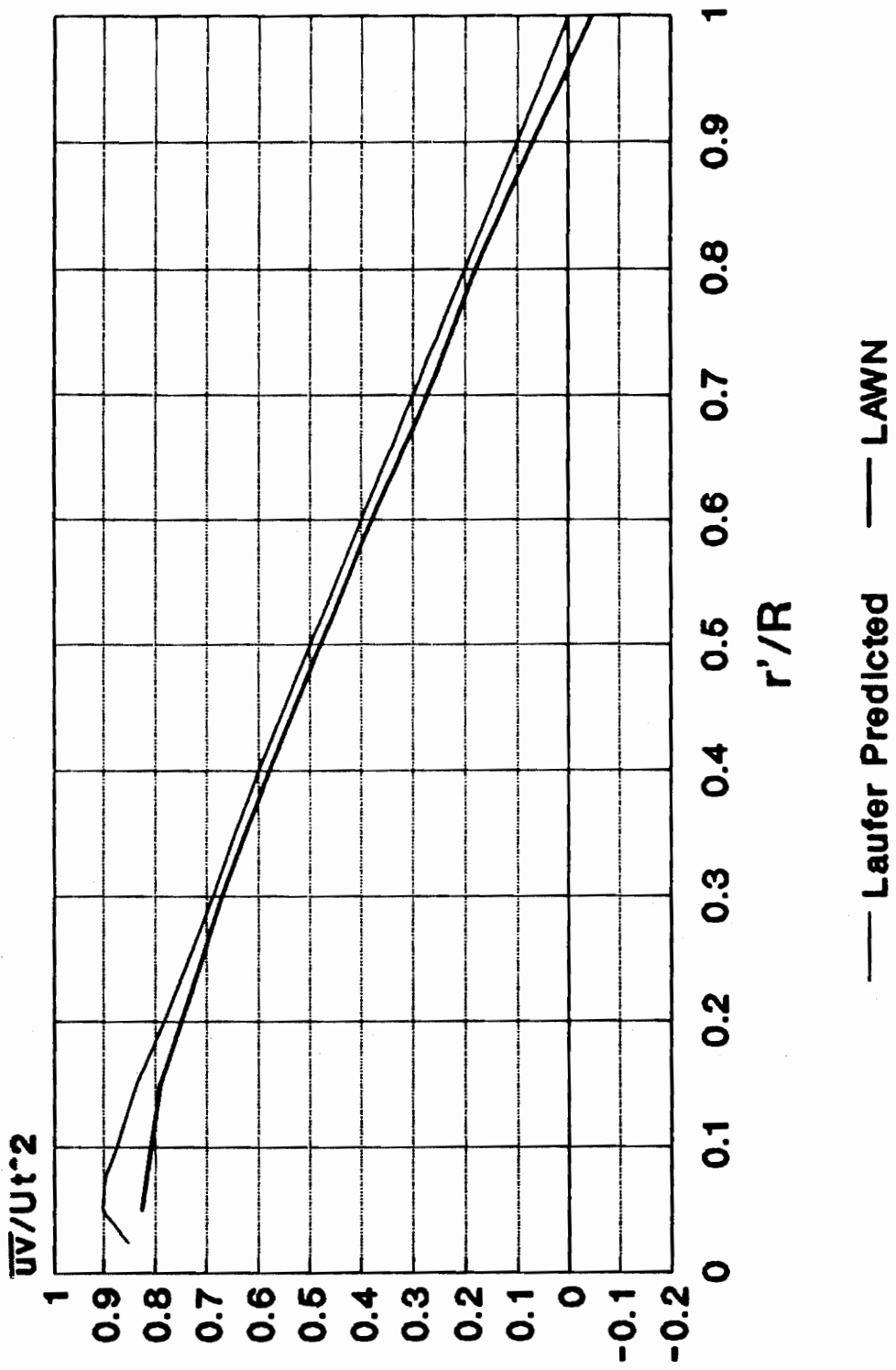


Fig. 6 Comparison of Laufer's and Lawn's Results for $\bar{u}v/Ut^2$ vs. r'/R [1], [2]

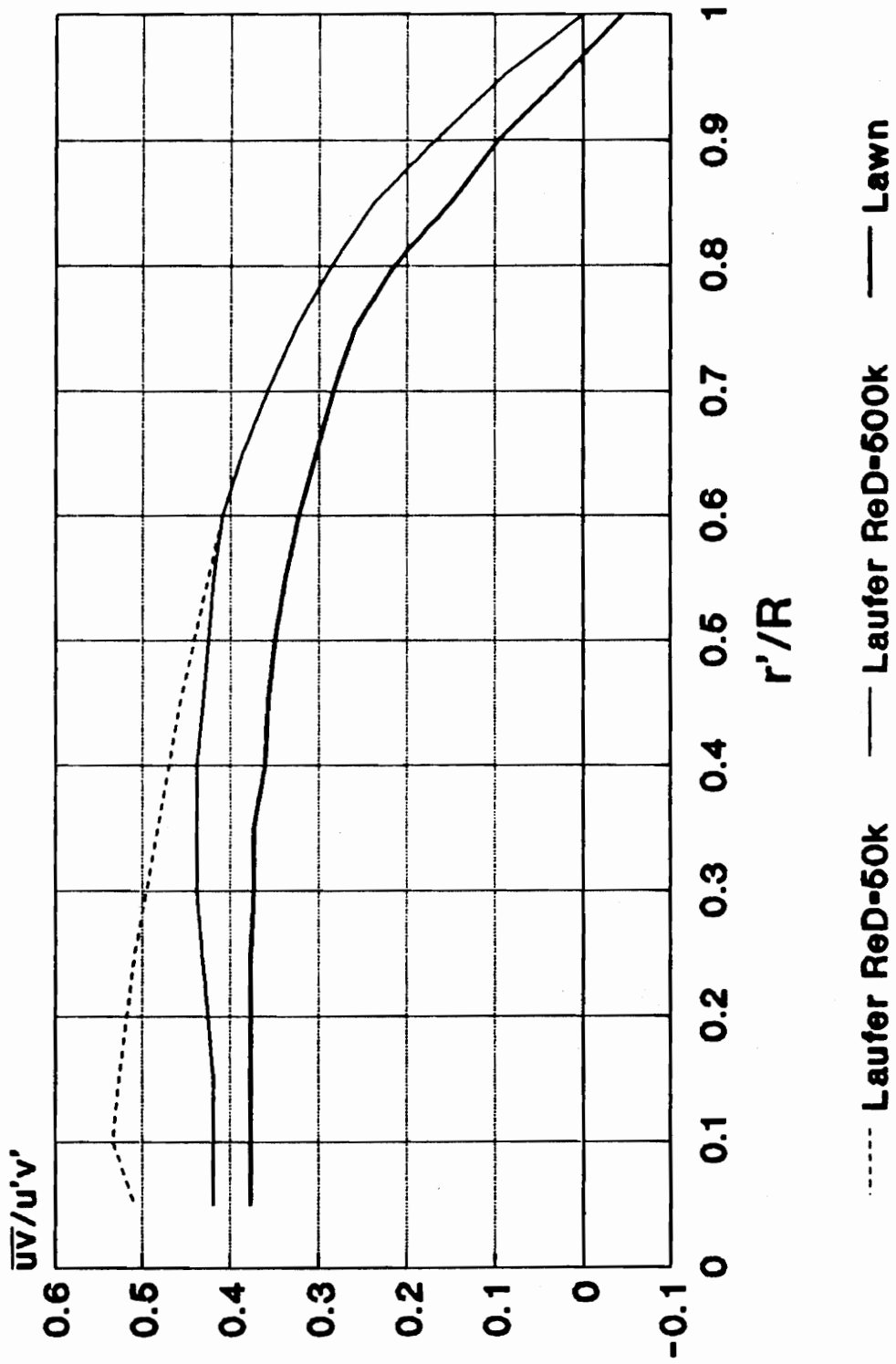


Fig. 7 Comparison of Laufer's and Lawn's Results for $\overline{uv}/u'v'$ vs. r'/R [1], [2]

asymmetric velocity profile should still provide an accurate correlation coefficient that should be the same as Laufer's $ReD = 500,000$ curve. Therefore, the error in Lawn's shear stress measurements may actually be due to measurement error and not asymmetry as he claimed.

The differences in these investigations demonstrate that there is a level of variation in turbulence measurements even in a well studied flow. This fact should be remembered when interpreting the measurements made with this or any other system.

2.4 Review Of Turbulence Measurement and Laser Anemometry

Many sources of information are available concerning turbulence measurement and LDA procedure. The following is a brief list of the related technical papers and books along with the work of previous graduate students. These authors will also be referenced in the appropriate chapters as subjects relating their work are discussed.

The two main methods of measuring turbulent velocity fluctuations are the hot-wire anemometer and the laser Doppler anemometer. The techniques for turbulence measurement with a hot wire were developed starting in the 1910's with the work of King [11], Dryden [12] and others. This was the first measurement device that was small enough and sensitive enough to make quantitative turbulence

measurements. Although the hot-wire technology is now well established, the technique can lead to errors since it interferes with the flow it is trying to measure.

A newer form of measurement first developed by Yeh and Cummins [13] in 1964 is the laser Doppler anemometer (LDA). Since then, its usefulness has developed from measuring simple mean velocities to measuring statistical turbulence quantities and Reynolds stresses. Along the way experimentalists have dealt with the problems inherent in LDA measurements.

Self and Whitelaw [14] presented an excellent description of LDA theory and the development of LDA techniques in the 1970's. They included descriptions of seeding, signal processing and LDA applications. One of the main goals during this period was to measure more than one component of velocity. Their paper showed that the first attempts used optical configurations that separated the velocity components according to polarization. Later, systems were developed that measured two or three components using a multiple color system. The information for each component was split by color separators and processed separately.

In concert with these developments, the ability to measure Reynolds stress also developed. One of the earliest attempts at Reynolds stress measurement was that of Johnson

and Rose [15] in 1973. They used a single component system that was rotated to three different orientations. Through geometric relations, they were able to calculate the Reynolds shear stress. However, since multiple component systems then became available, the standard procedure for obtaining Reynolds stresses became coincidence measurement. This procedure used the measurements from each velocity component and grouped them in sets according to when the measurement occurred. If the measurements from each channel occurred at the same time, or within a coincidence time window, they were grouped together. In 1979, Yanta [16] described a system for 3-D coincident measurements around a body at an angle of attack. Although he did not present Reynolds stress data, he demonstrated the ability to make coincident measurements. Also in 1979, Dimotakis, Lang, and Collins [17] made boundary layer measurements in several flow regimes. They were able to improve the previous Reynolds stress measurements that showed a maximum too far from the wall. They carefully documented their use of seeding, signal processing, and validation techniques. Reynolds stress measurement in boundary layers was also described by Orloff and Olson in 1980 [18]. They included excellent detail on coincidence windows and spatial correlation. Absil [19] made turbulence measurements behind a circular cylinder in 1980. He presented Reynolds stress

information and described specific techniques he used to make good quality measurements.

More modern investigations have developed the techniques even further. Johnson dealt with the problems of measurement in high speed flows in 1989 [20]. He included an excellent general description of LDA and biasing along with a discussion of the proper use of signal processing equipment. In 1990, Dancey [21] made 3-D Reynolds stress and turbulent kinetic energy measurements in an axial flow compressor. His paper included discussion about data rate and coincidence window effects.

Statistical bias is a significant factor in turbulence measurement and is covered by many authors. Statistical bias occurs when a turbulence quantity, such as the average velocity, is altered or biased by some aspect of the measurement system. Buchave and George [22] authored one of the first comprehensive descriptions of turbulence measurement with an LDA in 1979. They dealt extensively with bias and the use of different processors. "The Report of the Special Panel on Statistical Particle Bias Problems in Laser Anemometry" [23] is a concise description of all the types of bias and the proper means of correction. Direct measurements of bias in turbulent flows were made by Stevenson and Thompson [24]. They described the many types of bias and gave a history of the different correction

schemes that have been suggested. George [25] provided descriptions of statistical bias, bias correction, and the accuracy of statistics. Other papers on bias and bias correction include those by Brown [26], Carey [27], and Lacharme and Elena [28].

The size and reflectivity of the seed particles are significant concerns in LDA. The particles must be large enough to reflect light but not so large that they don't follow the flow dynamics. Discussions of seeding theory and practice are covered in papers by Samimy and Abu-Hijleh [29] and Cline and Lo [30]. Samimy and Abu-Hijleh discussed the use of polydisperse seed in a high speed flow. In addition, they discussed the effect of amplification on signal quality. Cline and Lo made LDA measurements in a transonic boundary layer. They included descriptions of statistical uncertainty and particle lag.

2.5 Previous Studies by Graduate Students

The related work of previous graduate students at VPI & SU includes the dissertations of Tree [31] and Nath [32] and the theses of Menna [33] and Shaffer [7]. Tree, Nath, and Menna all used the same LDA system that was used in this study. Tree used the system to make near wall measurements in a wing-body junction vortex. He wrote excellent descriptions of LDA theory and operations in his

dissertation and in the users manuals [34-37]. Future users should consider these as critical references. Menna used this system for differentiating between two sizes of seed in a flow. He includes a good description of LDA theory on a very basic and physical level. Shaffer used a hot-wire anemometer to make turbulence measurements in the same pipe that was used in this investigation. Although he used this pipe only for calibration before he moved on to other flows, his Reynolds stress measurements in this flow are an excellent reference.

3. BASIC LDA THEORY

This section introduces the basic concepts of LDA. Basic LDA theory is presented in many books including Hinze [4] and Durst [6]. Other excellent general descriptions are in technical papers by Self [14], Johnson [20], Yanta [16].

The Laser Doppler Anemometer (LDA) approximates the air velocity based on the Doppler shift of light reflected from a seed particle in the air stream. As the reflective seed particle passes through a laser beam, it absorbs and then emits light which is received by a photomultiplier tube (PMT). The light received at the PMT is Doppler shifted due to the particle moving in relation to the light source and also due to the particle moving relative to the receiving device. The frequency of this reflected light is linearly related to the velocity of this particle. Thus, no calibration curves are required to calculate the velocity as in hot-wire anemometry.

The most convenient way to measure the Doppler shift is with a dual-beam system. In this configuration shown in Fig. 8, two beams intersect and form an ellipsoidal probe volume. When a particle passes through the probe volume it reflects light from each beam which is then received by the PMT. The PMT can only respond to the frequency difference between the two signals. This "difference" signal is indicative of the component of velocity which is in the

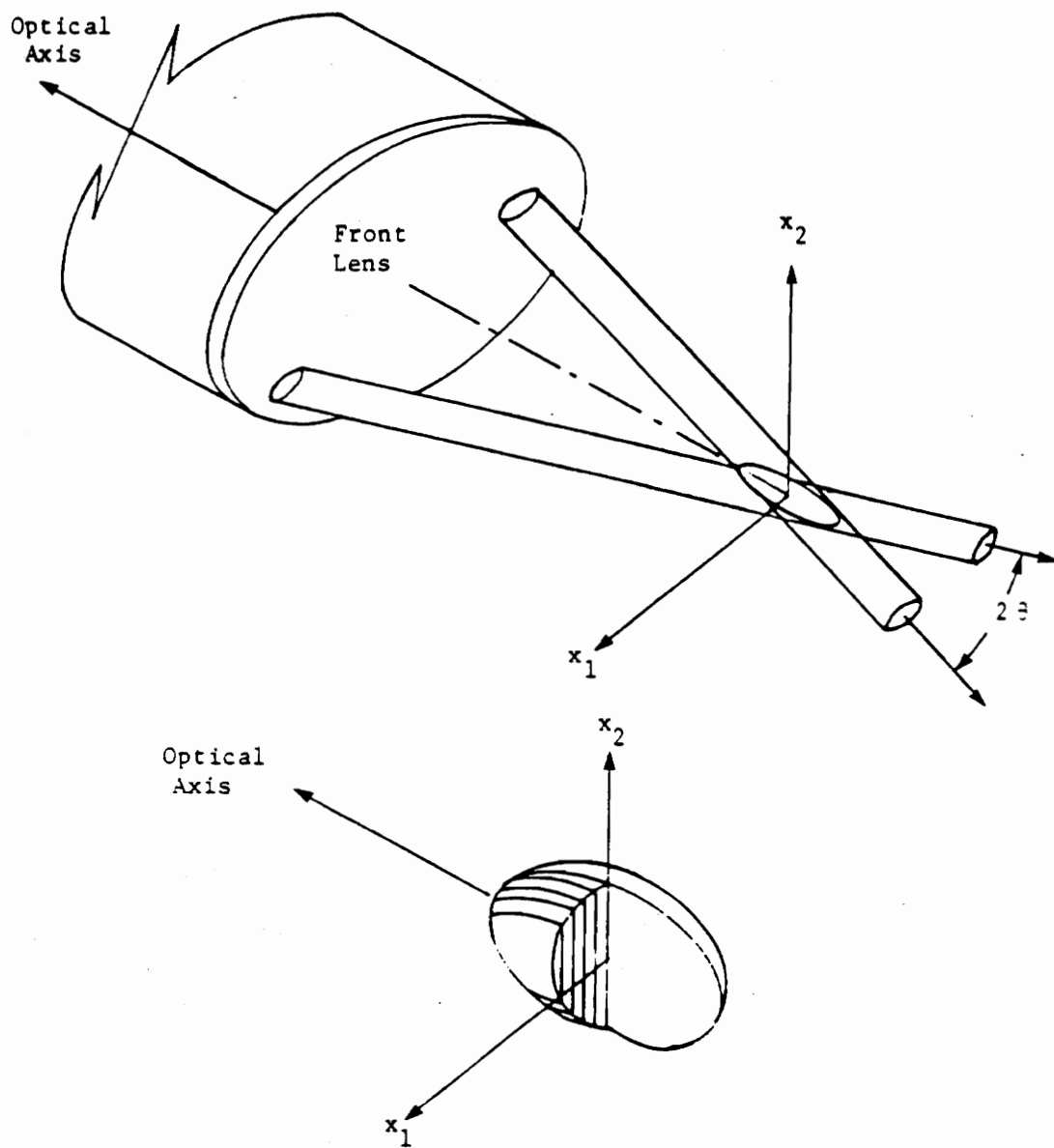


Fig. 8 Beam Intersection and Formation of Probe Volume [31]

plane of the beams and perpendicular to the optical axis as in Fig. 9. The appealing feature of the dual beam system is that the difference in the frequencies is independent of receiving direction. This allows the user to place the PMT at any location without needing to know its exact orientation to the probe volume.

A convenient physical model is to imagine that the two beams create a set of fringes as they intersect as shown in Fig 10. As a particle passes through the probe volume perpendicular to the fringes, it will encounter light and dark regions. The particle will absorb and then emit bursts of light every time it encounters a bright region. The frequency of the bursts, f_d , is equal to the particle speed, V_p , divided by the fringe spacing, D_f . If the particle passes through the probe volume at an angle ϕ , it will emit pulses at a frequency equal to $V_p \cos \phi / D_f$. Thus, the system is sensitive only to the component of velocity perpendicular to the fringes. If the particle passes through the probe volume parallel to the fringes the frequency of the pulses of light would be zero. The fringe spacing is calculated based on the wavelength, λ , and the half angle between the beams, θ ,:

$$D_f = \frac{\lambda}{2 \sin \theta} \quad (7)$$

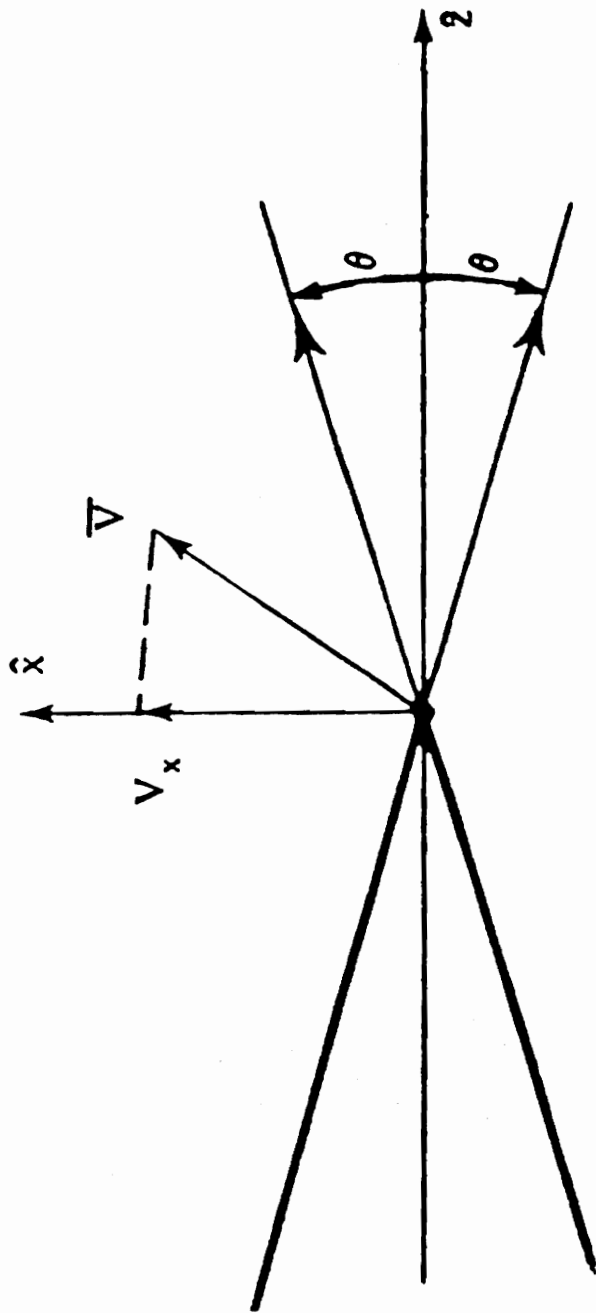
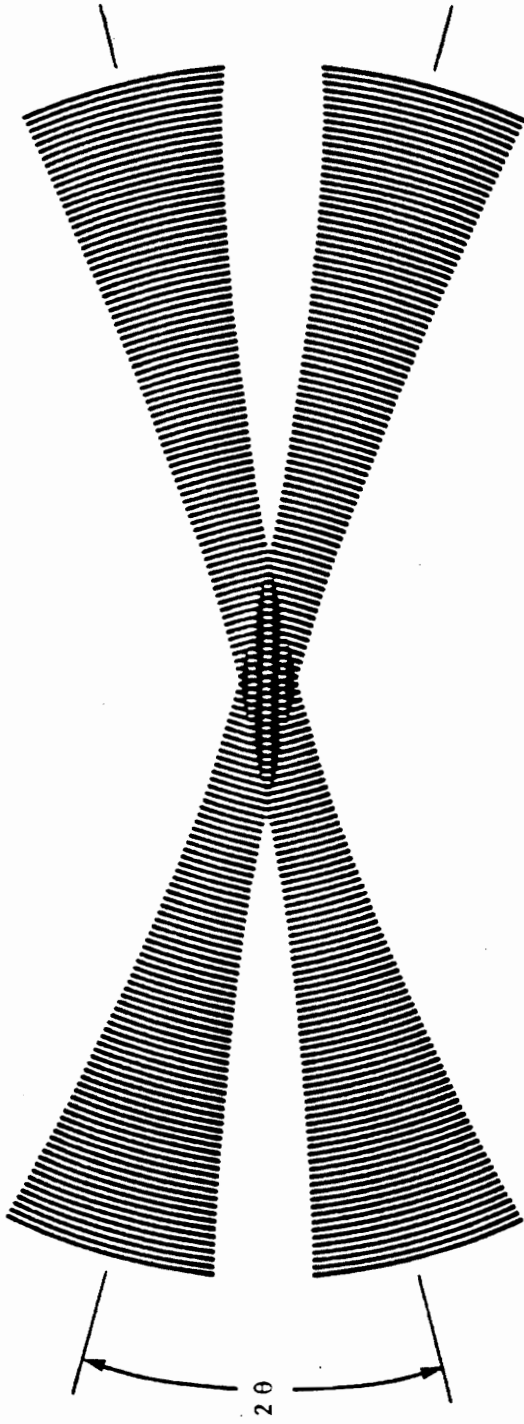


Fig. 9 Velocity Sensitivity of Dual Beam LDA [41]



Enlarged View of the Intersection Region

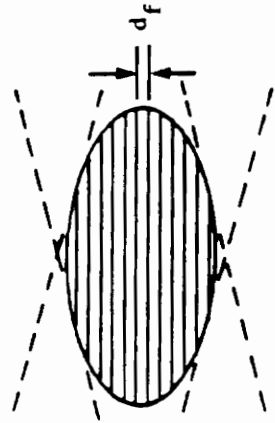


Fig. 10 Fringe Formation [31]

The signal received at the PMT looks like that in Fig. 11 where intensity is plotted versus time. The Doppler frequency is superimposed upon a low frequency "pedestal". The low frequency portion is due to the Gaussian distribution of light intensity across a laser beam as shown in Fig 12. The greater the intensity, the stronger the reflected light from the particle will be. Figure 13 shows Doppler bursts over a period of time plotted in the frequency domain. The peak near the origin is the pedestal while the other peak is the Doppler frequencies due to the various particles. For signal analysis, the pedestal is filtered out with a high-pass filter leaving bursts like Fig 14. The frequency of these bursts is determined to find the particle velocity.

The intensity of the reflected light is strongest in the "forward" direction as shown in a polar intensity plot in Fig. 15. Fig. 16a shows a forward scatter system while Fig. 16b shows a back scatter system. Forward scatter systems are desirable since they require only low power lasers on the order of 10-100 mW. The drawback is that the receiving optics and the transmitting optics must move together to stay in alignment. This makes doing large scale wind tunnel tests very difficult. Back scatter systems are desirable since the transmitting and receiving optics are part of one concentric unit and move together. However,

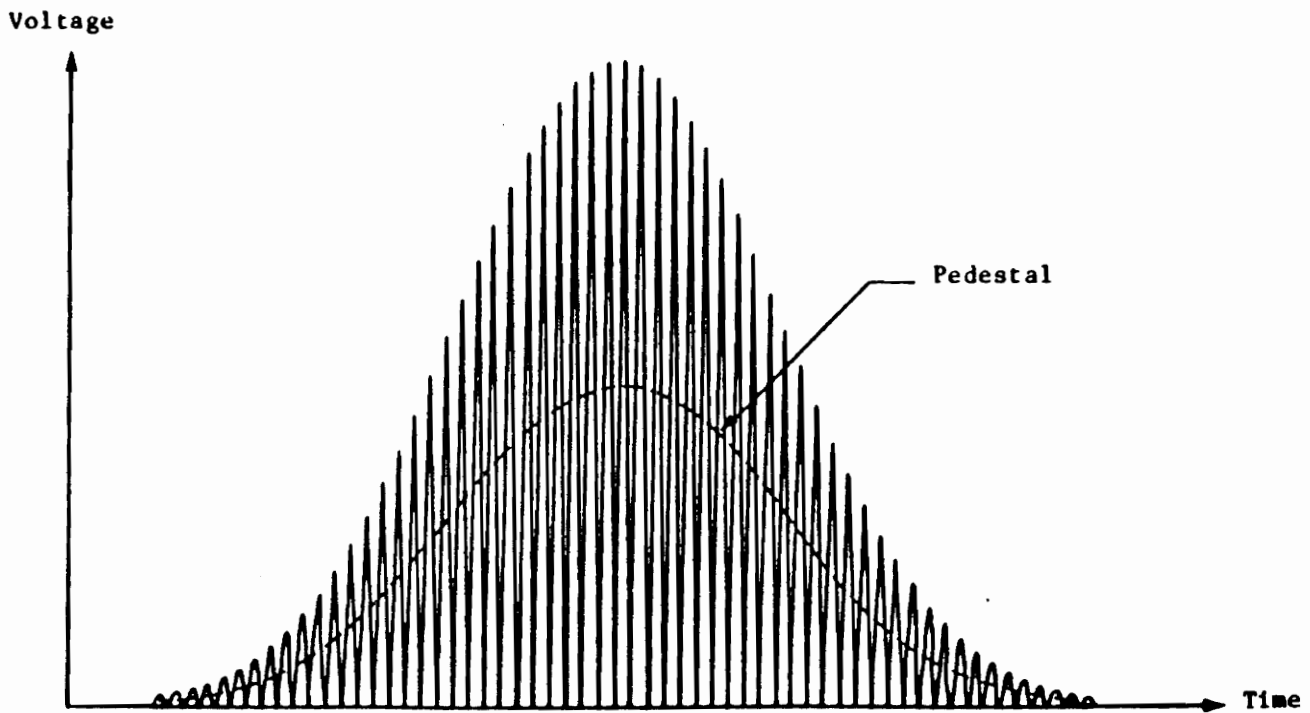


Fig. 11 Doppler Burst [31]

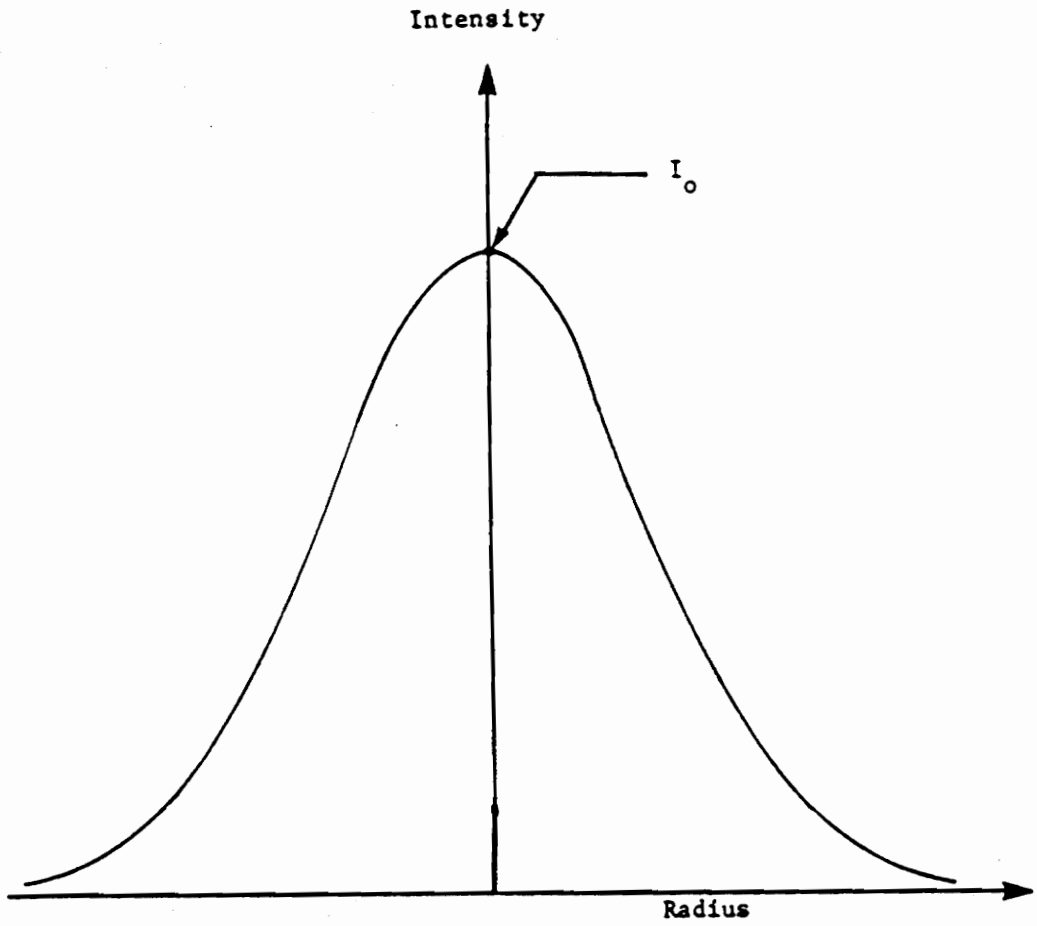


Fig. 12 Gaussian Distribution Of Intensity
Across a Laser Beam [31]

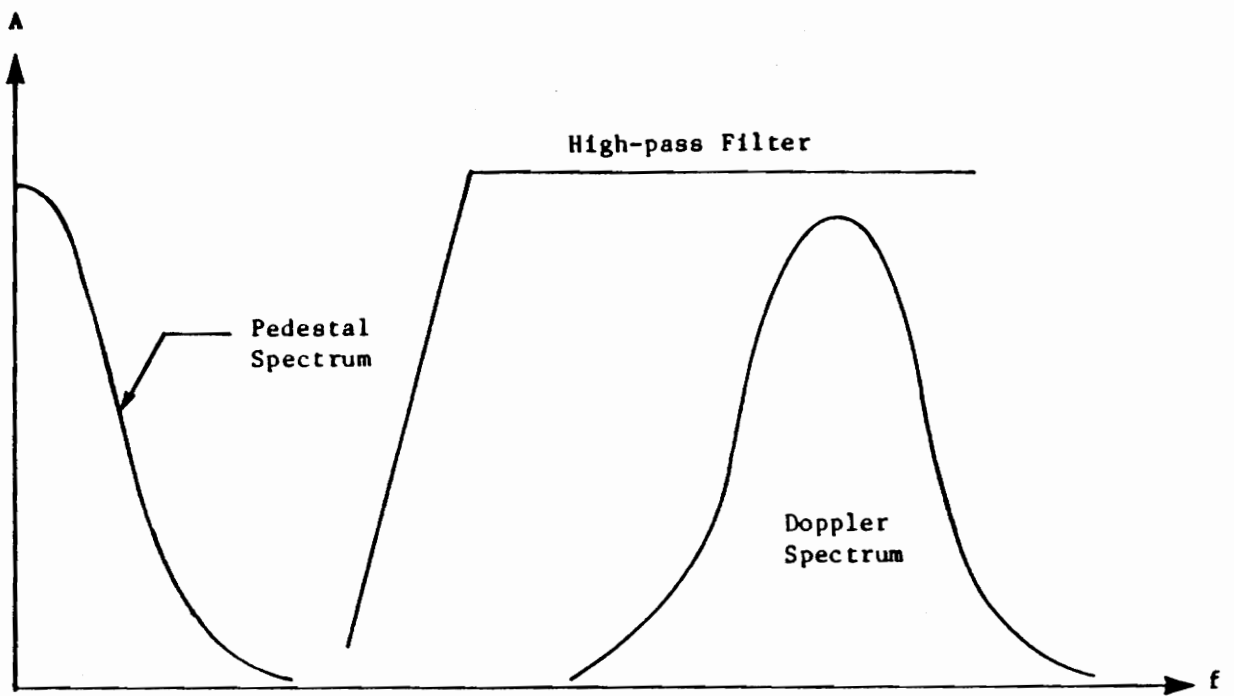


Fig. 13 Doppler Spectrum [31]

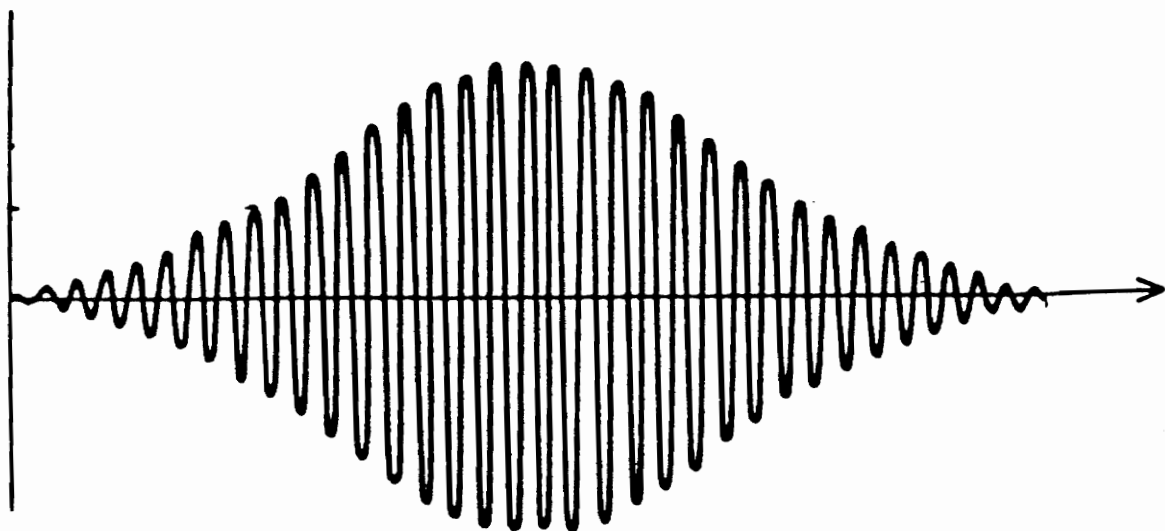


Fig. 14 Filtered Doppler Burst [6]

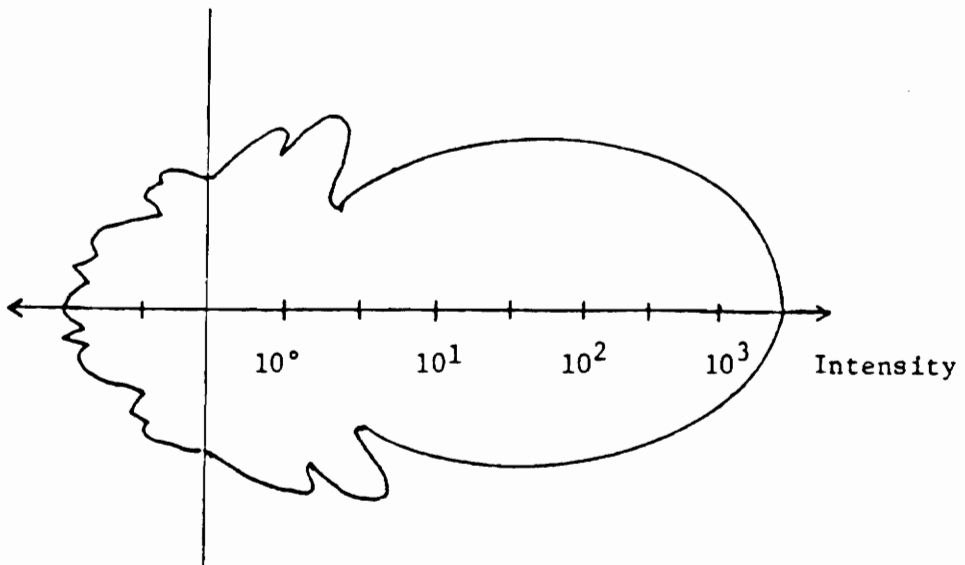
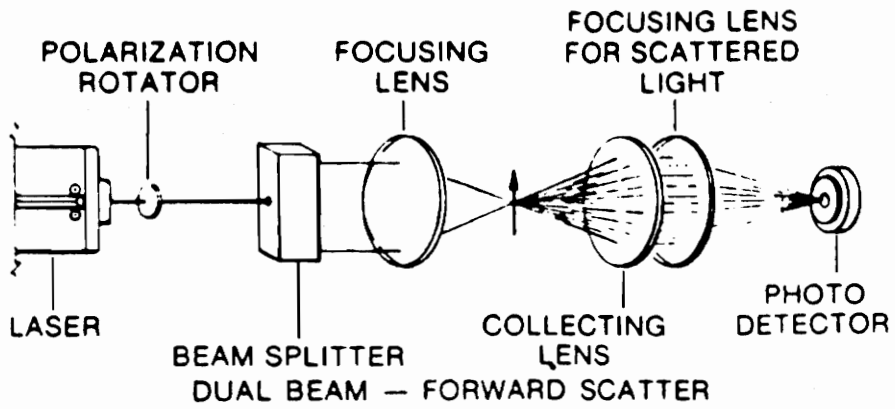
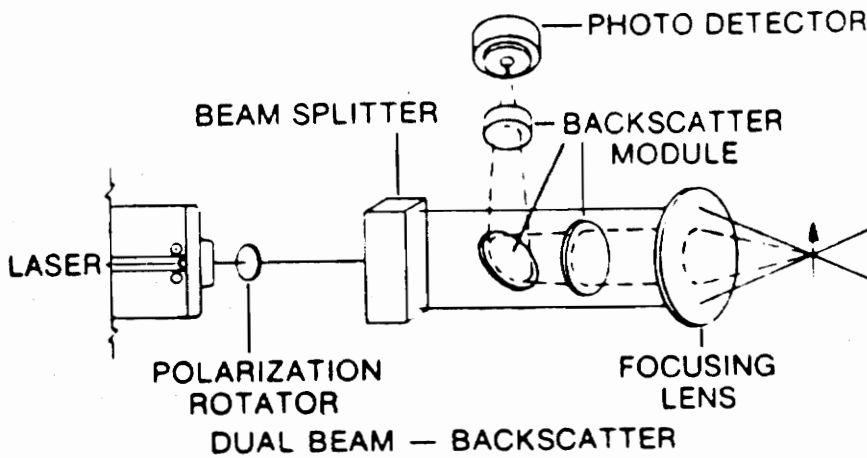


Fig. 15 Polar Intensity Plot of Scattered Light [33]



(a)



(b)

Fig. 16 Forward Scatter And Back Scatter LDA Systems

since the reflected light is weaker in backscatter, laser power must be on the order of 2-10 W.

If more than one component of velocity is desired, a multiple dual-beam system is used. Each component is measured by the shift of a different color laser light so that separation of the velocity component information is possible. The information for each component is sent to a different PMT and processed by separate frequency counter systems. The present LDA system uses three beams, a combination blue-green (cyan), a blue, and a green. As shown in Fig. 17, the three beams intersect to form a perpendicular set of fringes. The blue beam interferes only with the blue component of the blue green beam to form a set of blue fringes. The green beam interferes only with the green component of the blue-green beam to form the green set of fringes. The Doppler frequency from each set of fringes indicates the two perpendicular components of velocity in the x_1 and x_2 directions. These directions are in the plane perpendicular to the optical axis of the system.

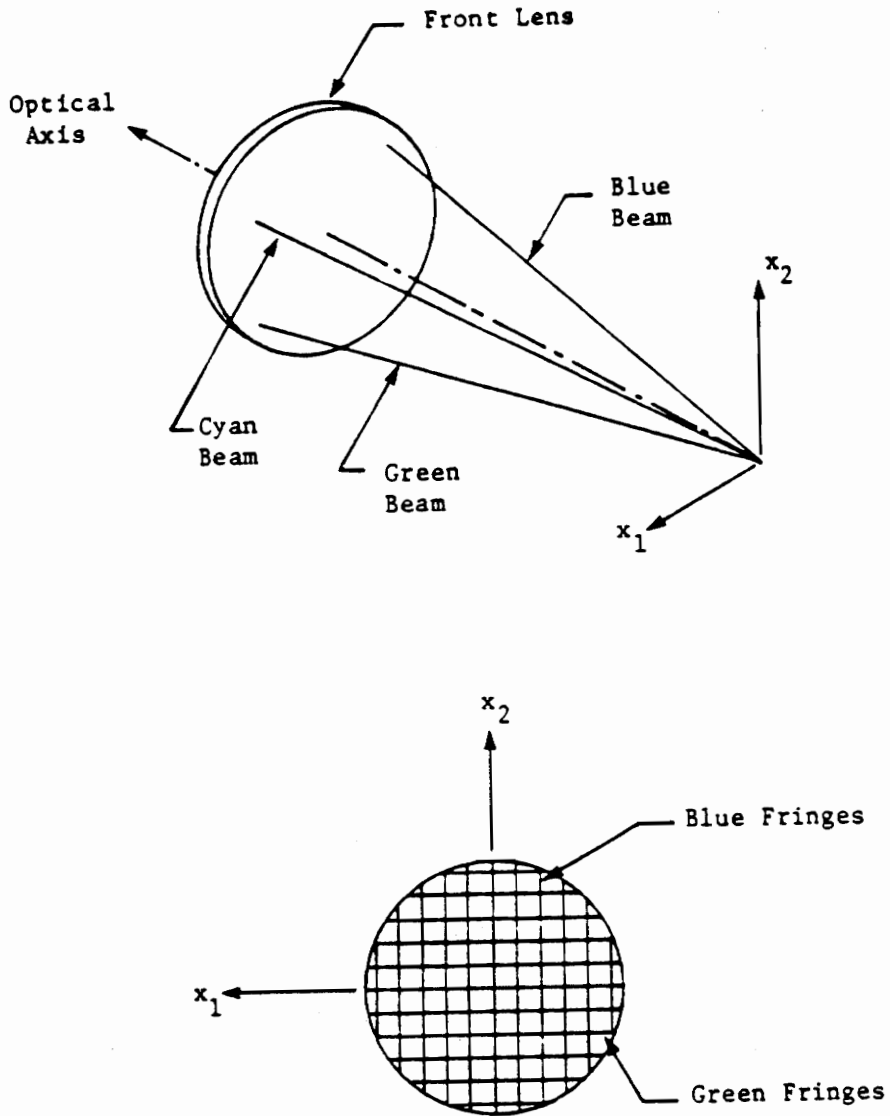


Fig. 17 Three Beam LDA System and Fringe Formation [31]

4. APPARATUS AND METHODS

The following description of the experimental set up and methods will introduce the LDA equipment and show how it was adapted it to measure Reynolds stresses in the fully developed pipe flow.

4.1 Pipe Description

As shown in Fig. 18, a centrifugal blower is attached to a copper alloy pipe with an inside diameter of 81 mm. Before the pipe inlet, the flow passes through honeycomb and screen to reduce the swirling effects of the blower. The pipe is approximately 200 diameters long which is longer than the 50 to 100 diameters needed to produce fully developed, turbulent flow at the pipe end measurement plane [8].

The butterfly valve varies the exit dynamic pressure from about 10 to 50 mm of H₂O (0.5 to 2.0 in of H₂O). These tests were run near the low value of about 10 mm which results in a center line exit velocity of about 14 m/s. Using a 1/7 power law, the average velocity is $.82 * 14 = 11.48$ m/s [7]. Using this value, the Reynolds number for the tests was about 60,000 which is significantly larger than the critical value of about 2300 for turbulent flow [8]. A full description of the experimental conditions is presented in Section 7.

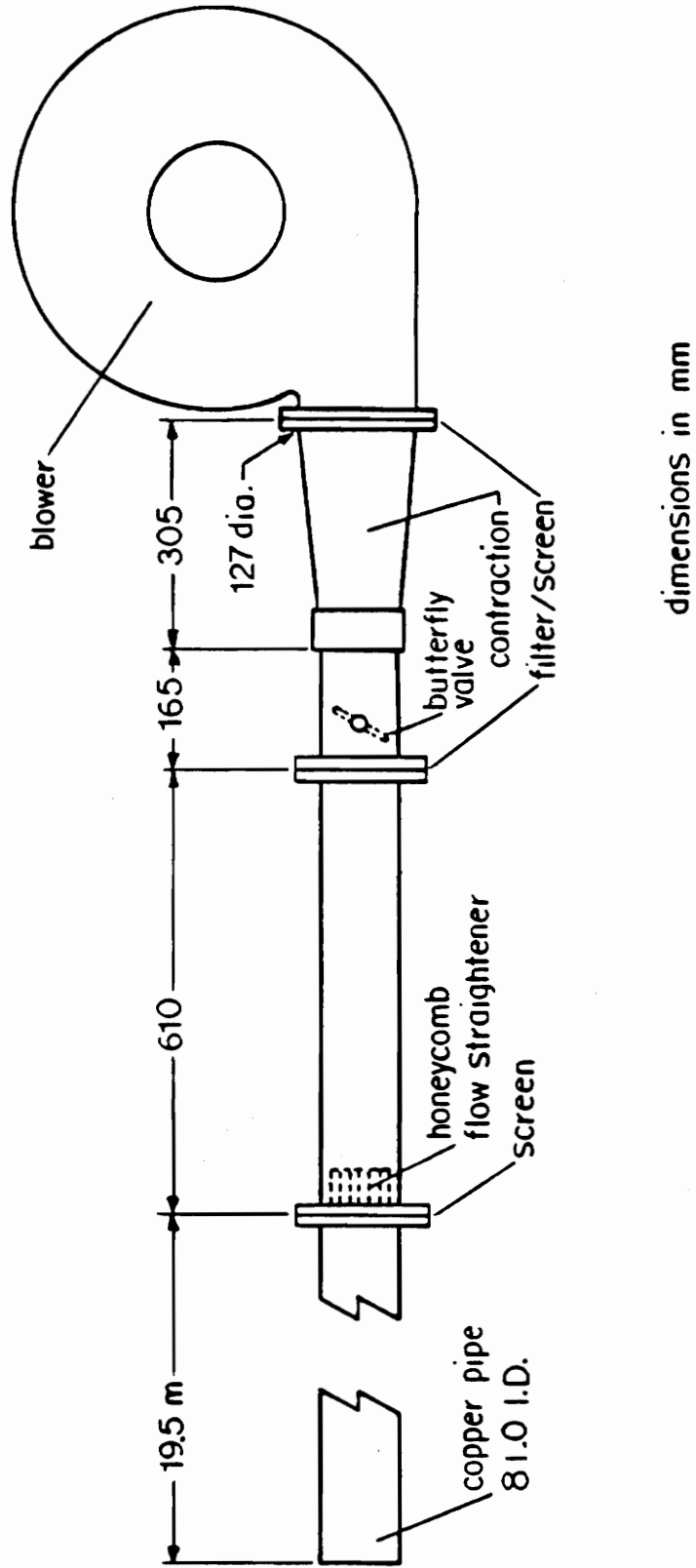


Fig. 18 Pipe and Blower [7]

The pressure drop along the pipe is measured using a static pressure tap 5.9 m upstream of the pipe exit. This pressure drop is used to calculate the friction velocity from Equation 5. The pressure drop is measured using a micromanometer that is readable to .0001 in of H₂O. The room static pressure is measured with a mercury barometer that is readable to .1 mm of Hg. The room static temperature is measured with a mercury thermometer that has single increments in degrees Fahrenheit.

4.2 LDV Equipment Description.

The LDA system is a combination of many pieces of equipment performing specialized tasks. To optimize turbulence measurements the user should have knowledge of each component and its theory of operation. To guide the user, the basic operation of each component will be discussed. Refer to Tree [31], and the manufacturers' manuals [38-41] for further detail.

4.2.1 Laser

A Spectra-Physics model 164-06 argon ion laser is used as the source of coherent light. Its nominal output is about 2.5 W at the laser head. The two dominant laser lines are 488 nm (blue) and 514.5 nm (green). The laser is water cooled and is powered by a 35 A, 240 V power supply.

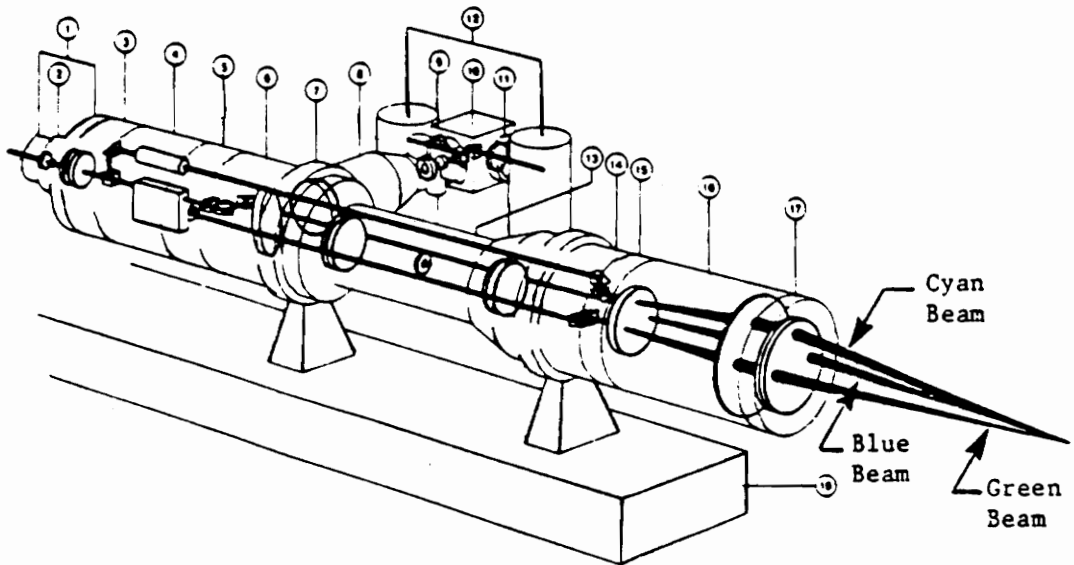
The laser is adjusted for peak power by moving the mirror at the end of the plasma tube. The optimal location of the mirror varies with temperature. The laser should only be adjusted when it has warmed up to a steady state temperature. This usually takes about 30 minutes.

4.2.2 Optical System

The optical system is a 55X modular system manufactured by DANTEK(DISA). Its purpose is to direct laser beams to cross at the probe volume and then gather the Doppler frequency information with photo detectors.

The transmitting path is shown in Fig. 19. From the laser head, the beam passes through a polarization rotator which correctly polarizes the beam to match the optics. This rotator is a $1/2$ wavelength plate which was added to the system. It replaces the set of two $1/4$ wavelength plates described in the DANTEK manual. The $1/2$ wavelength plate is mounted on a beam waist adjuster that places the beam waist at the beam intersection.

Next, the beam is split into two equal power beams and directed toward the Bragg cell. The Bragg cell uses acoustic waves to shift the frequency of one of the beams by 40 Mhz. The other beam is passed through unaltered. The next module splits the shifted beam into blue and green components using coated prisms. Finally, all three beams pass



Code No.	Description	Pos. No.
55X08	PM Section	12
55X12	Beam Expander	16
55X20	Cover and Retarder	1
55X22	Beam Waist Adjuster	2
55X23	Support	7
55X25	Beamsplitter Neutral	3
55X27	Beamsplitter Color	5
55X29	Bragg Cell Section	4
55X30	Backscatter Section	6
55X31	Pinhole Section	13
55X32	Beam Translator	14
55X33	Lens Mounting Ring	15
55X34	PM Optics	8
55X35	Color Separator	10
55X36	Interference Filter 488 nm	11
55X37	Interference Filter 514.5 nm	9
55X41	Mounting Bench	18
55X43	Tripod	-
55X58	Front Lens Achromatic (600 mm)	17

Fig. 19 Transmitting Path of LDA Optics [41]

through the 600 mm focal length front lens and are focussed at the probe volume.

The receiving path is shown in Fig. 20. The light emitted from the probe volume is transmitted back through the front lens and is directed on a pinhole. This pinhole masks out all light that is not directly from the probe volume. The light that makes it through the pinhole is reflected by a mirror at 45 degrees to the optical axis toward another pinhole. This further reduces any unwanted light. Beyond the pinhole is a color separator which separates the information for each velocity component. The Doppler information is then directed toward one of the two Photo-Multiplier Tubes (PMT). The PMT is sensitive to light intensity and outputs an analog voltage signal.

4.2.3 Signal Processing

The signal processing equipment takes the output signal from the PMT and converts it to velocity information. The frequency of the intensity variations detected by the PMT indicates the Doppler frequency. The signal processing is carried out by a frequency mixer, signal conditioners, frequency counters, a coincidence interface, and a micro-computer. The signal path is shown in Fig. 21.

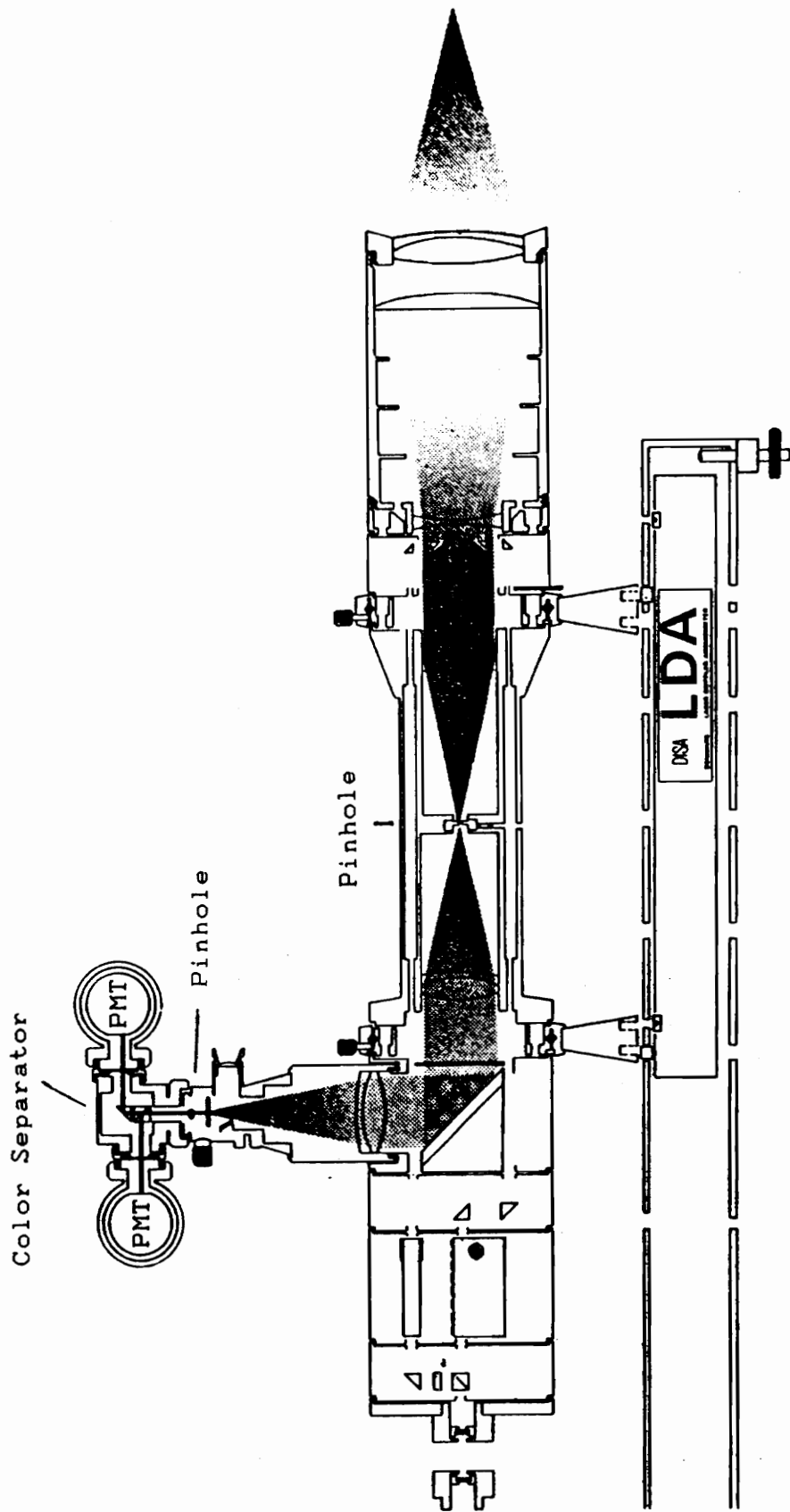


Fig 20. Receiving Path of LDA Optics [41]

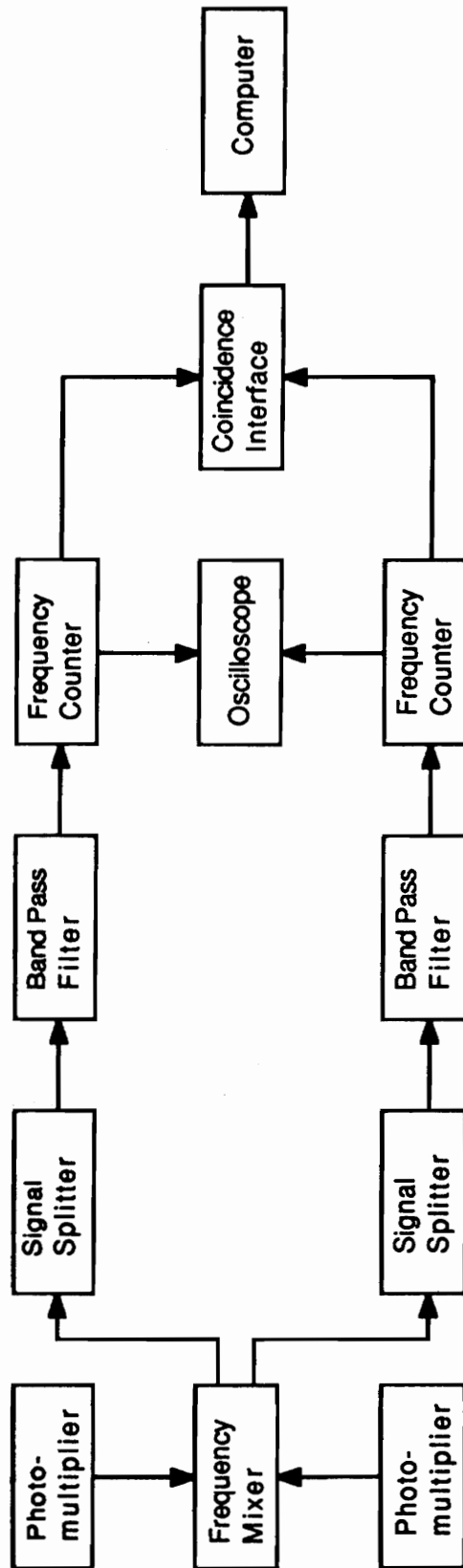


Fig. 21 Signal Path of LDA Signal Processing

4.2.3.1 Frequency Shifter

Frequency shifting is done in LDA systems to eliminate forms of statistical bias and to establish flow direction. Frequency shifting is a combination of optical and electronic shifting. The Bragg cell optically shifts one of the pair of laser beams up by 40 Mhz. After the collected light is converted into a voltage signal, the frequency shifter takes the PMT signal, filters out the low frequency pedestal, and mixes it with a generated frequency. The process downshifts the signal from the PMT by a user selected amount. The mixer also supplies the 40 Mhz voltage signal to power the Bragg cell. This system uses a DANTEK(DISA) model 55N10 frequency shifter. The use of frequency shifting as a correction for statistical bias is discussed in Section 5.2.1. Its theory and practice is well documented by Tree [31,36] and in the DANTEK(DISA) manual [40].

4.2.3.2 Signal Conditioners

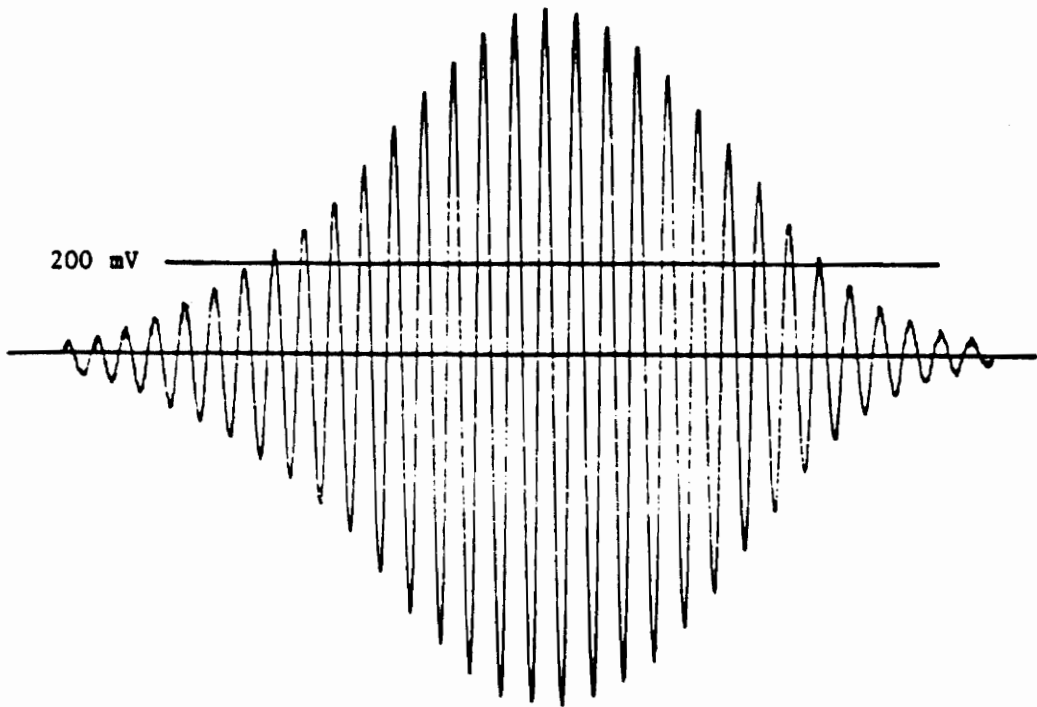
The resulting signal from the mixer is split into DC and AC components by the signal splitter. The DC component is displayed on a 0 to 100 μ A microammeter and indicates the PMT current. This current should be kept below 100 μ A to prevent damage to the PMTs. The AC component of the signal is passed to a TSI model 10099 amplifier. The amplifiers

are powered by a Zener diode controlled, 15 V power supply. After amplification, the signal is band-pass filtered by TSI model 1982 filters.

The use of filters is critical to turbulence measurements. If the band-pass filter width is too narrow, the signal variations may be clipped off. If the filter is too wide, it allows too much noise to pass. These filters were added to the system by Tree since the filters on the frequency counter do not allow enough flexibility in window selection. Filter window optimization is discussed in Sections 5.2.2 and 6.3

4.2.3.3 Frequency Counters

The frequency counters determine the frequency of the conditioned signals and send the information in digital form to the coincidence interface and the computer. This system uses DANTEK(DISA) model 55L90a frequency counters. The system is used in a mode where the counter determines the time for the passage of eight fringes. To demonstrate how it works, refer to Fig. 22. When a Doppler burst first crosses a 200 mV threshold, it starts a Schmitt trigger that cycles each time the threshold is crossed. The counter uses a 500 MHz clock to determine the time for eight cycles of the Schmitt trigger, τ_s . When the computer receives this information, the frequency of a burst is calculated by the



Schmitt Trigger Output

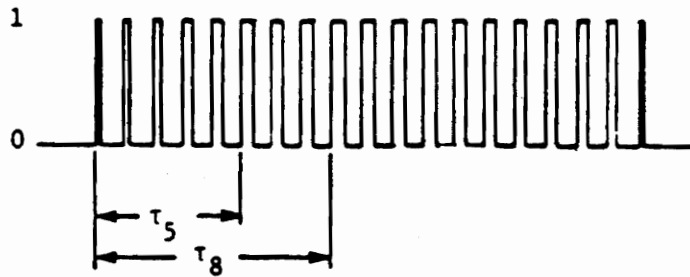


Fig. 22 LDA Counter Operation [31]

software as $8/\tau_1$.

Poor or noisy signals are eliminated by this system in two ways. First, all voltage levels below the threshold level are not recognized as signal. The user can adjust the amplification level of the incoming signal so that the Doppler bursts are the only portion of the signal that is recognized. Secondly, the time for eight crossings, τ_8 , and five fringe crossings, τ_5 , are compared to an accuracy tolerance. This determines the repeatability of the signal within the burst. The counter will reject signals that arise from multiple particles within the probe volume.

4.2.3.4 Coincidence Interface

The coincidence interface is a junction where the digital information from the two frequency counters is combined and sent to the computer. The coincidence interface determines whether the signals arriving from each counter are from the same particle. It measures the amount of time between the arrival of a signal in one channel and the arrival of a signal in the other. If the signals arrive within a time period called the coincidence window, they are considered to be from the same particle and are passed on to the computer. Coincidence window optimization is discussed in Section 6.4.

The coincidence interface was custom built by TSI to

accept information from the DANTEK counters. It consists of a 1998a master interface, a 1998s slave interface, and two 1998 interfaces. TSI modified the 1998 interfaces by cross wiring between the front panel and the back plane. Since DANTEK and TSI have different pin assignments for the same information, this cross wiring simply translates the information from DANTEK to TSI form.

4.2.3.5 Computer and Software

This system uses a Digital Equipment Corporation DEC-11/23 to record and analyze data. The data is transmitted from the coincidence interface over a 50 pin ribbon cable. The data is stored in direct memory access fashion (DMA) to receive the information as quickly as possible. This method bypasses the central processing unit (CPU) which eliminates many intermediate steps. The TSI DRP3 software controls the DMA and analyzes the data after it is stored. This program can calculate the mean and standard deviation of the velocity as well as the correlation between the two channels. The program calculates the velocity of each particle based on laser light wavelength and the angle between the beams. This information is provided by the user in addition to the desired sample size. The algorithms used to calculate the statistics are presented in Section 5.3.

4.2.4 Seeding System

The purpose of the seeding system is to introduce reflective, uniform particles into the flow. These particles should be small and light enough to follow any changes in the flow. If the particle is too large, it may not accelerate at the same rate as the air particles. This phenomenon is known as particle lag and is especially important in flows with large accelerations such as shock waves. The trade off is that larger particles reflect more light and improve signal to noise ratio. Thus, a compromise is necessary between signal quality and accurate particle dynamics. In this investigation, the effect of particle lag should be minimal since there are no large velocity gradients and small particles are used to seed the flow.

There are many choices for the seeding medium. In fact, any particle that reflects light is a candidate. Room dust and water spray both reflect light but are not uniform in size or stable enough to be good seed particles. Uniform size is necessary so that all particles have a statistically equal chance of being recognized by the counter processors. Particles that are too small or too large are not interpreted as valid signals but do reflect light which increases the noise level relative to the signal [42]. Although the frequency counters do have signal threshold levels to reject poor signals, a high signal to noise ratio is desirable to

insure that the data rate is high and that the sample is statistically valid.

The most common seeding systems use either oil droplets or uniform solid particles generated by an atomizer. One common method is to use uniform, expanded polystyrene spheres in a mixture with alcohol. As the mixture is atomized and injected into the air stream, the alcohol evaporates and the spheres follow the air stream into the test section. Another form of seeding is to atomize a solution that will dry into solid particles. The seeding system utilized in this investigation uses a 20% (by volume) solution of sugar and water. This seed was selected by Tree [31] due to low toxicity, ease of clean-up, and low cost.

A TSI model 9306 Six-Jet Atomizer is used to seed the flow. This works by spraying a jet of sugar solution against six plastic spheres thereby atomizing the solution. The atomizer injects this spray at a positive pressure into the flow. The user has the option of using from one to six of these jets to vary the amount of seed introduced. The present tests were conducted with 4 jets at an operating pressure of 82.7 KPa (12 psig). This pressure is indicated at the in-line pressure gauge.

As shown in Fig. 23, the atomized spray passes through a 2.5 mm I.D. tube to a manifold mounted below the pipe. The spray then passes into the pipe flow through a 5 mm I.D.

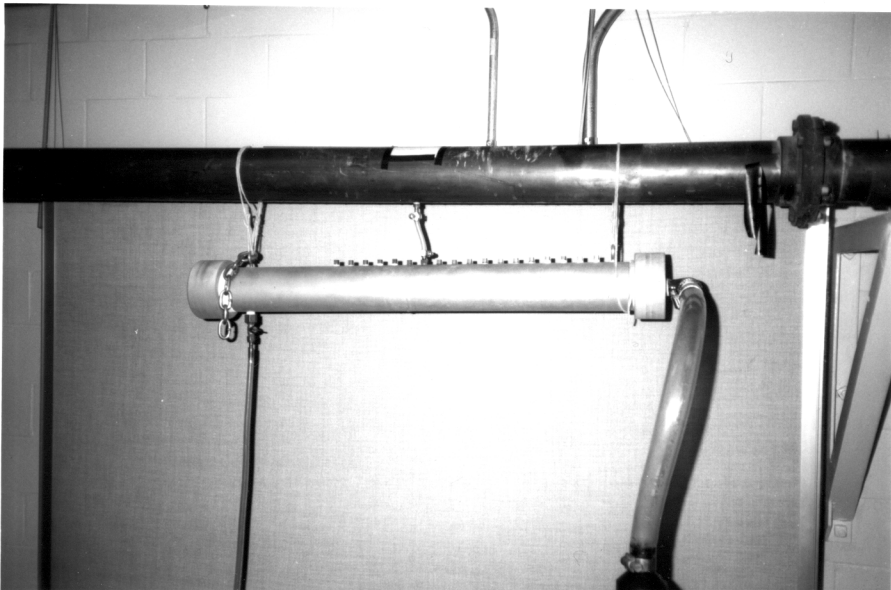
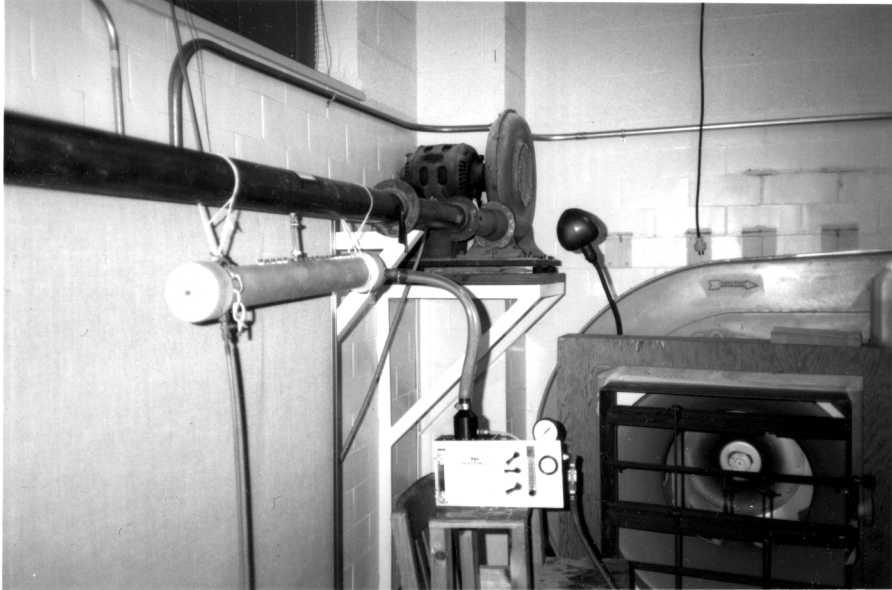


Fig. 23 Seeding System

tube approximately 200 diameters upstream of the measurement plane. This injection point was chosen to insure that the seed is uniformly distributed and that the final velocity profile is unaffected.

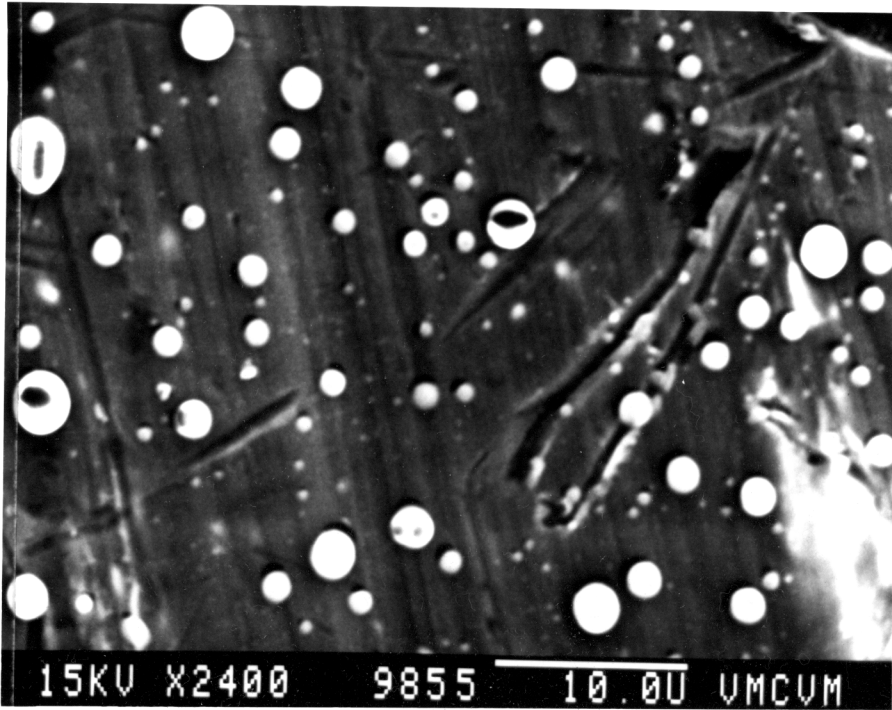
The size of the sugar seed particles depends on the concentration of the solution. Samples were gathered at the seeder manifold exit and examined with a scanning electron microscope. Figures 24a and 24b show the seed particles at magnifications of 2400X and 4000X respectively. Using the scale on the figure, the size of each particle can be determined. Based on 94 of the seed particles from Fig. 24a, the average seed size is 1.05 μm and the seed size varies from .3 to 2.8 μm .

4.2.5 Traverse System And Velocity Sensitivity

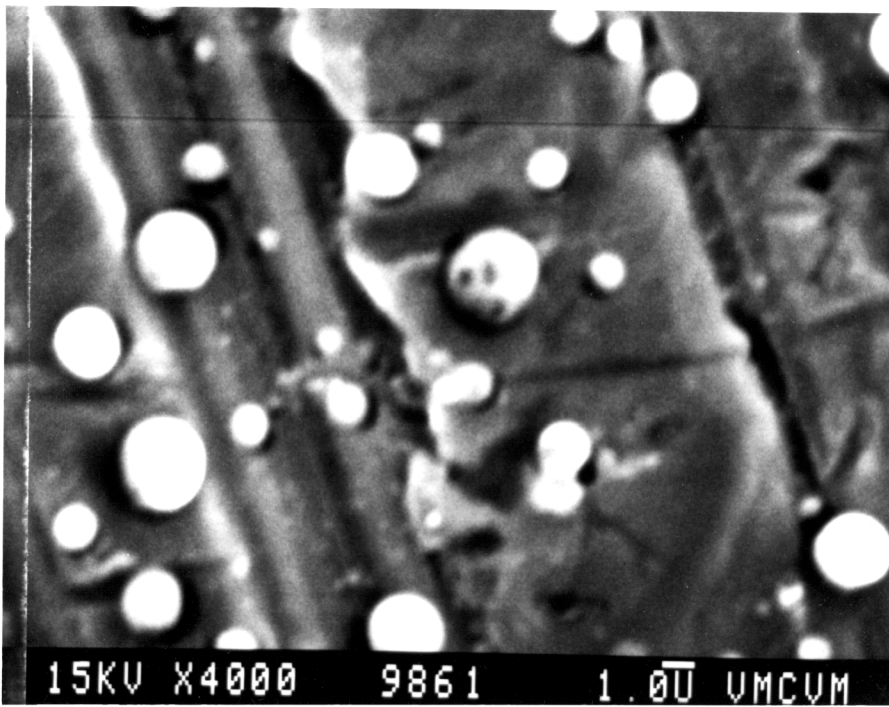
The traverse direction of the LDA as well as the orientation of the fringes determine the direction of velocity sensitivity in this investigation.

4.2.5.1 Traverse System and Optical Bench

The traverse system consists of a milling table and 3 linear dial-indicators which measure displacement in thousandths of an inch (25.4 μm). The milling table is manually operated and traverses in three directions orthogonal to the floor. The laser and the front optics are



(a)



(b)

Fig. 24 Scanning Electron Microscope View of Seed Particles

mounted on a metal box-beam called the optical bench. As shown in Fig. 25, the optical bench is mounted to the top of the milling table on a ramp with a 6 degree incline. This apparatus was originally used to make near wall measurements in a wind tunnel. In the present study, the optical bench was turned around to tilt the laser axis up to an angle of six degrees. This enabled the optical system to place the probe volume at the end of the pipe which is mounted about 2 meters above the laboratory floor.

4.2.5.2 Measurement Plane

The measurement plane is about 5 mm downstream of the pipe end and perpendicular to the axis of the pipe. This plane was chosen as the closest to the pipe end without having laser beam interference. Although the flow is no longer constrained by the non slip condition of the pipe wall, the core of the flow should still accurately simulate fully developed pipe flow. In this investigation, no near wall measurements were attempted. The closest measurement point is 5% of the radius away from the wall.

In this plane, any two perpendicular components of velocity can be measured at the same time. Shown in Fig. 26 is the range of velocity vectors that can be measured. In the present study, the front optics were rotated so that the fringes were at 45 degrees to the mean flow angle. This

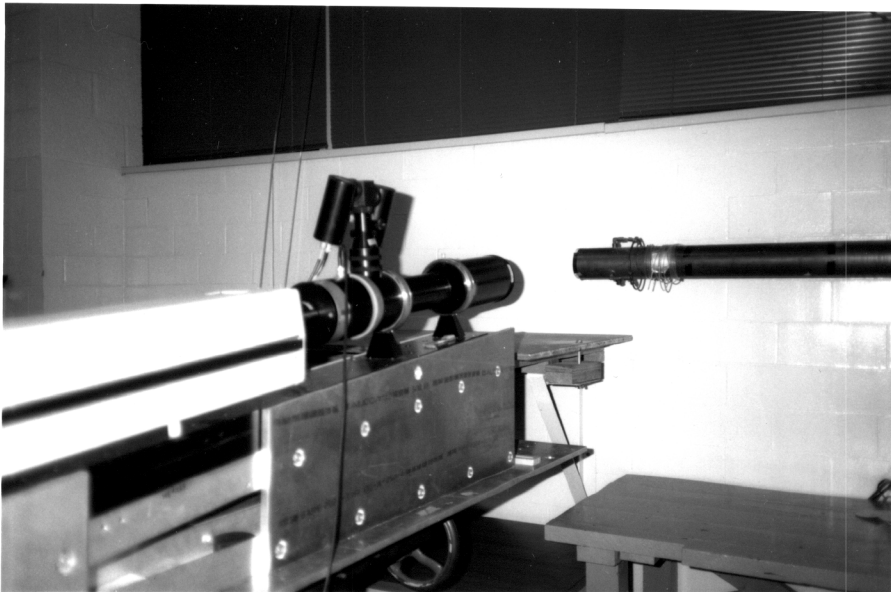
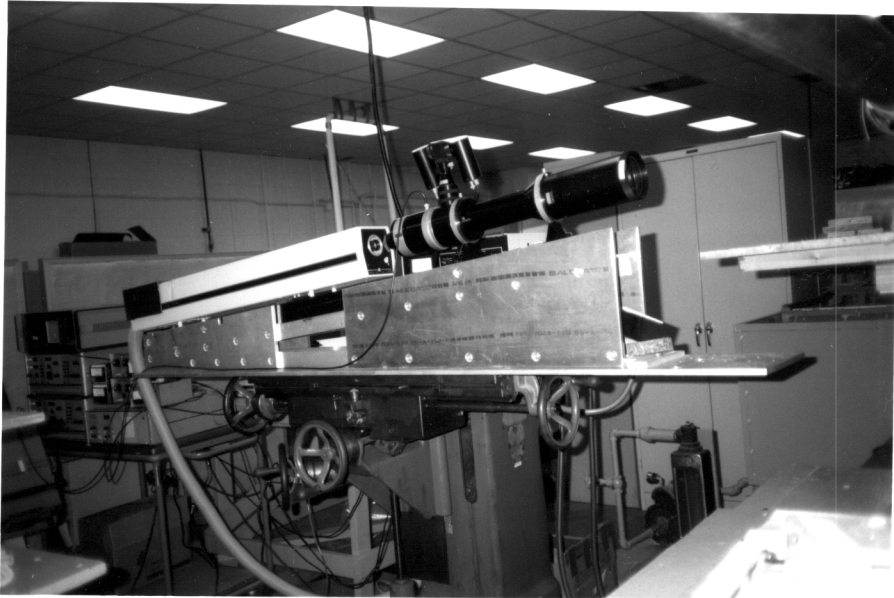


Fig. 25 Traverse System and Orientation to Pipe

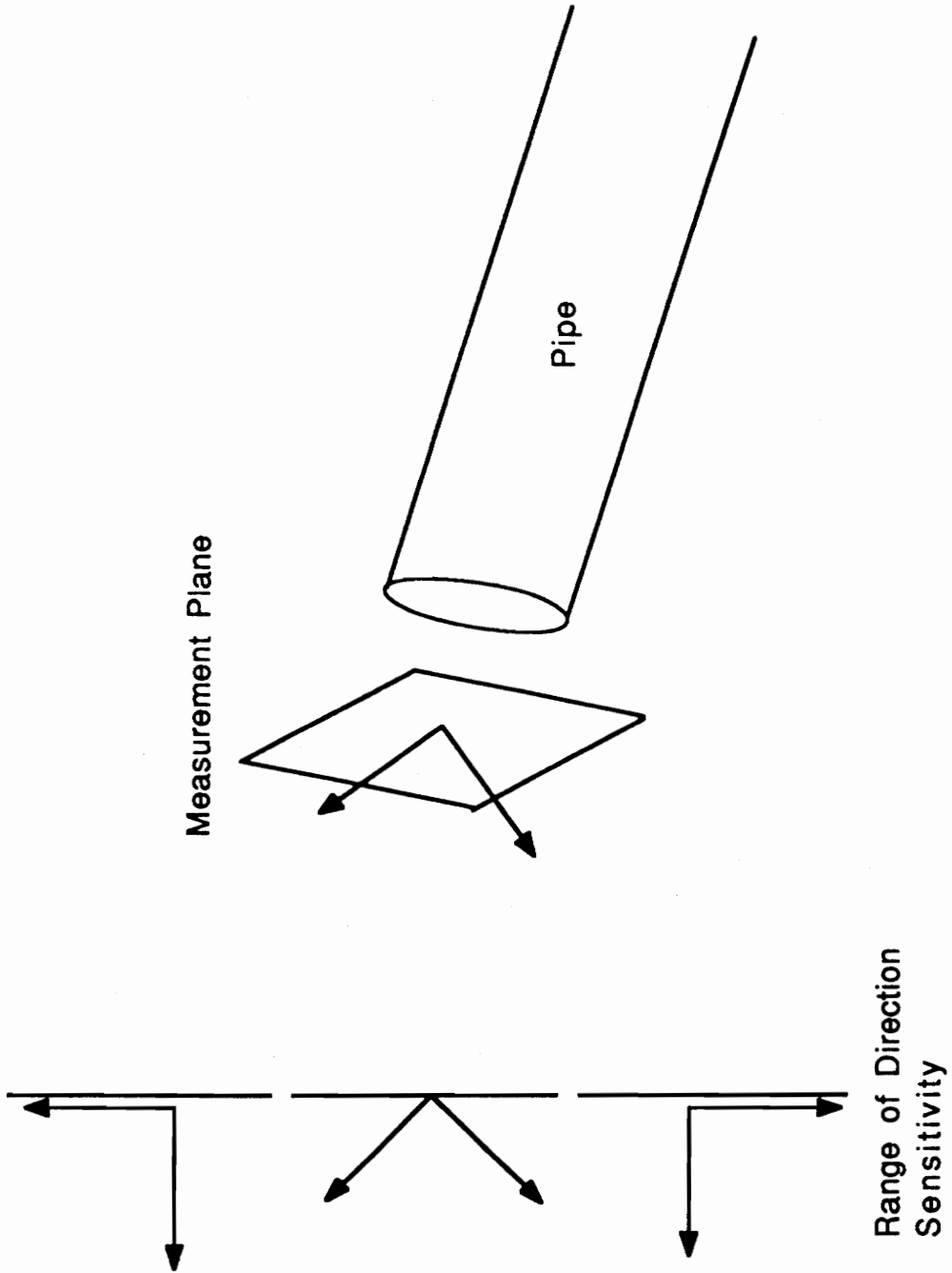


Fig. 26 Measurement Plane Orientation

insured that both channels would get roughly the same amount of particles at the same angle.

4.2.5.3 Velocity Sensitivity

Since the traverse direction is not aligned with the optical bench, special traverse directions were required to find the radial, axial, and circumferential velocity components of the pipe flow. To make the LDA system sensitive to only the axial and radial components, a declined, vertical traverse was chosen as shown in Fig. 27. If the traverse were taken in the direction shown in Fig. 28, the LDA system would be sensitive to only the axial and tangential components. Although all three components were measured, they were not taken coincidentally. Only two components were measured at the same time. This means that the Reynolds shear stress could be measured but the turbulence kinetic energy could not be measured.

4.2.5.4 Statistics Of Interest and Coordinate Transformation

As seen before, the instantaneous flow velocity, U_i , can be expressed as $U_i = \bar{U}_i + u_i$. In this investigation, the system was used to measure \bar{U}_i , the root-mean-square (RMS) of u_i , u' , and the correlation, $u_i u_j$. In pipe flow coordinates, this meant that the system measured the axial, radial, and tangential fluctuations, u' , v' , w' and the

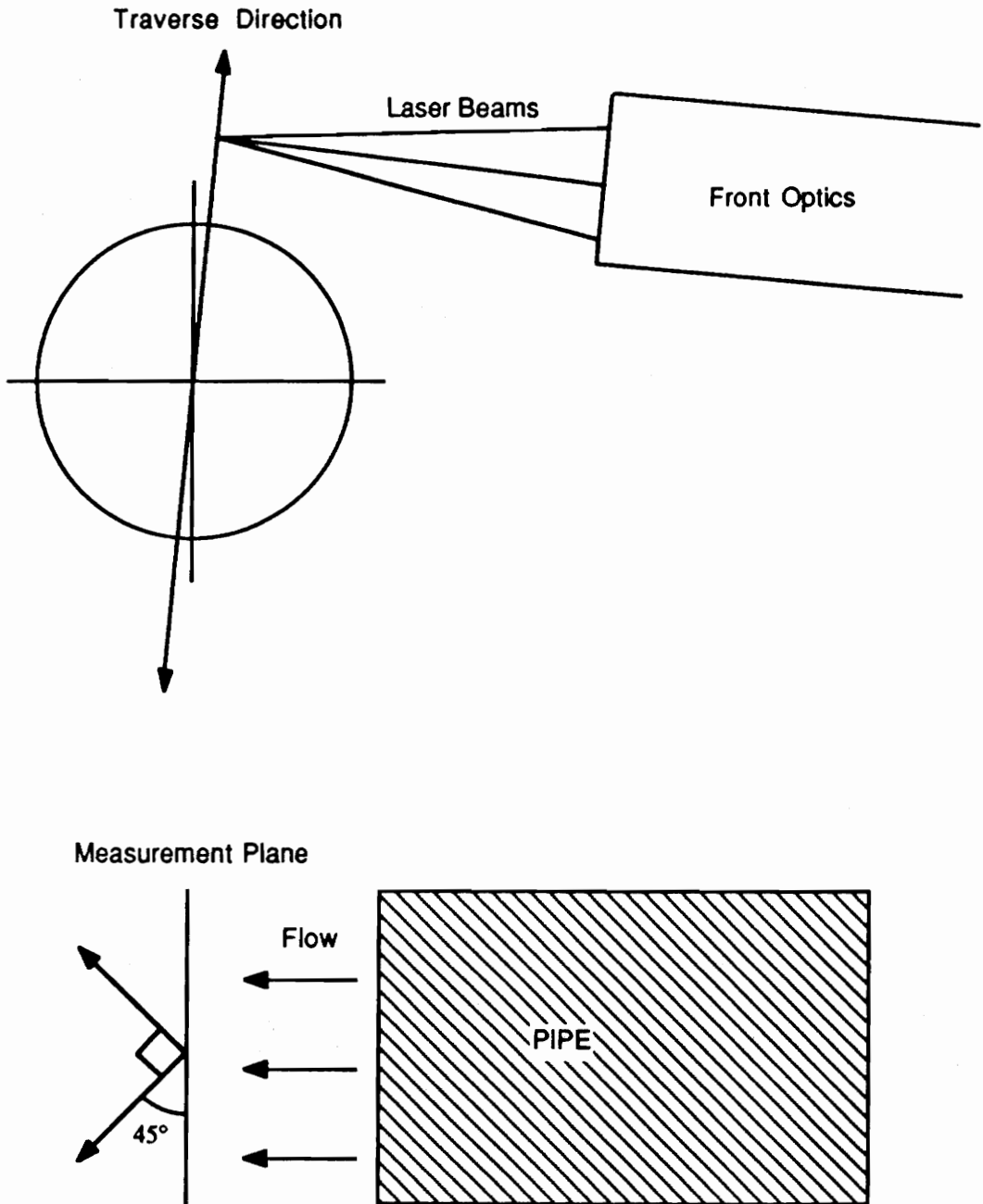


Fig. 27 Traverse Direction for U and V Sensitivity

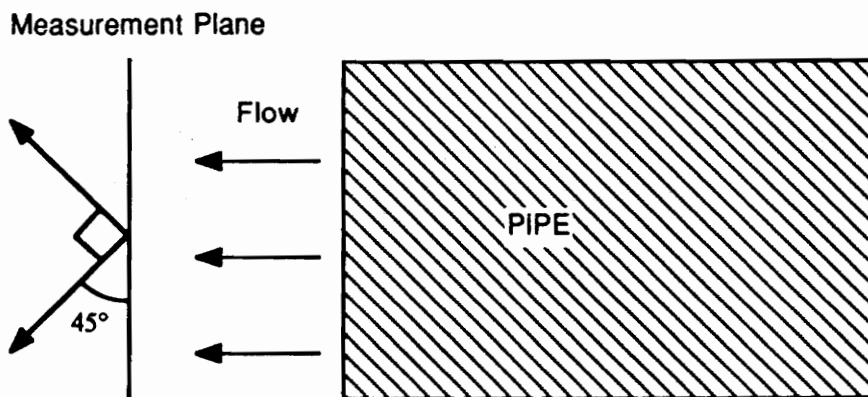
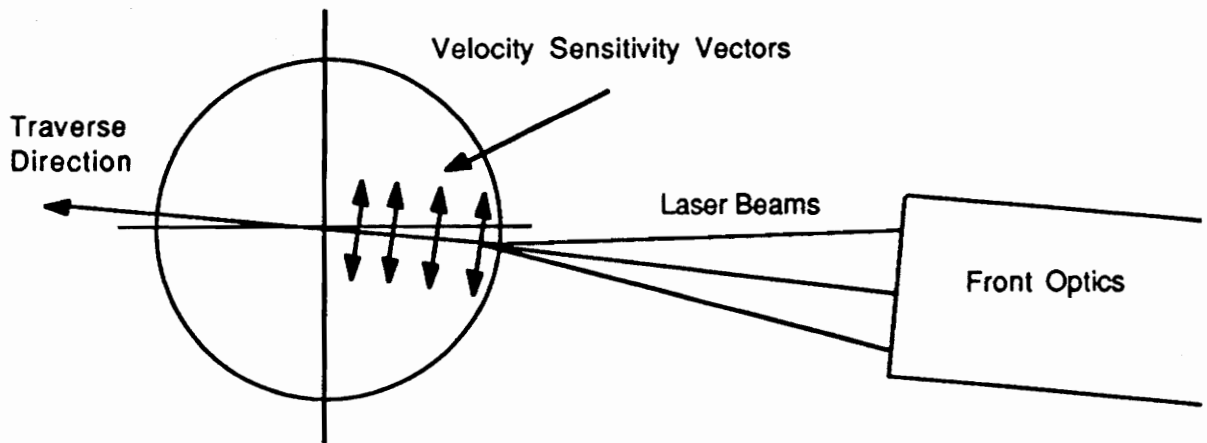


Fig. 28 Traverse Direction for U and W Sensitivity

correlation, \overline{uv} , along with the mean velocities. The velocity fluctuations are the square root of the Reynolds normal stresses while the correlation is the shear stress. Since the fringes were at 45 degrees to the main flow angle, these quantities couldn't be measured directly. A coordinate transformation was used to relate these quantities in the rotated coordinates to the pipe coordinates. Designating the b and g subscripts (blue and green) to correspond to the rotated coordinate system at an angle of θ with the pipe axis, the relations are as follows [43]:

$$u' = [\overline{u_b^2} \cos^2 \theta + 2\overline{u_b u_g} \cos \theta \sin \theta + \overline{u_g^2} \sin^2 \theta]^{\frac{1}{2}} \quad (8)$$

$$v' = [\overline{u_b^2} \sin^2 \theta - 2\overline{u_b u_g} \cos \theta \sin \theta + \overline{u_g^2} \cos^2 \theta]^{\frac{1}{2}} \quad (9)$$

$$\overline{uv} = (\overline{u_b^2} - \overline{u_g^2}) \sin \theta \cos \theta - \overline{u_b u_g} \cos [2\theta] \quad (10)$$

When $\theta = 45$ degrees is substituted for the rotation angle, Eqns. 8-10 reduce to:

$$u' = \frac{\overline{u_b^2}}{2} + \frac{\overline{u_g^2}}{2} + \overline{u_b u_g} \quad (11)$$

$$v' = \frac{\overline{u_b^2}}{2} + \frac{\overline{u_g^2}}{2} - \overline{u_b u_g} \quad (12)$$

$$\overline{uv} = \frac{\overline{u_b^2}}{2} - \frac{\overline{u_g^2}}{2} \quad (13)$$

Note that these are for the traverse that is sensitive

to the axial and radial fluctuations. When the user traverses the system in the direction sensitive to U and W, the relations are the same except that v' is replaced with w' .

4.2.6 Beam Angle Determination

Careful beam angle determination is vital to accurate turbulence measurements with a LDA. As seen in Section 3, the instantaneous velocity of a seed particle, V_p , is determined from:

$$V_p = f_d * \lambda / (2 * \sin\theta) \quad (14)$$

where f_d is the Doppler frequency, λ is the laser light wavelength, and θ is the half angle between the beams. If the wrong beam angle is used to calculate the velocity, the velocity measurement will be wrong by some unknown, constant offset. This will affect the mean velocity calculations as well as the standard deviation of the velocity fluctuation. Since the Reynolds stress measurement depends on the standard deviation of the velocity fluctuations of both components, it is critical that the beam angles are measured correctly.

The DANTEK manual [41] lists the nominal beam angle as 2.55 degrees for both sets of beams for the 600 mm lens and the widest beam separation. While optimizing the system, the actual value may change significantly. The variation experienced in this study was +/- .5 degrees. To accurately

measure the beam angles, two methods may be used.

The first method is to allow the three beams to pass through the probe volume and strike a far wall [35]. Rotate the optics to 45 degrees as shown in Fig. 29. First, measure the distance, d , between the probe volume and the wall along one of the beams. Next, measure the distance between the images of the beams. The beam angle is calculated using similar triangles. The half angle between the beams is then:

$$\theta = \sin^{-1}\left(\frac{c}{2d}\right) \quad (15)$$

While this method is valuable when there is sufficient space behind the probe volume, the distance between the probe volume and the wall was only about 1 m in the present set up. This method would not be accurate enough over such a short distance.

The second method uses a pinhole and the traverse table to measure the angle as suggested by Dancey [43]. This procedure measures three vectors from the probe volume, one along each laser beam. After the coordinates for each vector are measured, the results are inputted into a BASIC program to compute the angles. This program is listed in Appendix A. The procedure for this process is:

1. Remember safety. Use goggles for this procedure and

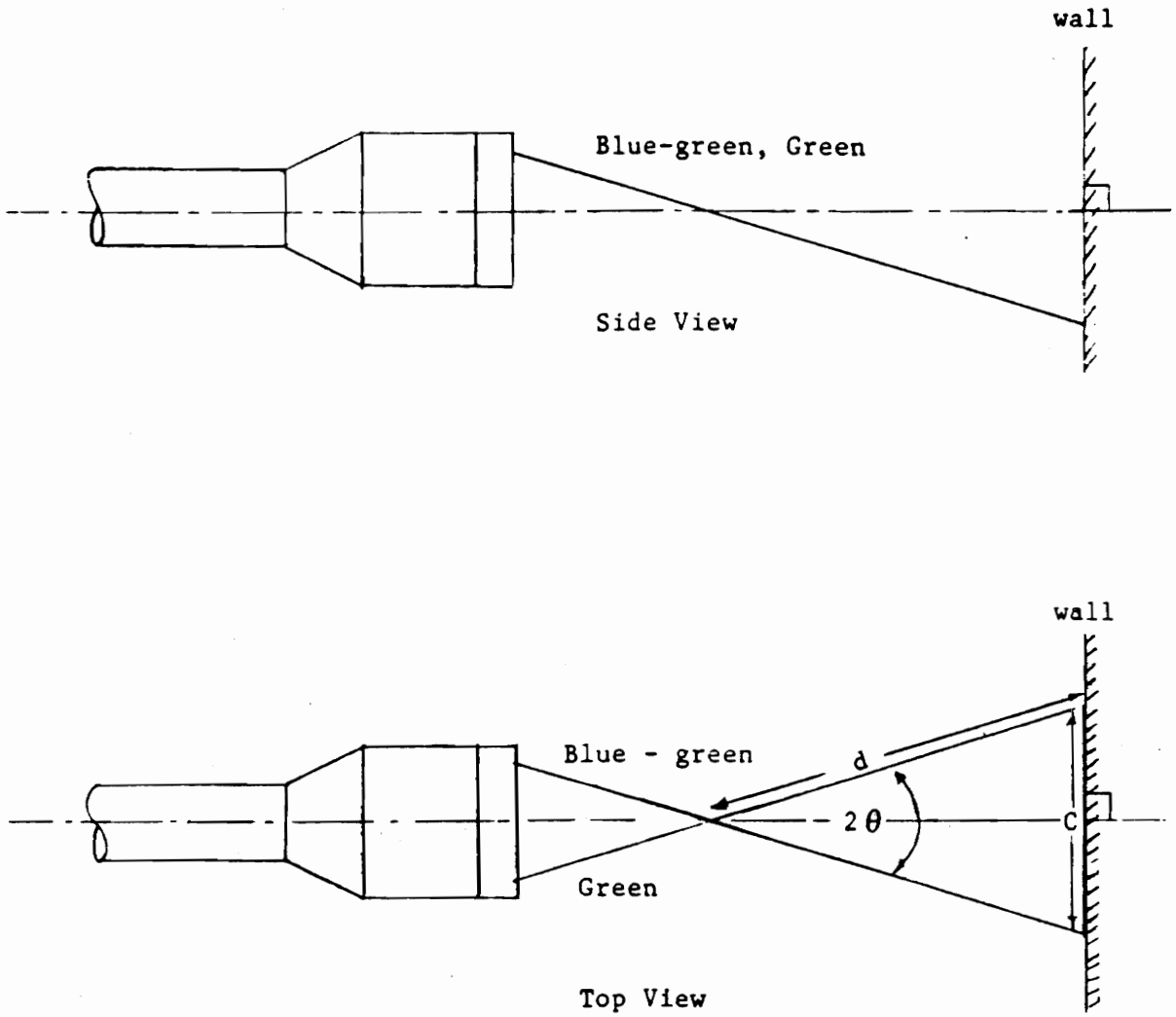


Fig. 29 Half Angle Determination [37]

watch out for stray reflections.

2. Warm up the laser for approximately 30 minutes and completely align system. Alignment procedures are available in the DANTEK manual [41], Tree's alignment report [37], and Doty's alignment supplement [44].

3. Place a pinhole near the beam intersection.

4. Move the traverse table until the beam intersection is at the pinhole and note the coordinates. All three beams should pass through the pinhole and hit the wall behind the measurement plane. The images on the wall should be as strong as possible and have a concentric diffraction pattern. These are the "center coordinates" asked for in the BASIC program.

5. Move the traverse table back a convenient distance, noting the change in the x coordinate. Greater distances yield better results but are limited by the method of distance measurement. With this traverse system, the limitation was about 38 mm (1.5 in)

6. Locate all three beams and note their coordinates. Again move the traverse table until each beam image on the wall is as strong as possible and exhibits a diffraction pattern.

7. Input the coordinates into the program and determine the beam angles. Note that the program provides the whole angle between the beams.

After this procedure, the user should not alter the beam angles in order to optimize the signal quality. All optimization should be done before the beam angles are measured. Remember that the laser alignment mirrors and all the beam steering adjustments change the beam angles.

It was found that the measurements with the micrometers were repeatable to within $\pm .01$ in ($\pm .25$ mm). This error would propagate through the beam angle calculations and would alter the calculated beam angle. A conservative estimate based upon the parameters in this system and several measurements indicates that the variation of the beam angle, measured in radians, was less than 2%.

5. Turbulence Measurements With An LDA

Gathering turbulence statistics with an LDA requires knowledge of the characteristic scales of turbulence and the types of statistical bias that are present. To see this, the following sections will examine the characteristics of turbulence and how the sampling rate and the averaging time affect measurements. They will also describe the forms of statistical bias that have been identified in the literature and how this bias was reduced.

5.1 Turbulence Scales and Sampling Rate

Hinze [4] describes turbulence as "an irregular condition of flow in which the various quantities show a random variation with time and space coordinates, so that statistically distinct average values can be discerned." The averages are calculated based upon a large number of statistically independent samples. The question to the experimentalist is: what is the measure of statistical independence?

5.1.1 Statistical Independence

In turbulent flows there are periodic patterns or eddies which emerge in the flow and produce correlation. In pipe flow, the largest eddies are on the order of the pipe diameter. However, within these eddies are smaller ones

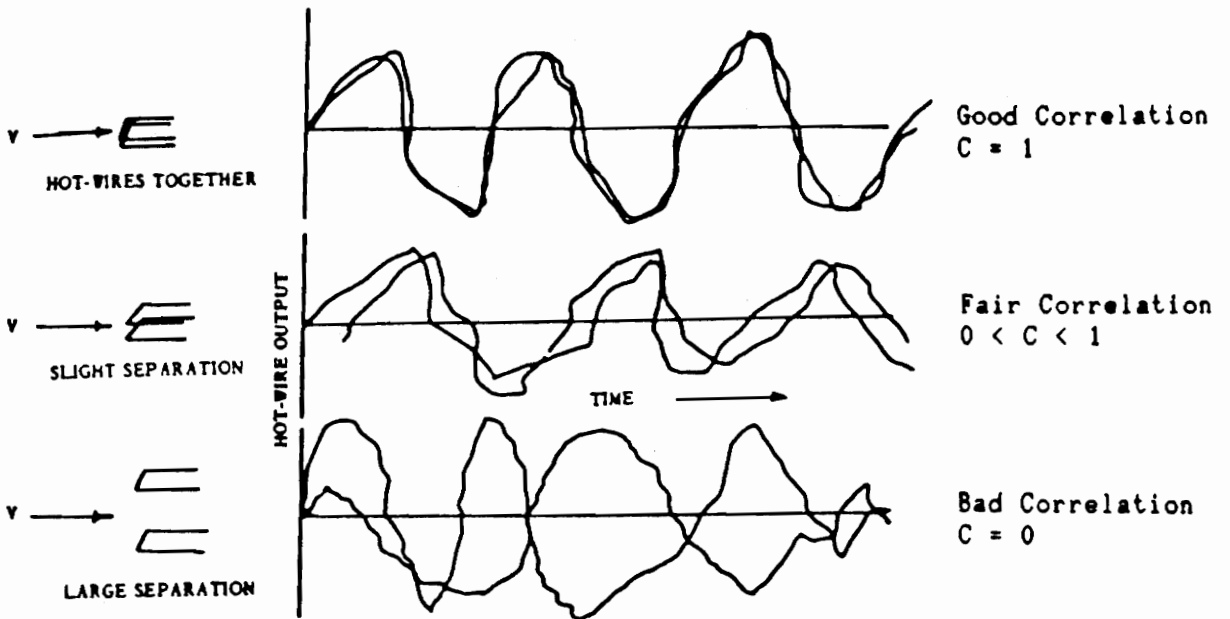
which feed upon the energy of the larger ones. Since these patterns do exist it is necessary to define turbulence length and time scales in order to make statistically valid averages with a LDA.

To illustrate the concept of turbulence scales, refer to Fig. 30a. If the two-hot wire probes shown were to measure the velocity very close to each other, they would measure about the same time history of the velocity [45]. This means that the finite volume of fluid that encompasses the two probes is moving as a unit. However, if the probes are separated by an ever increasing distance, there is less and less correlation between the two. When the two traces are completely independent of each other they are no longer within the same eddy and are statistically independent. The spatial correlation, C , is defined as [45]:

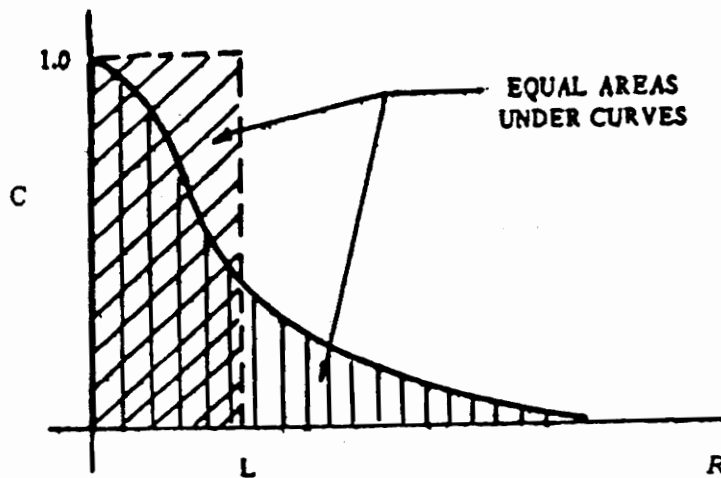
$$C = \frac{\overline{u_1 u_2}}{u_1' u_2'} \quad (16)$$

where u_1 and u_2 are the axial velocity fluctuations from the mean measured at two radial positions and u_1' and u_2' are the corresponding RMS values.

To define the average eddy size, the correlation coefficient is integrated over the radius of the pipe to find the length scale, L :



(a)



(b)

Fig. 30 Spatial Correlation of Two Signals [45]

$$L = \int_0^R C \, dr \quad (17)$$

This is graphically displayed in Fig. 30b and represents the separation distance, L , that would result in $C(r) = 1$ for a mean eddy. For pipe flows, G. I. Taylor found this to be $0.14*(d/2)$, where d is the diameter [46].

Associated with the length scale is a time scale, T , which indicates the time between the passage of each average eddy. This is found from $T=L/U$ where U is the mean axial velocity. To make statistically independent velocity samples with an LDA system, the sampling frequency should be slower than the time scale of the turbulence. If the sampling frequency were greater than T , the samples would be correlated. As shown by George [25], if the velocity samples are correlated, they do not contribute to greater accuracy.

It is important to note that neither the time history nor the spectra of the velocity are required to measure Reynolds stresses. The only required quantities are the mean velocities and standard deviations away from these means. These mean velocities are calculated based on a large number of statistically independent samples. If extremely detailed time histories are desired, the small scales of turbulence such as the Taylor microscale or the Kolmogorov scale would be important. They would insure that

there was sufficient resolution in the samples to capture all the important fluctuations. However, since the statistical distribution of velocity is the only quantity of interest, multiple samples in each eddy are not required. As seen before, if two samples are taken from the same eddy, they are not statistically independent and don't indicate the level of velocity fluctuation.

Figure 31 shows three examples of sampling methods. In Fig. 31a, the velocity is sampled at a high rate (relative to the turbulence scale) and averaged over many eddies. This method will give accurate averages if the sample time is sufficiently long. However, a large amount of data must be collected since the samples are not statistically independent. Figure 31b shows samples that were taken over a short time and don't encompass all the variation in the flow. In Fig. 31c, the velocity samples are statistically independent and averaged over a long time. With this method, the averages will be valid and will require much less data storage space.

5.1.2 Sampling Rate of This System

In this investigation of fully developed pipe flow, the sampling rate is approximately one sample per 28 ms or a sampling frequency of 35 Hz. Using Taylor's result of $L = .14 * (d/2)$, the length scale would be about 5.7 mm based on

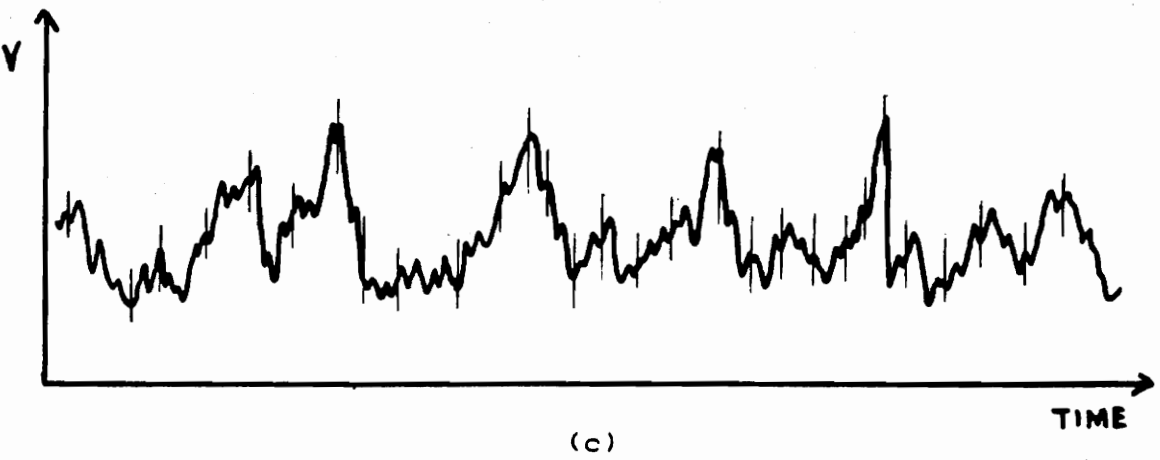
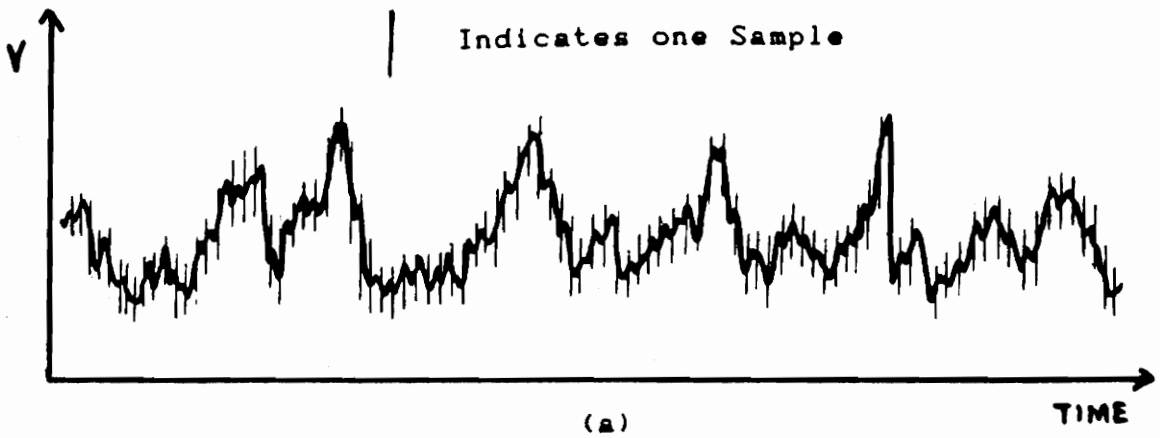


Fig. 31 Sampling Methods

the pipe diameter, d , of 81 mm. The associated time scale calculated with an axial velocity of 14 m/s would be about 412 μs or a sample rate of 2.5 kHz. Thus, the sampling rate in this experiment is 89 times slower than the average eddy frequency and is sufficiently slow for statistically independent velocity measurements. In the worst case, the largest eddy would be on the order of the pipe diameter and the time scale would be about 579 μs or a sample rate of 172 Hz. The measurements would still be statistically independent since the samples are taken approximately every 6 eddies.

5.2 Statistical Biasing

Although the LDV system is a powerful tool for making statistical measurements, it has some inherent problems. The literature on turbulence measurements reveals that there are several sources of statistical particle bias that affect the measured statistical quantities. These sources of bias can be minimized by appropriate use of corrective procedures. [23]

5.2.1 Fringe Bias

Fringe or directional bias occurs when particles pass through the probe volume at an extreme angle relative to the fringes. If a particle passes through the probe volume on a

trajectory, V , as shown in Fig. 32, it will not pass through enough fringes to trigger the counter processor. As a result, this particle will not be counted in the statistical measurements and the results will be biased toward particles that pass more normal to the fringes. The angle labeled B in the figure is the dead zone. All velocity directions inside the zone defined by this angle will not be counted by the system. To alleviate this problem, a Bragg cell is used to optically shift the frequency of one of the incident laser beams. This shift causes the apparent fringes to move across the probe volume. This process reduces the bias by increasing the chances that a particle (ideally at any angle relative to the fringes) will pass through a sufficient number of fringes to be detected. The drawback of the Bragg cell is that it tends to lower the signal-to-noise ratio in the signal.

5.2.2 Filter Bias

Filter bias occurs when the filter windows used to condition the Doppler signal are too small. In a turbulent flow, the Doppler frequency will vary greatly around the mean value. If the filter window is small enough to clip off the extrema of the Doppler frequency, the measured turbulence level will be too small. Proper use of the filter window involves calculating the maximum and minimum

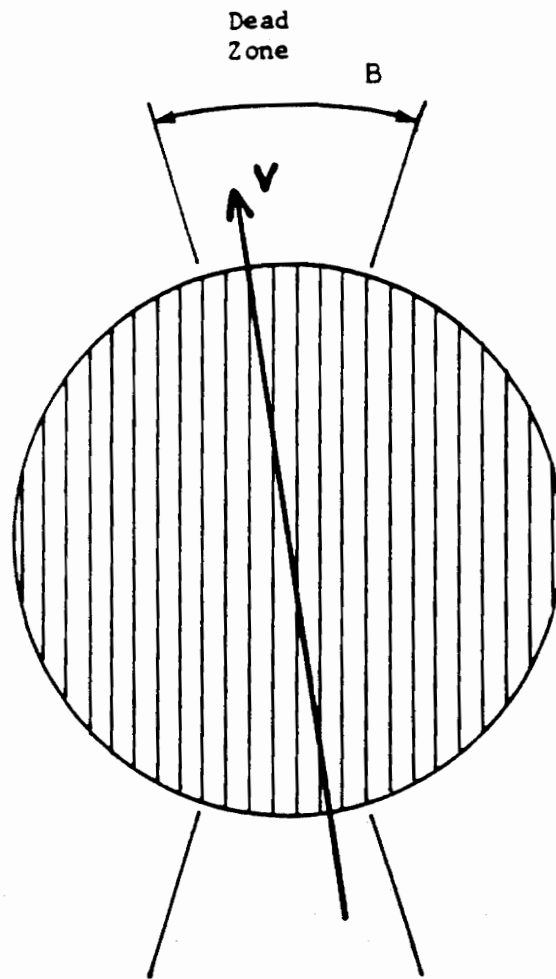


Fig. 32 Dead Zone in Unshifted LDA Measurements [31]

possible frequencies at a given point in the flow and ensuring that the filter will not clip off these frequencies. Also note that filters have a characteristic roll-off region in the frequency spectrum where the signal is passed through but at an attenuated level. This roll-off region is near each edge of the filter window and its width depends on the filter design. If a particular Doppler signal falls in this region, it may not be counted since its amplitude may drop below the threshold of the counter processor.

5.2.3 Velocity Bias

Velocity bias is a result of sampling the velocity at non-uniform intervals. Especially in turbulent flows, the particle arrival rate will not be independent of the flow velocity [23]. For a given surface in the flow, more high velocity particles will cross the surface in a unit of time than slow particles. This means that simple arithmetic averaging will give improper results since the results will be biased toward the faster particles. Edwards [23] states that this type of biasing can be eliminated by "constructing a time series with the same statistics as that of the flow". In essence, the digital samples are converted to an analog signal. Although several methods have been developed to produce this series such as the McLaughlin and Tiedermann

method [47], Edwards [23] and George [25] recommend residence time weighting as the best correction for our type of system. Residence time refers to the amount of time the scattering particle spends in the viewable probe volume. The more time it spends in the probe volume, the more it is weighted. Thus, the bias is reduced since the slower particles are given more weight than the more prevalent faster particles. Note that the viewable probe volume is defined by the placement of the pinhole and how much of the probe volume it masks out. The average velocity is then:

$$\bar{v} = \sum_{j=1}^N \frac{U_j \Delta T_j}{\Delta T_j} \quad (18)$$

where U_j is the velocity of the j th particle and ΔT_j is the time that particle spends in the viewable probe volume. With this method, the time series is integrated only over the amount of time particles are in the probe volume thus eliminating velocity bias.

5.3 Residence Time Weighting and Software Algorithms

Residence time weighting is implemented in this investigation by a combination of hardware and software settings. The frequency counters operate in a "Combined Mode" where the time for 8 fringe crossings, τ_8 , and the total number of fringes, T_f , is passed to the computer. The

software calculates the residence time using this information. It assumes the particle velocity is constant across the probe volume and calculates the residence time, ΔT_i , as:

$$\Delta T_i = \frac{\tau_s \times T f_i}{8} \quad (19)$$

The software algorithms used to calculate the averages, standard deviations, and correlations all use the residence time weighting factors. Each of the channels is identified by a subscript u or v and the j subscript refers to the jth measurement. When a correlation measurement is taken between two channels, the residence time, ΔT_{uv} , is the smaller of the residence times in each channel. The equations used in the software are then:

$$\bar{U} = \sum_{j=1}^N \frac{U_j \Delta T_j}{\Delta T_j} \quad (20)$$

$$u' = \left[\left(\sum_{j=1}^N \frac{U_j \Delta T_j}{\Delta T_j} \right)^2 - \bar{U}^2 \right]^{\frac{1}{2}} \quad (21)$$

$$\overline{uv} = \sum_{j=1}^N \frac{U_j V_j \Delta T_{uvj}}{\Delta T_{uvj}} - \bar{U} \sum_{j=1}^N \frac{V_j \Delta T_{uvj}}{\Delta T_{uvj}} - \bar{V} \sum_{j=1}^N \frac{U_j \Delta T_{uvj}}{\Delta T_{uvj}} + (\bar{U} * \bar{V}) \quad (22)$$

where N = number of samples

5.4 Errors Due to Finite Sample Size

Another source of uncertainty in LDA measurements is the error due to finite sample size. As shown in Yanta

[16], and Strazisar [48], the error bounds on the sample can be calculated to within some confidence level. The error in the mean velocity is depends on both the standard deviation and the mean velocity:

$$\frac{V_m - V}{V} = C_v = \frac{Z}{\sqrt{N}} \left[\frac{V'}{V} \right] \quad [23]$$

where Z is the confidence level, N is the number of samples, V_m is a measured mean velocity, V' is the true standard deviation, and V is the true velocity. For a 95% confidence level, $Z=1.97$ and using the extreme values from this experiment of 1.1 and 9.8 for V' and V , the percent error in the mean velocity is $\pm .3\%$ based on 4000 samples. The possible error in the standard deviation depends only on the sample size:

$$\frac{V_m' - V'}{V'} = C_{v'} = \frac{Z}{\sqrt{2N}} \quad [24]$$

Using the same values for Z and N , the percent error is 2.2%. These results illustrate that a given number of samples will give a better approximation to the mean velocity than the standard deviation.

6. OPTIMIZATION OF LDA SYSTEM

As an LDA system is used by more and more people, they incorporate the ideas of previous users and develop new optimization procedures particular to that system. The following is a discussion of the procedures that were found crucial to making Reynolds stress measurements.

6.1 Alignment

The alignment procedures developed by Tree in his alignment manual [37] are an excellent guide. As the system has been used, additional guidelines have been developed.

In general, alignment is a process designed to correctly focus the three laser beams at the probe volume with the highest possible power and the correct polarity. The revised alignment procedure is to follow Tree's guidelines but to align the system for only one rotational position of the optics. Ideally, the optics should remain aligned as they are rotated. In practice it was found that the system would go out of alignment if it was rotated, no matter how carefully the system was aligned.

Some new equipment and procedures were added to Tree's alignment guide. The beams are made to cross correctly at the probe volume by using an ORIEL 100 μm pinhole that is mounted in a holder. The pinhole is placed at the probe volume and then the beams are "steered" through it. The

goal is to get all three beams to pass through the pinhole and cast the strongest image on the wall.

It was found that the primary tool used for adjusting and aligning the system is the oscilloscope. The basic alignment is made using the pinhole, then once the blower and seeder are started, the Doppler bursts are viewed on the oscilloscope. The signal comes from the monitor output of the frequency counter.

The general procedure is to first rotate the $1/2$ wavelength plate at the front of the optics to get the strongest signal in each channel. Next, make fine adjustments of the beam angles, again get the strongest signal. Finally, vary the amplification level to get the noise below the 100 mV threshold of the counter. Further optimization is accomplished with amplification, filter selection, flow velocity, and coincidence window selection.

6.2 Choice of Amplification

As shown by Samimy [29], the PMT gain has a considerably more positive effect on signal-to-noise ratio (SNR) than the amplifiers on the counter. Therefore, to get the best signal, the gain is raised on the PMTs as much as safely possible by adjusting the supply voltage to about 1750 V. This is above the normal operating level of 1250 V but safely below the maximum voltage of 2000 V. The counter

amplifiers are only used to further amplify the signal if necessary. For instance, if there is a weak signal, first amplify as much as possible with the gain on the PMT and then bring the signal up to the counter threshold level with the counter amplifiers. Further fine adjustments are made with the PMT gain. It was found that the "validated data rate" and the "percent validated" as indicated by the counters are both higher when this is done.

6.3 Filter Width and Flow Rate Selection

The width of the filter window was found to have a pronounced effect on our measurements. If the window were too large, a larger percentage of noise was included in the signal. This reduced the "validated data rate" as well as the "percent validated". It also tended to overestimate the standard deviation of the velocity. If the window were too small as shown in Fig. 33, the filter would not pass through all the frequency fluctuations, especially in regions of high turbulence. This would decrease the standard deviation and underestimate the turbulence.

The original filters with this system are part of the frequency counters. Tree added some TSI filters and amplifiers to increase the signal quality and add flexibility. For this flow, a filter window of 300 KHz to 2 MHz was selected and the frequency shifter was used to place

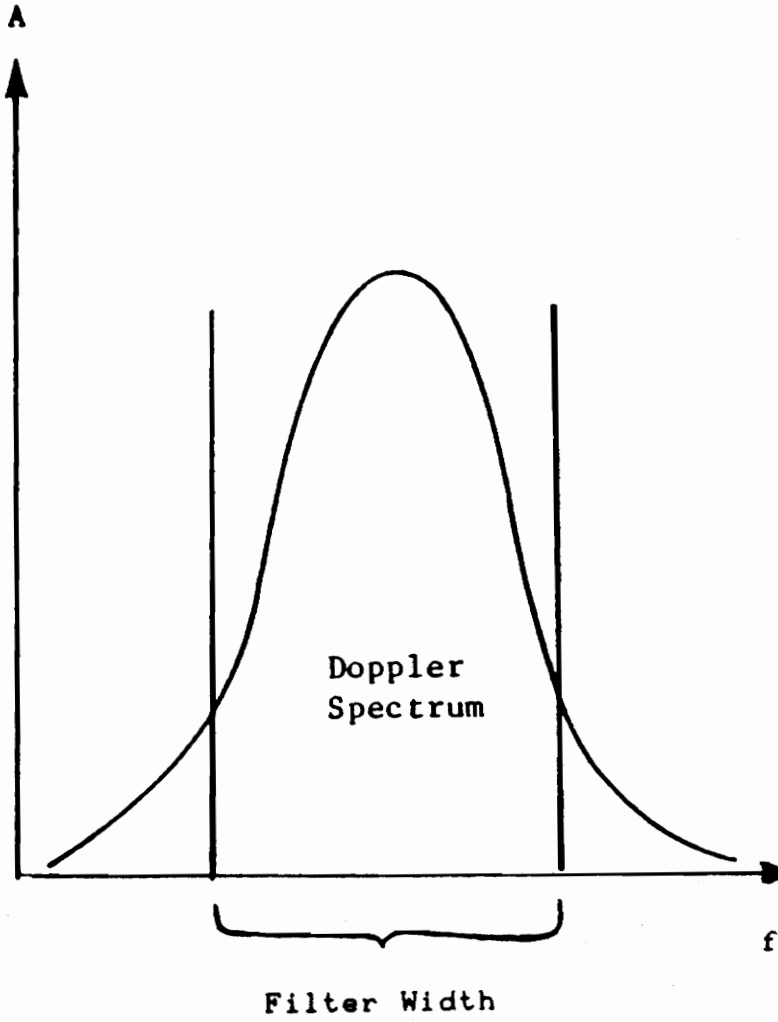


Fig. 33 Clipped Doppler Spectrum

the mean signal frequency at about 1.05 Mhz. As the traverse progresses across the pipe, the frequency varies so the shift was adjusted to keep the mean frequency at this value. For a flow with a dynamic pressure of about 13 mm of H₂O (.5 in of H₂O), it was found that these filter settings would not clip off any relevant frequency fluctuations but would eliminate most of the noise in the signal.

6.4 Coincidence Window

The coincidence window refers to the size of a time window in which two measurements are to be considered coincident in time. Recall that each seed particle passes through two sets of fringes in the probe volume. The frequency information from each set is received by a separate PMT and processed by a separate system. After the counters determine the frequency in each channel, the information is passed to the coincidence interface. Because of differences in laser power, processing speed, and signal quality, the signals from each channel may not arrive at the same time. To illustrate, consider Fig. 34 where Doppler bursts from a single particle in two different channels are shown. The signal in channel 1 is stronger and is recognized before the signal from channel 2. In this example, it is recognized 4 fringes sooner. Based on a fringe spacing of 5.6 μm , and a velocity of 14 m/s, the

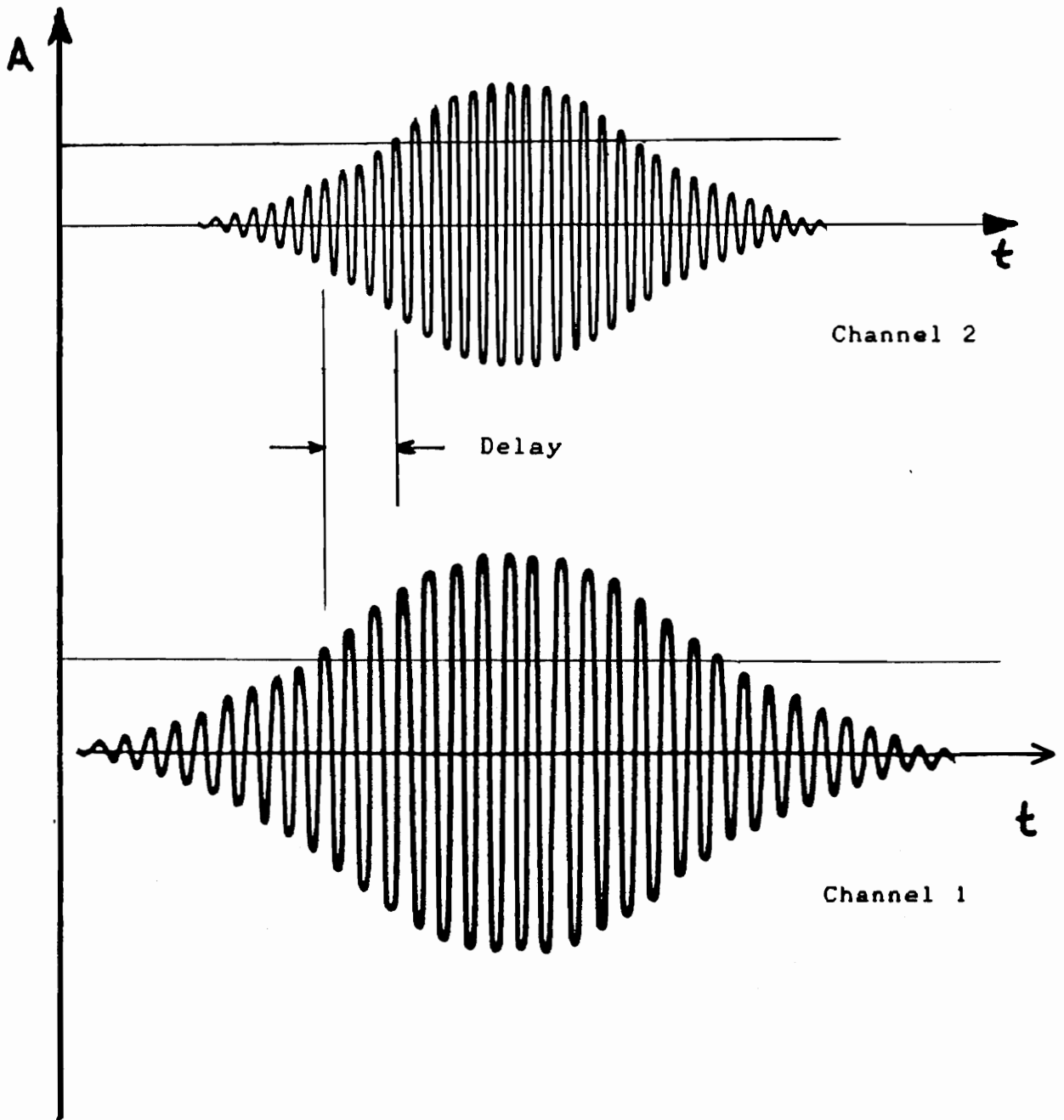


Fig. 34 Delay Due to Disparate Signal Strength

delay between the signals would be:

$$\text{Delay} = \frac{5.6 \mu\text{m}}{\text{Fringe}} * 4 \text{ Fringes} * \frac{1}{14 \text{ m/s}} = 1.6 \mu\text{s} \quad (25)$$

When the coincidence interface attempts to combine the information, it measures the amount of time between frequency measurements on the two channels. If they are close enough, they are considered to be from the same particle. We use these coincident measurements to correlate the two channels and make Reynolds stress measurements.

Choosing the correct coincidence window is a compromise between data rate and measurement variability. If the window is too small, very few particles will satisfy the time increment and the data rate will be low. Figure 35 shows the variation in data rate versus coincidence window for this system. The test was conducted with an average data rate of 450 Hz coming into the coincidence interface on each channel. As the coincidence window size increases, the coincident data rate increases before it levels off. Although not shown, at an extreme window size of 5 ms, the coincident data rate is about 200 Hz.

If the window is too large the system will start interpreting signals from different particles as coincident. This will tend to decrease the repeatability or stability of the measurements. To find out the dependence in this

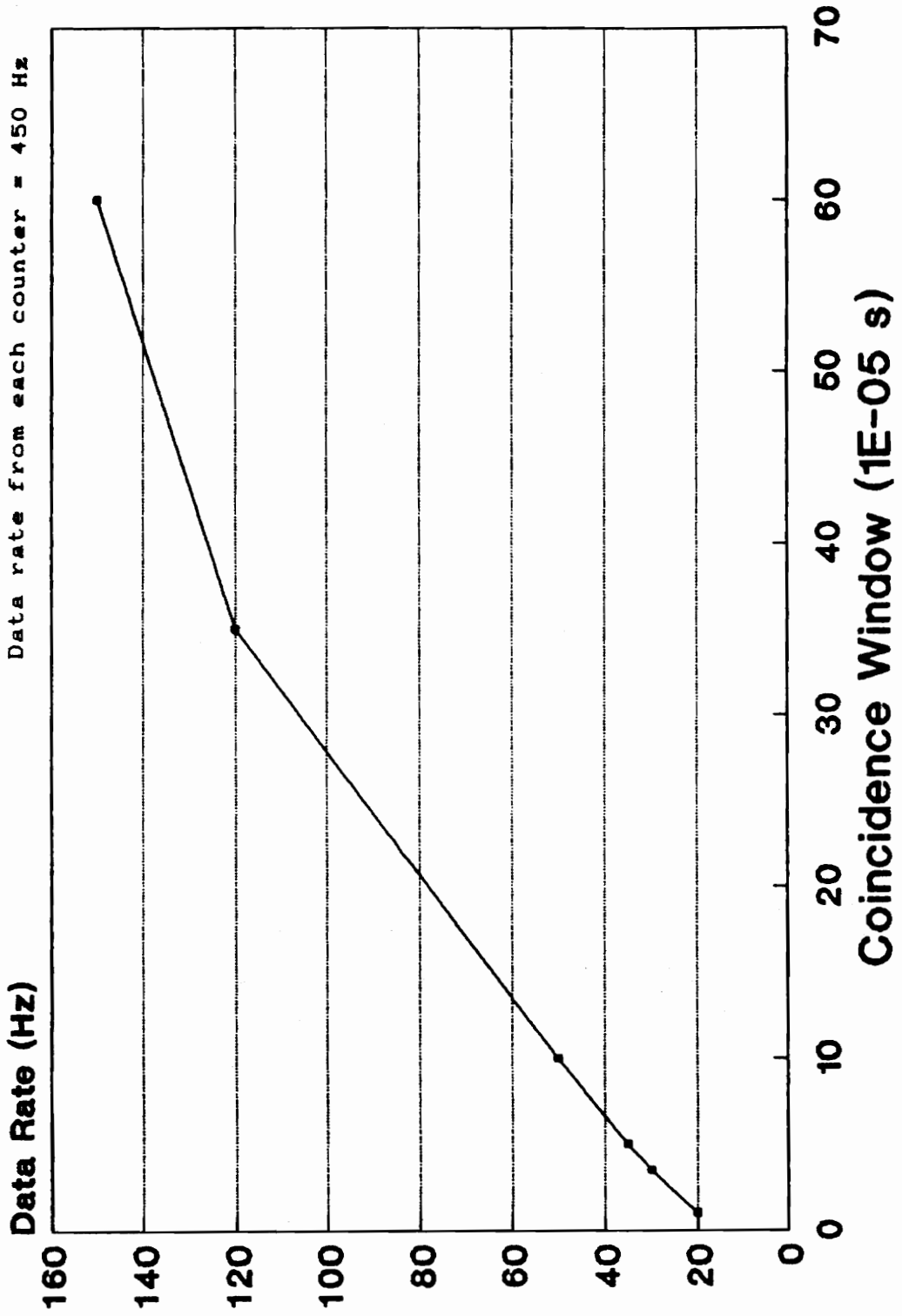


Fig. 35 Coincident Data Rate vs. Coincidence Window Size

system, a basic test was conducted to see how much the statistics varied with coincidence window at a radial location near the pipe wall. The results are shown in Fig. 36. The axial and radial fluctuations along with the Reynolds stress show very little variation with coincidence window up to about 300 μ s. The fluctuations that are present can not be attributed to the coincidence window alone and are a combination of all the possible sources of error in the system.

A coincidence window of 50 μ s was chosen to insure high quality measurements. A larger window could have been chosen based on Fig. 36, but this choice allowed a sufficient margin to insure that only coincident measurements were taken. It was also desired that only statistically independent measurements were collected so too high a data rate would not be suitable. This coincidence window size provided a data rate of about 35 Hz and consistent statistics.

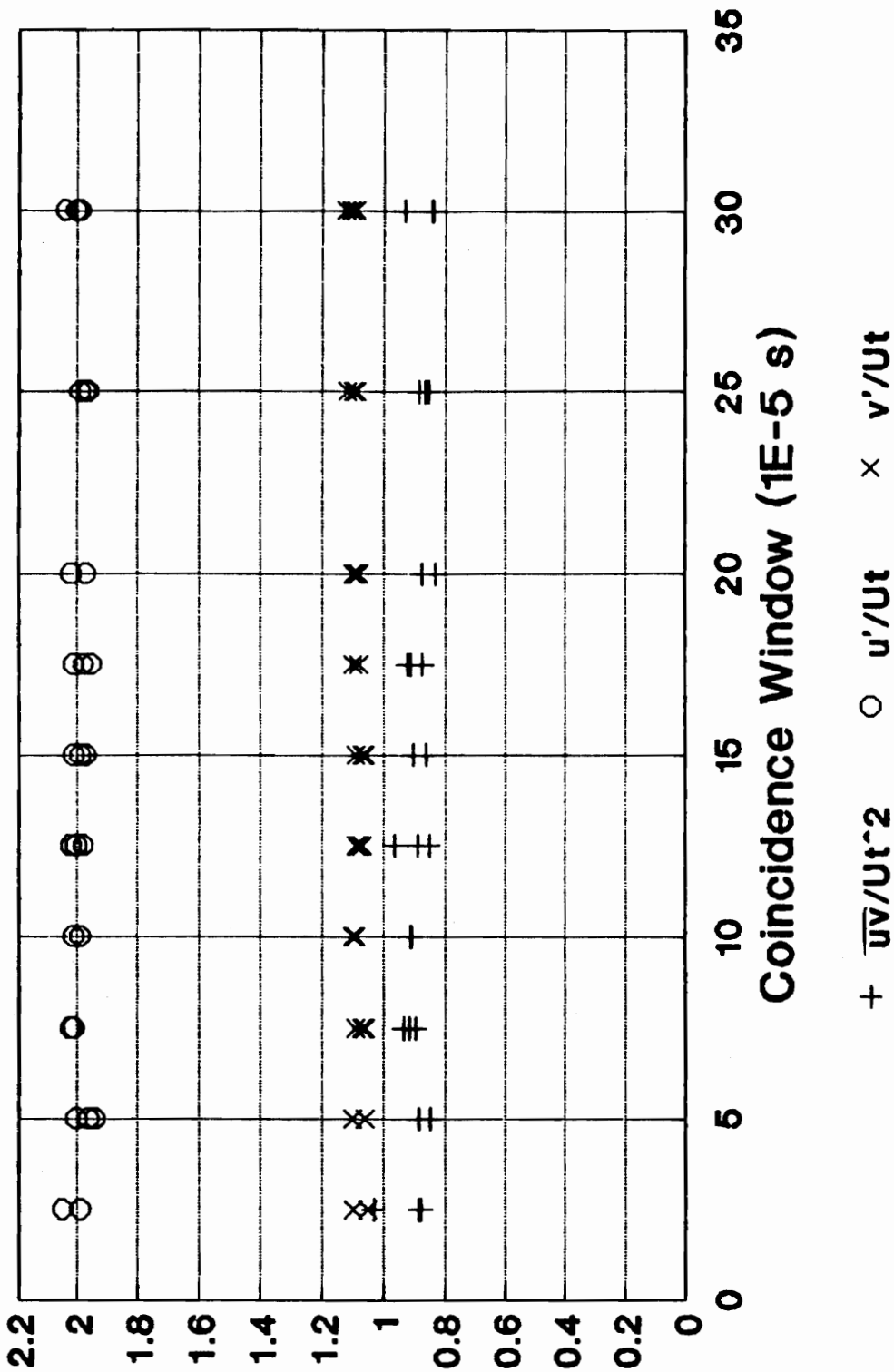


Fig. 36 Measurement Variability vs. Coincidence Window Size

7. RESULTS AND DISCUSSION

The experimental results of this investigation are discussed in the following sections. The data are plotted along with the results of Lawn [2], Laufer [1], and Shaffer [7]. Lawn's and Laufer's data were compared in Section 2.3. The results using this system will be evaluated on the basis of agreement to Laufer and Lawn as well as repeatability. All of the data, except the mean velocity, are nondimensionalized by the friction velocity and are plotted versus radius, r'/R . When $r'/R = 0$ the location is the pipe wall while at $r'/R = 1$, the location is the pipe center line. The repeatability of the measurements is demonstrated by plotting several points at each radial location consisting of 4000 samples each. Recall that in Section 5.4, the estimated error range in standard deviation was about $\pm 2.2\%$. All of the experimental data are tabulated in Appendix B and the experimental conditions are summarized in Table 1.

7.1 Mean Velocity Profile

The mean velocity profile for the fully developed pipe flow is shown in Fig. 37. The mean center line velocity is used to nondimensionalize the values. The experimental data show reasonable agreement with Laufer's curve which is for a Reynolds number based on diameter (ReD) of 50,000. Since

Table 1: Experimental Conditions

For the data presented in Fig. 37:

Pressure drop along Pipe	95.93 Pa
Static Temperature	296.43 K
Static Pressure	93.7 KPa
τ_w	0.329 N/m ²
Ut	0.546 m/s
Reynolds number (diameter)	51,000

For the data presented in Figs. 38,39,41,and 42:

Pressure drop along Pipe	102.9 Pa
Static Temperature	295 K
Static Pressure	94.9 KPa
τ_w	0.353 N/m ²
Ut	0.561 m/s
Reynolds number (diameter)	55,000

For the data presented in Fig. 40:

Pressure drop along Pipe	112.8 Pa
Static Temperature	294 K
Static Pressure	95.5 KPa
τ_w	0.387 N/m ²
Ut	0.585 m/s
Reynolds number (diameter)	57,000

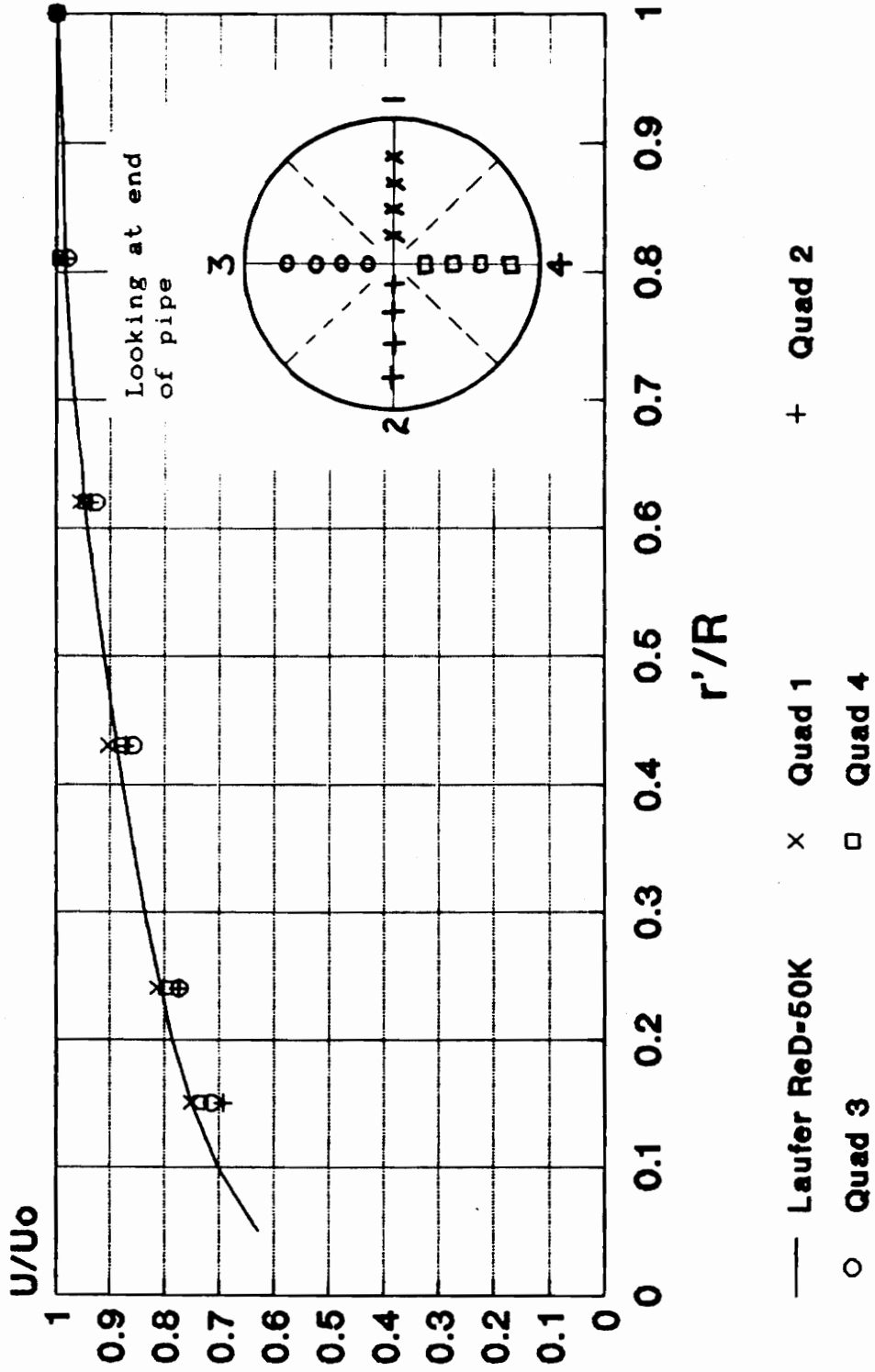


Fig. 37 Comparison of U/U_0 vs. r'/R to Reference Curve [1]

the ReD here was about 50,000, this agreement is expected. Data is shown from four quadrants of the pipe to assess the symmetry of velocity profile. The agreement between the quadrants is best near the center line and decreases toward the wall. The slight degree of asymmetry may be due to the layer of sugar seed particles which accumulated on the pipe wall or due to positioning error in the traverse. The measurements from all quadrants agree with Laufer's results to within .05 at all of the points measured. The Reynolds stress measurements discussed in subsequent sections were made in quadrants 1 and 3. Lawn and Shaffer do not present these curves in their results so no comparison is shown.

7.2 Velocity Fluctuations

The velocity fluctuations in the axial, radial and tangential directions are shown in Figs. 38-40. Note that u' is defined as the RMS value of u , where $U = \bar{U} + u$ and v' and w' are defined similarly. The RMS value is the square root of the Reynolds normal stress. The measured axial fluctuation, u' , shows very close agreement to Lawn's curve and Shaffer's data as shown in Fig. 38. The measured values are higher than Laufer's through the core of the flow but have better agreement with the reference curves near the wall. The results are repeatable since the variation in the 4000-sample measurements is less than .08. They are within

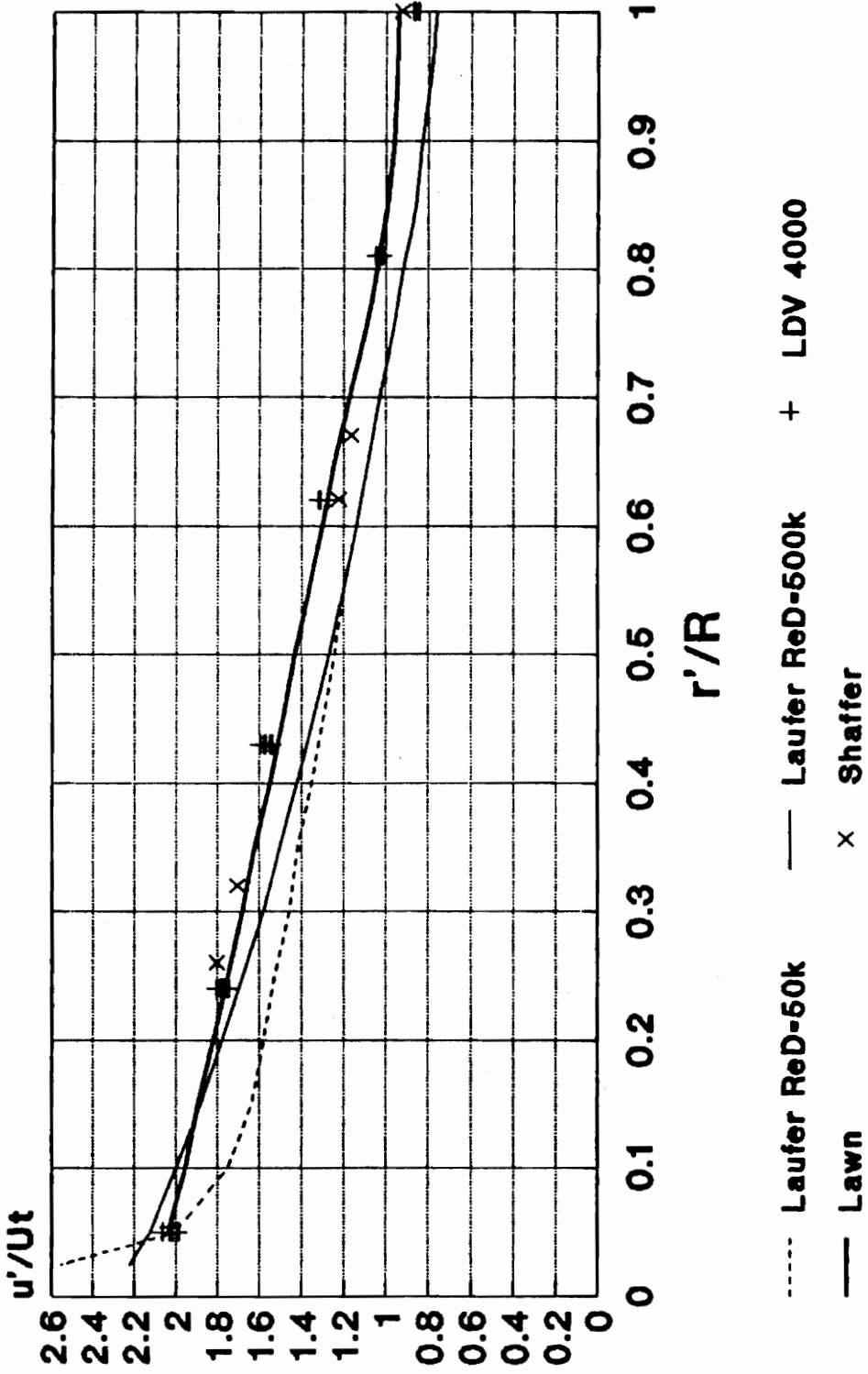


Fig. 38 Comparison of u'/U_t vs. r'/R to Reference Curves [1], [2], [7]

the expected variation of $\pm 2.2\%$ at all radial locations. The differences between Laufer's and Lawn's curves are within .3 throughout the flow. Since the experimental data from this system are all within .1 of Lawn's data and there is a significant difference between Laufer's and Lawn's curves, the agreement of this experimental data with the reference curves is reasonable.

The data for the radial fluctuations, v' , show reasonable agreement throughout the flow as shown in Fig. 39. The data is lower than both Laufer's and Lawn's near the center of the pipe. As the wall is approached, the data fall between Laufer's and Lawn's curves. At $r'/R = .05$, the data agree very closely to Lawn's curve. Considering that Lawn and Laufer's curves agree to within only about .2 near the wall, these results show reasonable agreement to their curves. Shaffer's data is close to Lawn's curve but slightly higher at most of the radial locations. Repeatability is demonstrated since the data vary no more than .045 within the set of measurements at each radial location. The variability is within the expected $\pm 2.2\%$ error bounds.

The results for the tangential fluctuations, w' , are shown in Fig. 40. The measured results are lower than Laufer's and Lawn's throughout the pipe. They do however, show the same general profile and are within .2 of Laufer's

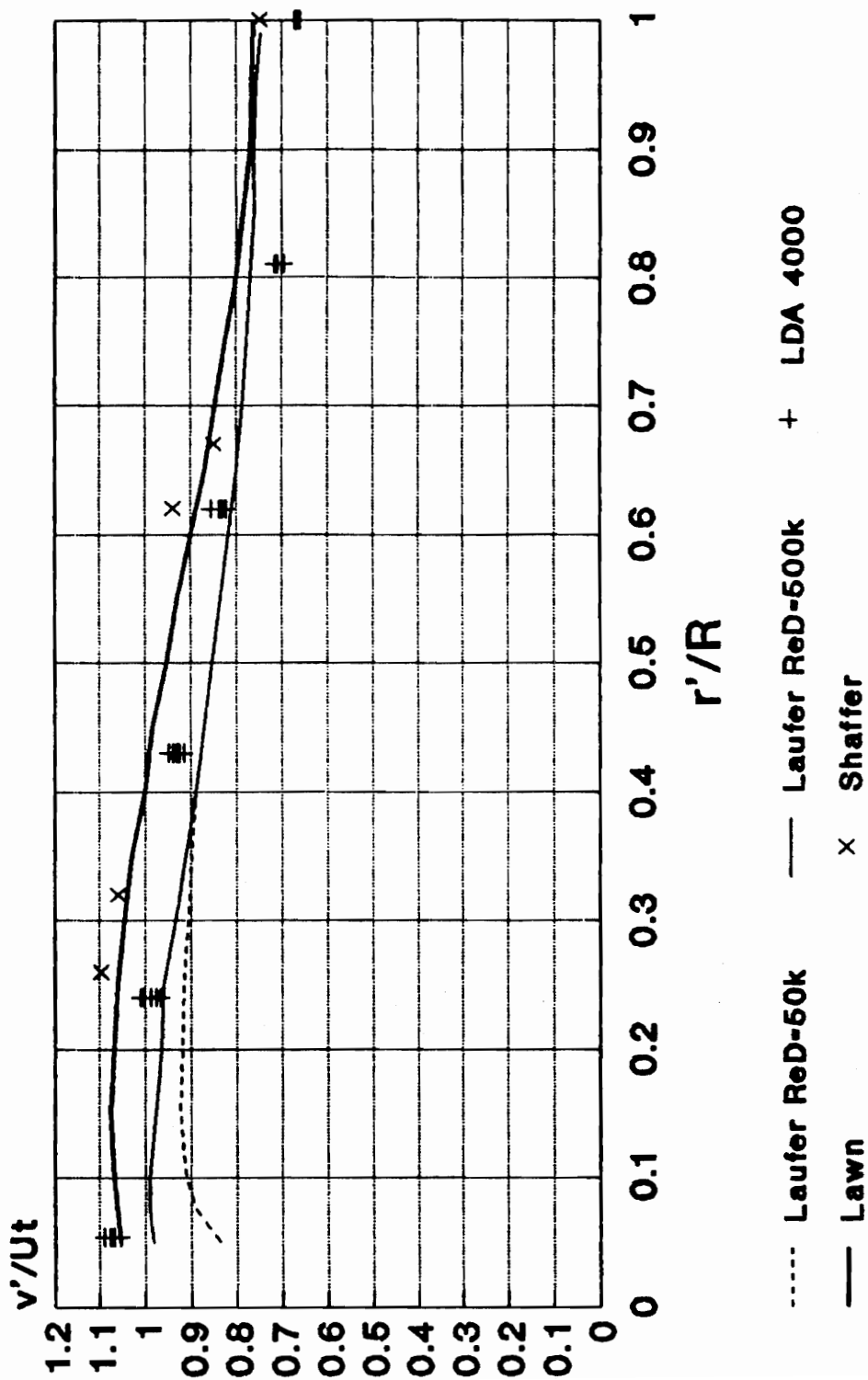


Fig. 39 Comparison of v'/Ut vs. r'/R to Reference Curves [1], [2], [7]

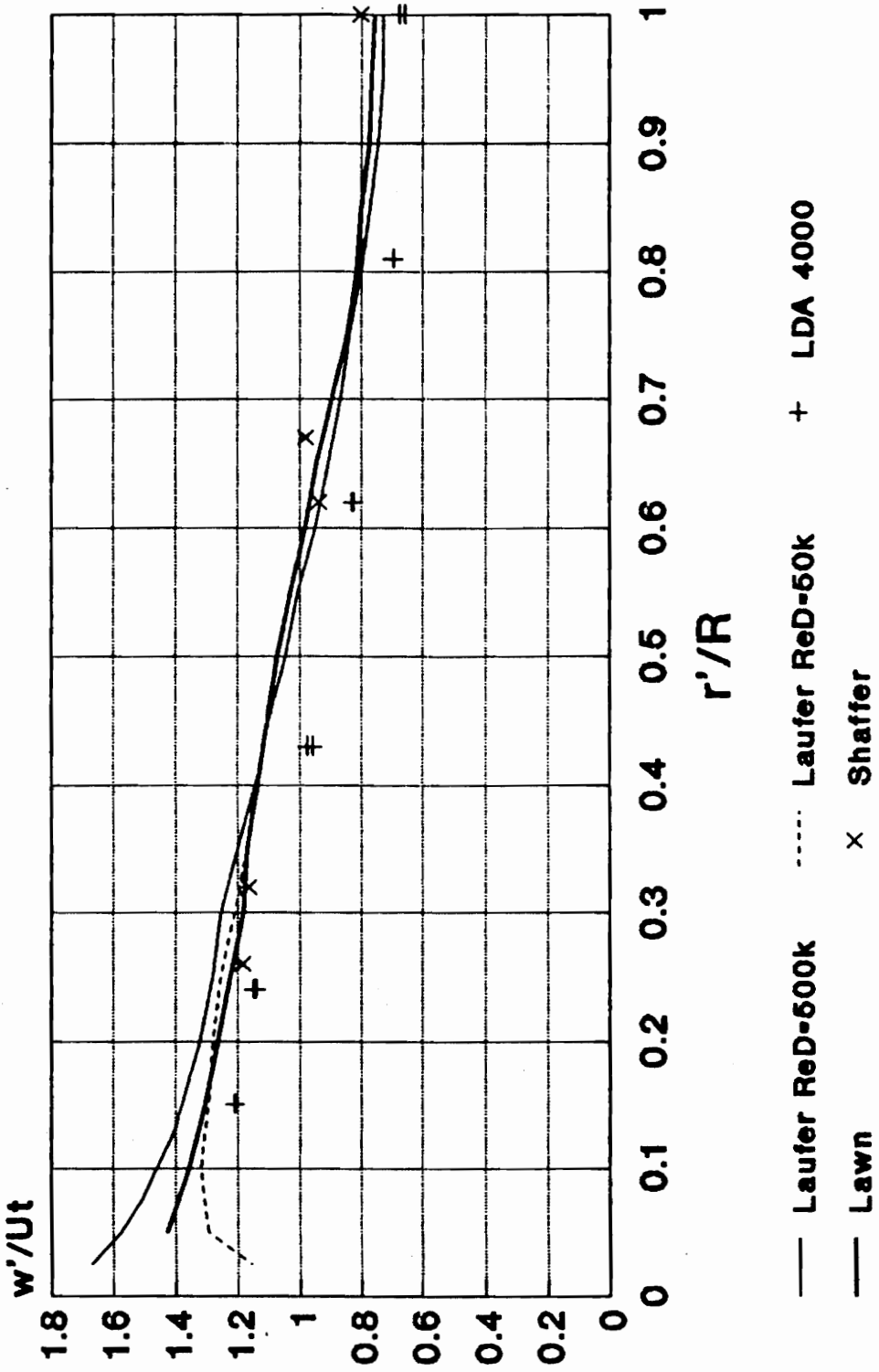


Fig. 40 Comparison of w'/U_t vs. r'/R to Reference Curves [1], [2], [7]

and Lawn's curves. Shaffer's data was very close to the other curves so the results using this system are clearly different and cannot be attributed to normal variation in measurement technique. The error could be due to the decreased spatial resolution while traversing in this direction. As shown in Appendix C, the ellipsoidal probe volume has dimensions of about 3.5 mm by .15 mm along its long and short axes respectively. Thus, when traversing along its long axis, the system is sensitive to a greater portion of the radius which decreases resolution. Even with the offset, the results were very repeatable. Only two groups of 4000 samples were taken for the tangential traverse since the results varied less than .02.

7.3 Reynolds Shear Stress

Fig. 41 shows the Reynolds shear stress profile across the pipe. This is the only curve for which there is a theoretical distribution. Through the core of the flow, the distribution should be linear. Near the wall, the turbulent shear stress should decrease as the viscous shear stress begins to dominate. The theoretical curve from Laufer is calculated based on his velocity profile assuming a symmetrical, fully developed pipe flow for $Re_D = 50,000$.

In the core region of the flow, the data closely match the curve from Laufer. As shown in Section 2.3, Lawn's data

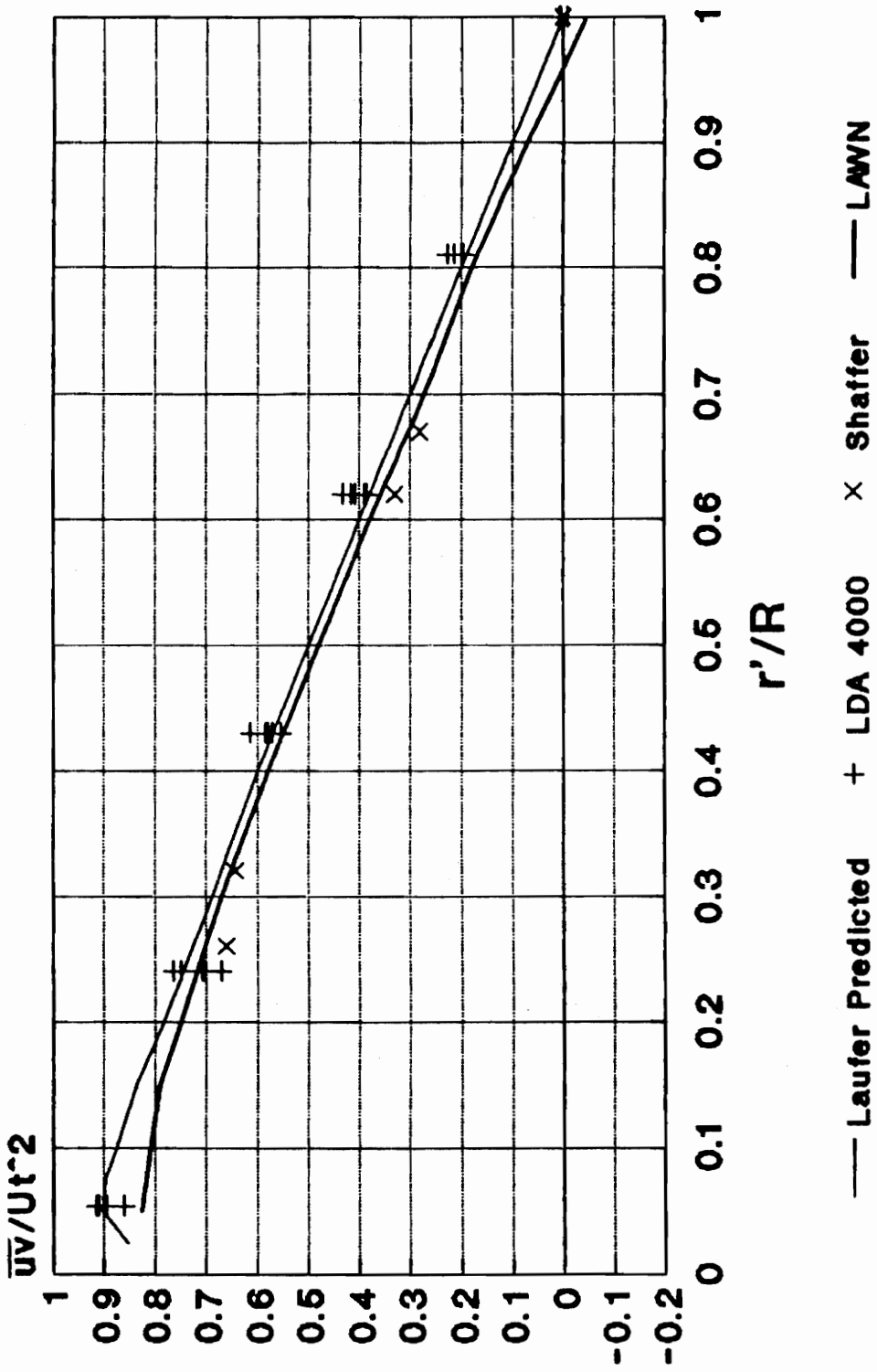


Fig. 41 Comparison of $\bar{u}\bar{v}/U_t^2$ vs. r'/R to Reference Curves [1], [2], [7]

have an offset from the expected linear distribution and are shown to illustrate the variability that exists in other measurements of turbulence in pipe flows. The experimental data from this system show close agreement with Laufer's calculated distribution. The maximum error increases from .01 at the center line to .094 near the wall. Within the groups at each radial location, the measurements vary less than .10 but the variability decreases toward the centerline.

7.4 Correlation Coefficient

The correlation coefficient $\overline{uv} / u'v'$ is displayed in Fig. 42. The value is about zero at the center line which indicates that there is no correlation between the axial and radial velocity. The correlation coefficient rises to about .4 and remains nearly constant across the radius of the pipe. The experimental data closely match the $ReD = 500,000$ curve from Laufer. As described before, Lawn's curve is low since his shear stress measurements were low. However, Lawn does demonstrate that the correlation coefficient is independent of Reynolds number which is not shown by Laufer. The experimental results at each radial location vary less than .04 between the groups of 4000 samples.

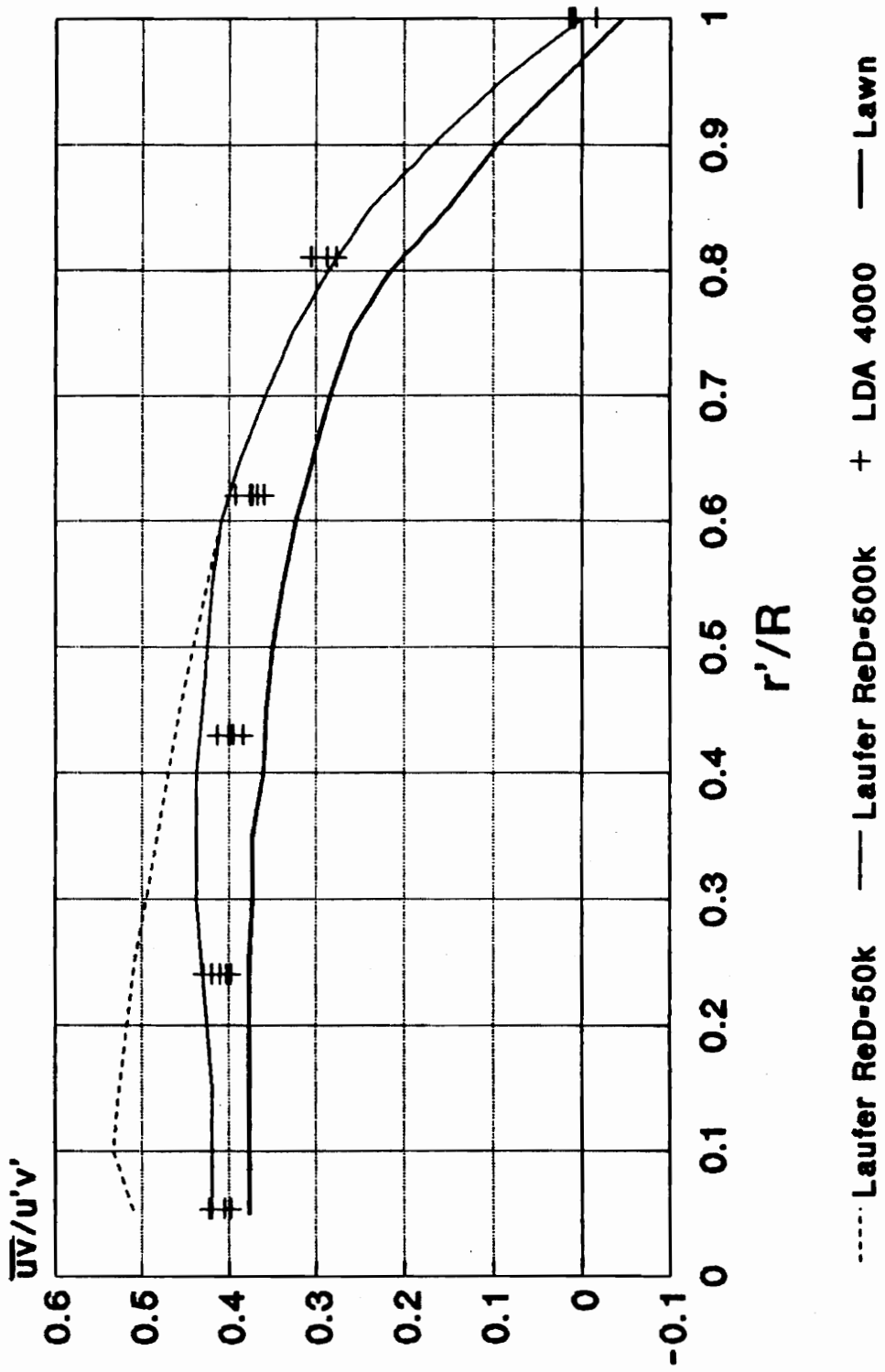


Fig. 42 Comparison of $\overline{uv}/u'v'$ vs. r'/R to Reference Curves [1], [2], [7]

8. CONCLUSIONS

The ability to make Reynolds shear stress measurements with the Mechanical Engineering Department's two component laser Doppler anemometer (LDA) system has been successfully demonstrated. The measurements were made in a fully developed, turbulent pipe flow. It was found that accurate turbulence measurements with an LDA depend on many factors.

Statistical bias has a pronounced effect on turbulence measurements. The effects of bias can be reduced through the methods described in Section 5.2: 1. The filter width must be chosen very carefully to avoid filter bias. 2. A Bragg cell should be used to reduce the effects of fringe bias. 3. Residence time weighting should be implemented to reduce the effects of velocity bias.

The choice of amplification can play an important role in optimization of the system. Using the gain on the PMT rather than the amplifiers on the frequency counters provides higher quality signals.

A low sample rate can be used successfully to make mean and turbulence measurements. This was based upon an estimate of the time scales of turbulence and how they relate to the sample rate.

The errors due to inexact angle measurement and finite sample size were estimated to be at most $\pm 2\%$ and $\pm 2.2\%$ respectively. It was found that the variation in the

repeated measurements made at the same radial location were within the $\pm 2.2\%$ error that was expected.

The results of the experiment were compared with those of Laufer and Lawn. The level of variability in the results of these two authors shows that the techniques for turbulence measurement are inexact and are still evolving. Therefore, no one author's results should be taken as absolutely correct. In fact, the values for the Reynolds normal stresses don't appear to be better known than about $\pm 10\%$. Also, while there is a theoretical shear stress distribution, it does not appear to be possible to make measurements with an accuracy better than about $\pm 5\%$.

This investigation has added another set of measurements that can be used for comparison to evaluate turbulence measurement equipment. The results using this system are within the range of variability and show reasonable agreement with Laufer's and Lawn's results. Based on these results, this system is suitable for Reynolds shear stress measurements in other flows of research interest.

REFERENCES

1. Laufer, J., "The Structure of Turbulence in Fully-Developed Pipe Flow," NACA Report No. 1174, 1954.
2. Lawn, C. J., "The Determination of Dissipation in Turbulent Pipe Flow," Journal of Fluid Mechanics, Vol. 48, Pt. 3, 1970, pp. 477-505.
3. Reynolds, O., "An Experimental Investigation of the Circumstances Which Determine Whether the Motion of Water Shall Be Direct or Sinuous, and of the Law of Resistance in Parallel Channels," Phil. Trans. Roy. Soc., Vol. 174, 1883, pp. 935-982.
4. Hinze, J.O., Turbulence, 2nd Edition, McGraw-Hill, New York, 1975.
5. Moran, J., An Introduction to Theoretical and Computational Aerodynamics, John Wiley & Sons, New York, 1984.
6. Durst, F., Melling, A., and Whitelaw, J. H., Principles and Practice of Laser-Doppler Anemometry, 2nd Edition, Academic Press, London, 1981.
7. Shaffer, D, "Reynolds Stress Measurement Downstream of a Turbine Cascade," Master's Thesis, Virginia Polytechnic Institute and State University, Blacksburg, VA, 1985.
8. Schlichting, H., Boundary-Layer Theory, 7th Edition, McGraw-Hill, New York, 1979.
9. Berman, N, and Dunning, J., "Pipe Flow Measurements of Turbulence and Ambiguity Using Laser-Doppler Velocimetry," Journal of Fluid Mechanics, Vol. 61,. Pt. 2, 1973, pp. 289-299.
10. Kim, J., Moin, P., and Moser. R., "Turbulence Statistics in Fully Developed Channel Flow at Low Reynolds Number," Journal of Fluid Mechanics, Vol. 177, 1987, pp. 133-166.
11. King, L., "On the Convection of Heat From Small Cylinders in a Stream of Fluid: Determination of the Convection Constants of Small Platinum Wires with Application to Hot-Wire Anemometry," Phil. Trans. Roy. Soc., Ser. A, Vol. 214, 1914, pp. 373-432.

12. Dryden, H. L., and Keuthe, A., "The Measurement of Fluctuation of Air Speed by the Hot-Wire Anemometer," NACA Report No. 320, 1929.
13. Yeh, Y., and Cummins, H., "Localized Fluid Flow Measurements with an He-Ne Laser Spectrometer," Applied Physics Letters, Vol. 4, No. 10, May, 1964, pp. 176-178.
14. Self, S., and Whitelaw, J., "Laser Anemometry for Combustion Research," Combustion Science and Technology, Vol. 13, 1976, pp. 171-197.
15. Rose, W., and Johnson, D., "Laser Velocimeter and Hot-Wire Anemometer Comparison in a Supersonic Boundary Layer," AIAA Journal, Vol. 13, No. 4, April, 1975, pp. 512-515.
16. Yanta, W., "A Three-Dimensional Laser Doppler Anemometer (LDV) for Use in Wind Tunnels," ICIASF Record, Sept. 1979, pp. 294-300.
17. Dimotakis, P.E., Lang, D.B., and Collins, D.J., "Laser Doppler Velocity Measurements in Subsonic, Transonic, and Supersonic Turbulent Boundary Layers," Laser Velocimetry and Particle Sizing, Hemisphere, Washington, D.C., 1979.
18. Orloff, K. and Olson, L., "High Resolution LDA Measurements of Reynolds Stress in Boundary Layers and Wakes," AIAA Paper No. 80-0436, 1980.
19. Absil, L., "Laser Doppler Measurements of Mean Turbulence Quantities, Time- and Spatial-Correlation Coefficients in the Wake of a Circular Cylinder," 4th International Symposium on the Applications of Laser Anemometry to Fluid Mechanics, Lisbon, Portugal, July 11-14, 1980, pp. 45-61.
20. Johnson, D., "Laser Doppler Anemometry," A Survey of Measurements and Measuring Techniques in Rapidly Distorted Compressible Turbulent Boundary Layers, AGARD Proceeding No. 315, May, 1989, pp. 6.1-6.10.
21. Dancey, C.L., "Measurement of Second Order Turbulence Statistics in an Axial-Flow Compressor via 3-Component LDA," AIAA/SAE/ASME/ASEE Joint Propulsion Conference, Orlando, FL, July 16-18, 1990.

22. Buchave, P., George, W. K., and Lumley, J. L., "The Measurement of Turbulence with the Laser-Doppler Anemometer," Annual Review of Fluid Mechanics, Vol. 11, 1979, pp. 443-503.
23. Edwards, R.V., "Report of the Special Panel on Statistical Particle Bias Problems in Laser Anemometry," Journal of Fluids Engineering, Vol. 109, June, 1987, pp. 89-93.
24. Stevenson, W., and Thompson, H., "Direct Measurement of Laser Velocimeter Bias Errors in a Turbulent Flow," AIAA Journal, Vol. 20, No. 12, 1982, pp. 1720-1723.
25. George, W., "Quantitative Measurement with the Burst-Mode Laser Doppler Anemometer," Experimental Thermal and Fluid Science, Vol. 1, 1988, pp. 29-40.
26. Brown, J. L., "Geometric Bias and Time Coincidence in 3-Dimensional Laser Doppler Velocimeter Systems," Experiments in Fluids, Vol. 7, 1989, pp. 25-32.
27. Carey, C., "Statistical Bias of the Data From Two-Channel Laser-Doppler Anemometer Systems," 10th International Symposium on Applications of Laser-Doppler Anemometry to Fluid Mechanics, Lisbon, Portugal, 1986.
28. Lacharme, J. P., and Elena, M., "Effect of Angular Bias on LDA Measurements in Supersonic Turbulent Flow," Experiments in Fluids, Vol. 6, 1988, pp. 435-442.
29. Samimy, M., and Abu-Hijleh, B.A., "Performance of Laser Doppler Velocimeter with Polydisperse Seed Particles in High-Speed Flows," Journal of Propulsion, Vol. 5, No. 1, Jan.-Feb., 1989, pp. 21-25.
30. Cline, V.O., and Lo, C.F., "Application of the Dual-Scatter Laser Velocimeter in Transonic Flow Research," Applications of Non-Intrusive Instrumentation in Fluid Flow Research, AGARD Conference Proceeding No. 193, May, 1976, pp. 4.1-4.12.
31. Tree, I., "Laser Doppler Velocimeter Measurements in a Turbulent Junction Vortex," PhD Dissertation, Virginia Polytechnic Institute and State University, Blacksburg, VA, 1986.

32. Nath, S. "Spectral Estimates and Flow Characteristics From Non-uniformly Sampled LDV Data in a Turbulent Junction Vortex," PhD Dissertation, Virginia Polytechnic Institute and State University, Blacksburg, VA, 1988.
33. Menna, J., "A Particle Biasing Technique for a Two-Color Laser Doppler Anemometer with Counter Processing," Master's Thesis, Virginia Polytechnic Institute and State University, Blacksburg, VA, 1979.
34. Tree, I. and Pierce, F.J., "Principles of Laser Doppler Anemometry", 1982.
35. Tree, I., and Pierce, F.J., "LDA -- Miscellaneous Topics", 1982,
36. Tree, I. and Pierce, F. J., "Practical Aspects of Implementing DISA'S 55X Optical-Electronic Frequency Shift System," 1983.
37. Tree, I., Menna, J., and Horne, M., "Alignment of the DISA Two Color Optics," 1985.
38. Model 164 General Laboratory Ion Laser Instruction Manual, Spectra-Physics, 1977.
49. DISA 55L90 LDA Counter Processor Instruction Manual, DISA Information Department
40. DISA 55N10 LDA Frequency Shifter Instruction Manual, DISA Information Department
41. DISA 55X Modular LDA Optics Instruction Manual, DISA Information Department
42. Argarwal, J. K., and Johnson, E., "Generating Aerosol for Laser Velocimeter Seeding," TSI Quarterly, Vol. 7, Issue 3, July-September, 1981, pp 5-12.
43. Dancey, C.L., Personal Interviews, January-March, 1992.
44. Doty, M.C., "Alignment Supplement For LDA", December, 1992.
45. Dean, R.C., Ed., Aerodynamic Measurements, 7th Edition, Eagle Enterprises, New York, 1961.
46. Taylor, G.I., "Correlation Measurements in Turbulent Flow Through A Pipe," Proc. Roy. Soc., A157, 1936, pp. 537-546.

47. McLaughlin, D.K., and Tiederman, W.G., "Biasing Correction For Individual Realization of Laser Anemometer Measurements in Turbulent Flows," Phys. Fluids, Vol. 16, 1974, pp. 2082-2088.
48. Strazisar, A.J., "Application of Laser Anemometry to Turbomachinery Flowfield Measurements," Measurement Techniques in Turbomachines, von Karman Institute Lecture Series No. 3, Belgium, February 25 - March 1, 1985.

Appendix A. Beam Angle Determination Program

```

1000 'ANGLE CALCULATION PROGRAM FOR 3 BEAM LDV SYSTEM
1010 'COORDINATES FOUND USING A PINHOLE AND TRAVERSE TABLE WITH
1020 'MICROMETER DIAL INDICATORS TO INDICATE POSITION
1030 ' First locate the center coordinates where all three beams go through
1040 ' pinhole. Next traverse the table away from the pinhole about 1.5 inches
1050 ' and locate all three beams. Locate beams by traversing table in remaining
1060 ' two coordinate directions until the desired beam goes through the pinhole
1070 ' Note the coordinates for each beam and enter into this program.
1080 DIM X(4),Y(4),Z(4),UNVECI(4),UNVECJ(4),UNVECK(4),VECI(4),VECJ(4),VECK(4)
1090 DIM VLEN(4)
1100 'read in data
1105 PRINT "center,blue,green,and blue-green coordinates
1106 PRINT"      x              y              z"
1110 FOR N=1 TO 4
1120 READ X(N),Y(N),Z(N)
1125 PRINT X(N),Y(N),Z(N)
1130 NEXT N
1140 FOR N = 2 TO 4
1150 ' calculate vector length
1160 VLEN(N) = ((X(N)-X(1))^2+(Y(N)-Y(1))^2+(Z(N)-Z(1))^2)^.5
1170 VECI(N) = X(N)-X(1)
1180 VECJ(N) = Y(N)-Y(1)
1190 VECK(N) = Z(N)-Z(1)
1200 ' calculate unit vector components
1210 UNVECI(N)=VECI(N)/VLEN(N)
1220 UNVECJ(N)=VECJ(N)/VLEN(N)
1230 UNVECK(N)=VECK(N)/VLEN(N)
1240 NEXT N
1250 PRINT "          i " , "          j", "          k"
1260 PRINT "vector b:";
1270 PRINT USING " #.#####"          "; UNVECI(2), UNVECJ(2), UNVECK(2)
1280 PRINT "vector g:";
1290 PRINT USING " #.#####"          "; UNVECI(3), UNVECJ(3), UNVECK(3)
1300 PRINT "vector bg:";
1310 PRINT USING " #.#####"          "; UNVECI(4), UNVECJ(4), UNVECK(4)
1320 'calculate dot products
1330 BDOTBG=UNVECI(2)*UNVECI(4)+UNVECJ(2)*UNVECJ(4)+UNVECK(2)*UNVECK(4)
1340 GDOTBG=UNVECI(3)*UNVECI(4)+UNVECJ(3)*UNVECJ(4)+UNVECK(3)*UNVECK(4)
1350 PRINT "B VECTOR DOT BG VECTOR=",BDOTBG
1360 PRINT "G VECTOR DOT BG VECTOR=",GDOTBG
1370 ' calculate angles from arcosine(dot product)
1380 ANGBBG=-ATN(BDOTBG/SQR(-BDOTBG*BDOTBG+1))+(3.1415927#/2)
1390 ANGGBG=-ATN(GDOTBG/SQR(-GDOTBG*GDOTBG+1))+(3.1415927#/2)
1400 PRINT "angle between blue and blue-green beam is:",ANGBBG*(180/3.1415927#)
1410 PRINT "angle between green and blue-green beam is:",ANGGBG*(180/3.1415927#)
1420 'center coordinates(x,y,z)
1430 DATA 1.693,1.045,1.052
1440 'blue coordinates(x,y,z)
1450 DATA 0.193,0.988,1.052
1460 'green coordinates(x,y,z)
1470 DATA 0.193,0.805,1.052
1480 'blue green coordinates(x,y,z)
1490 DATA 0.193, 0.900,0.949

```

Appendix B. Experimental Data

	Radial Location r'/R						
	1	0.81	0.62	0.43	0.24	0.15	0.05
u'/Ut	0.8649	1.011	1.2715	1.5355	1.7517		1.984
	0.8439	1.0436	1.3108	1.574	1.7706		2.026
	0.8749	1.021	1.3105	1.5966	1.761		2.061
	0.8737	1.044	1.319	1.5452	1.7797		2.018
			1.3169	1.566	1.744		2.025
				1.802			
v'/Ut	0.6659	0.7109	0.8239	0.9389	0.9766		1.0683
	0.6718	0.7096	0.8299	0.9305	1.0098		1.0687
	0.6623	0.696	0.8537	0.9151	1.004		1.0899
	0.6607	0.7148	0.8368	0.9252	0.989		1.0534
			0.8227	0.9479	0.9666		1.077
				0.987			
w'/Ut	0.675	0.6938	0.8265	0.9589	1.15	1.211	
	0.66	0.6975	0.832	0.9768	1.143	1.2105	
\overline{uv}/Ut^2	0.0065	0.1995	0.385	0.5542	0.7017		0.895
	-0.009	0.227	0.409	0.5797	0.75		0.8605
	0.0089	0.1966	0.4175	0.5854	0.703		0.9098
	0.005	0.2148	0.4329	0.5707	0.7078		0.8959
			0.3899	0.6144	0.67		0.9149
				0.7636			
$\overline{uv}/u'v'$	-0.016	0.2775	0.3675	0.3844	0.4101		0.4222
	0.014	0.3065	0.3759	0.3958	0.4194		0.3974
	0.011	0.2766	0.373	0.4006	0.3976		0.405
	0.0086	0.2879	0.3922	0.399	0.4021		0.4214
			0.3598	0.4139	0.3974		0.4195
				0.4293			
U/U_0							
Quad 1	1	0.9907	0.9538	0.9029	0.8123	0.75	
U/U_0							
Quad 2	1	0.9815	0.936	0.8707	0.773	0.6915	
U/U_0							
Quad 3	1	0.976	0.9244	0.8751	0.7713	0.7127	
U/U_0							
Quad 4	1	0.991	0.9438	0.876	0.7955	0.732	

Appendix C. Probe Volume Dimensions

From reference 41, a pair of laser beams that intersect will form an ellipsoidal probe volume with the following dimensions:

$$dx = \frac{bw}{\cos \theta}$$

$$dy = bw$$

$$dz = \frac{bw}{\sin \theta}$$

where:

$$bw = \frac{4 f \lambda}{\pi E b}$$

f = focal length of front lens

λ = laser light wavelength

E = expansion ratio of beam expander

$\pi = 3.1415927\dots$

b = beam waist diameter of unfocused laser beam

θ = half angle between the beams

Using the values for this system:

$f = 600 \text{ mm}$

$\lambda = 488 \text{ and } 514.4 \text{ nm}$

$E = 1.9$

$b = 1.25 \text{ mm}$

$\theta = 2.55 \text{ deg}$

for $\lambda = 488 \text{ nm}$

$dx = 0.1571 \text{ mm}$

$dy = 0.1569 \text{ mm}$

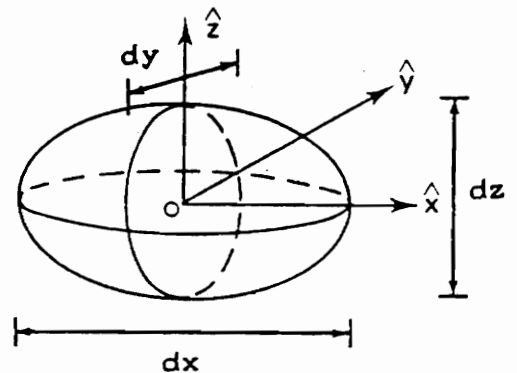
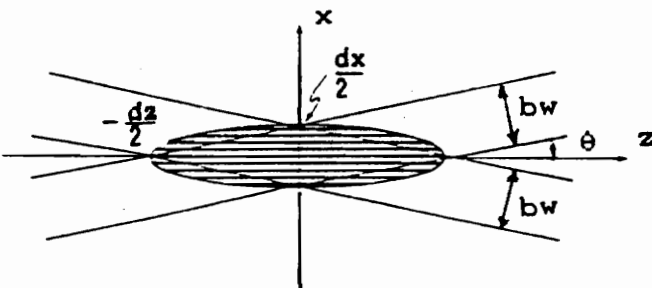
$dz = 3.528 \text{ mm}$

for $\lambda = 514.5 \text{ nm}$

$dx = 0.1650 \text{ mm}$

$dy = 0.1648 \text{ mm}$

$dz = 3.705 \text{ mm}$

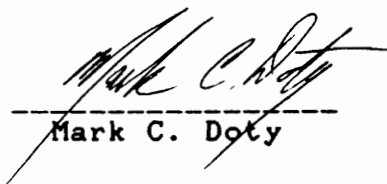


Vita

Mark Clayton Doty was born in Radford, Virginia on January 4, 1968. His family moved to Denver, Colorado in 1970 where he later completed elementary and junior high school. In 1983, his family moved to Baltimore, Maryland where he completed high school.

In September, 1986, he began his undergraduate studies in Aerospace Engineering at Virginia Polytechnic Institute and State University. During his undergraduate career he completed the cooperative education program. He graduated with honors in May, 1991.

In August, 1991, he began graduate studies in Mechanical Engineering at Virginia Polytechnic Institute and State University. This thesis is the culmination of his efforts there.



Mark C. Doty